Vol. 5, 4, 311-384 (1998)

Archives of Computational Methods in Engineering
State of the art reviews

Continuum Modelling and Numerical Simulation of Material Damage at Finite Strains

E.A. de Souza Neto, D. Perić and D.R.J. Owen

Department of Civil Engineering
University of Wales Swansea
Singleton Park
Swansea SA2 8PP, UK

Summary

This paper describes in detail a general framework for the continuum modelling and numerical simulation of internal damage in finitely deformed solids. The development of constitutive models for material deterioration is addressed within the context of Continuum Damage Mechanics. Links between micromechanical aspects of damage and phenomenological modelling within continuum thermodynamics are discussed and a brief historical review of Continuum Damage Mechanics is presented. On the computational side, an up-to-date approach to the finite element solution of large strain problems involving dissipative materials is adopted. It relies on an implicit finite element discretization set on the spatial configuration in conjuction with the full Newton-Raphson scheme for the iterative solution of the corresponding non-linear systems of equations. Issues related to the numerical integration of the path dependent damage constitutive equations are discussed in detail and particular emphasis is placed on the consistent linearization of associated algorithms. A model for elastic damage in polymers and finite strain extensions to Lemaitre's and Gurson's models for ductile damage in metals are formulated within the described framework. The adequacy of the constitutive-numerical framework for the simulation of damage in large scale industrial problems is demonstrated by means of numerical examples.

1 INTRODUCTION

Techniques for numerical simulation of the behaviour of solids, mostly based on the finite element method, are today becoming routinely used by an ever increasing number of design engineers. In many areas, such techniques have reached a high degree of predictive capability and comprise an essential component of the design process.

During early developments of computer codes for stress analysis, the constitutive description of the response of materials had been mostly dominated by the classical and mathematically well established theories of elasticity and elasto-plasticity. Over the years, following the increasing industrial demand for accurate predictive tools, the finite element procedures originally based on such material models have been continuously modified and adapted to cope with more complex deformation processes involving large deflections, finite strains, viscous effects, etc.

Despite the great achievements realised regarding the simulation of many materials under a wide variety of circumstances, the description of the general non-linear behaviour of solids undergoing large deformations is far from settled. For many industrial applications, the description of the mechanical response by means of standard elastic or elasto-plastic models can lead to very poor representations of the real processes. Of particular importance are situations in which internal damaging of the material in the form of growth of cracks and microcavities plays an essential role in the overall constitutive behaviour. As pointed out by Krajčinović [49], in spite of the fundamental differences between the microscopic nature of damage mechanisms and elastoplastic processes, the classical theory of plasticity has been frequently stretched beyond its limits of applicability and used to describe materials whose behaviour is dominated by internal damage evolution. In such cases, the development and

 ISSN: 1134–3060 Received: December 1996

computational implementation of new and more refined constitutive models deserves careful consideration.

This paper describes a general framework for the development of continuum models along with the appropriate computational algorithms for numerical simulation of internal damage in finitely deformed solids.

The development of constitutive models is addressed within the context of *Continuum Damage Mechanics* [10, 55]. Inaugurated by Kachanov [44] in 1958, this new branch of continuum mechanics has since been attracting increasing attention within the applied mechanics community. Based on a solid mathematical and thermodynamical foundation, acquired over the last two decades or so of its development, Continuum Damage Mechanics is today recognised as an effective tool of mathematical modelling, which can help bridge the gap between the microscopic analysis of the internal deterioration of materials and engineering models suitable to design work.

On the computational side, an up-to-date approach to the implicit finite element solution of finite strain problems involving dissipative materials is described. It provides an efficient tool for simulation of damage in large scale industrial problems. Its basic ingredients comprise: the development of algorithms for numerical integration of the path dependent constitutive equations, leading to incremental versions of the original constitutive laws; a finite element discretization of the corresponding (equilibrium) incremental boundary value problem set on the spatial configuration and; the use of the full Newton-Raphson scheme for the iterative solution of the resulting non-linear system of equations. Due to the use of the Newton method, particular emphasis is placed on the derivation of exact tangent moduli.

Specific examples of application of the described framework are given with the formulation of three distinct damage models:

1. A model for finite strain *elastic* damage capable of describing the *Mullins effect* [67] in filled rubbery polymers.
2. A finite strain extension to Lemaitre's *elasto-plastic* damage model [57]. Lemaitre's theory includes damage evolution as well as non-linear isotropic and kinematic hardening in the description of the behaviour of ductile metals.
3. A finite strain extension to Gurson's [32] voids growth theory, also applicable to the description of ductile damage in metals.

The extensions to Lemaitre's and Gurson's theories are based on the framework for multiplicative hyperelastic-based finite elasto-plasticity described in references [25, 84, 85, 95, 98, 118]. Among other advantages, this approach allows the formulation of integration algorithms for the constitutive equations that, essentially, preserve the format of the now classical return mapping schemes of infinitesimal elasto-plasticity. In addition, a relatively simple structure for the associated consistent spatial tangent modulus can be derived, making the resulting formulation particularly attractive for computational implementation.

This article is divided into eight sections. After this introductory one, Section 2 sets out some basic concepts of continuum mechanics and thermodynamics which form the basis for constitutive modelling of damage described in subsequent sections. Section 3 reviews some micromechanical aspects related to internal damage in solids and Section 4 presents a brief historical review of the development of *Continuum Damage Mechanics*. Section 5 describes a general framework for the implicit finite element simulation of finite strain problems involving dissipative materials. It provides a common basis for the numerical simulation of the damage models presented in Sections 6 and 7. In Section 6, a damage model for finitely strained filled polymers is described, along with all relevant aspects related to the numerical integration of the constitutive equations and corresponding consistent linearization. Numerical examples show the effectiveness of the numerical model. At its outset, Section 7 describes in detail a general framework for the treatment of finite elasto-plasticity which, subsequently, is applied to the finite strain formulation of Lemaitre's and Gurson's ductile damage models. Issues related to the integration of constitutive equations and corresponding consistent linearization are addressed. Numerical examples, including an industrial metal forming problem, are provided to demonstrate the adequacy of the adopted constitutive-numerical framework for the efficient numerical simulation of ductile damage at finite strains. Finally, concluding remarks are presented in Section 8.

2 CONTINUUM CONSTITUTIVE MODELLING

Some basic concepts of thermodynamics of continuous media are briefly reviewed in this section. The material presented here is standard and well established in the continuum mechanics literature [112, 33]. Nevertheless, its inclusion at this point is convenient for later discussion. By emphasizing the link between micromechanical processes and their mathematical representation within the framework of continuum thermodynamics with internal variables, the purpose of the present section is to establish a clear logical sequence in the development of continuum constitutive models of general dissipative materials. Application of the fundamental principles reviewed to the constitutive description of material damage is discussed in Sections 4, 6 and 7.

2.1 Fundamental Laws of Thermodynamics

Consider a generic continuum body $\mathscr{B}$ which occupies a region Ω, with boundary $\partial\Omega$, of the three-dimensional Euclidean space $\mathscr{E}^3$ in its reference configuration. Let $\mathscr{B}$ be subjected to a *motion* $\boldsymbol{\varphi}$ so that for each time t, the *deformation*

$$\boldsymbol{\varphi}(\cdot, t) : \mathscr{E}^3 \longrightarrow \mathscr{E}^3$$

maps each material particle $\boldsymbol{p}$ of $\mathscr{B}$ into the place $\boldsymbol{x}$ it occupies at time t. In order to state the fundamental laws of thermodynamics, it is convenient to introduce the scalar fields $\theta(\boldsymbol{x}, t)$, $e(\boldsymbol{x}, t)$, $s(\boldsymbol{x}, t)$ and $r(\boldsymbol{x}, t)$ defined over the deformed configuration $\boldsymbol{\varphi}(\Omega, t)$ of $\mathscr{B}$ which represent, respectively, the *temperature*, *specific internal energy*, *specific entropy* and the *density of heat production*. In addition, the tensor field $\boldsymbol{\sigma}(\boldsymbol{x}, t)$ will denote the *Cauchy stress* and the vector fields $\boldsymbol{b}(\boldsymbol{x}, t)$ and $\boldsymbol{q}(\boldsymbol{x}, t)$ will denote, respectively, the *body force* and *heat flux*.

Conservation of mass

The postulate of conservation of mass requires that:

$$\boxed{\dot{\rho} + \rho \, \mathrm{div}[\boldsymbol{v}] = 0 \, ,} \tag{1}$$

where ρ is the *mass density* field, $\boldsymbol{v}$ is the spatial *velocity* and $\mathrm{div}[\cdot]$ denotes the *spatial divergence* of $[\cdot]$.

Momentum balance

In its local form, the momentum balance can be expressed by the equations

$$\boxed{\begin{array}{ll} \left.\begin{array}{r} \operatorname{div}[\boldsymbol{\sigma}] + \rho\, \boldsymbol{b} = \rho\, \dot{\boldsymbol{v}} \\ \boldsymbol{\sigma}^T = \boldsymbol{\sigma} \end{array}\right\} & \text{in } \boldsymbol{\varphi}(\Omega) \\ \quad \boldsymbol{f} = \boldsymbol{\sigma}\, \boldsymbol{n} & \text{in } \boldsymbol{\varphi}(\partial\, \Omega) \end{array}} \tag{2}$$

where $\boldsymbol{n}$ is the outward normal vector to the deformed boundary $\boldsymbol{\varphi}(\partial\,\Omega)$ of $\mathscr{B}$, $\boldsymbol{f}$ is the boundary traction vector field and $\dot{\boldsymbol{v}}$ stands for the *acceleration* field. Equation $(2)_2$, which expresses the balance of angular momentum, is restricted to *nonpolar* media, i.e., stress couples are assumed absent.

The first principle

The first principle of thermodynamics, which postulates the conservation of energy, is explicitly expressed by the equation

$$\boxed{\rho\, \dot{e} = \boldsymbol{\sigma} : \boldsymbol{D} + \rho\, r - \operatorname{div}[\boldsymbol{q}]\,,} \tag{3}$$

where

$$\boldsymbol{D} = \tfrac{1}{2}(\nabla \boldsymbol{v} + \nabla \boldsymbol{v}^{\,T})$$

is the *rate of deformation* or *stretching* tensor, with $\nabla(\cdot)$ denoting the spatial gradient of $(\cdot)$,

The second principle

The second principle of thermodynamics postulates the irreversibility of entropy production. It is expressed by means of the inequality:

$$\rho\, \dot{s} + \operatorname{div}\left[\frac{\boldsymbol{q}}{\theta}\right] - \frac{\rho\, r}{\theta} \geq 0\,. \tag{4}$$

The Clausius-Duhem inequality

By combination of the first and second principles stated above, one easily obtains the fundamental inequality:

$$\rho\, \dot{s} + \operatorname{div}\left[\frac{\boldsymbol{q}}{\theta}\right] - \frac{1}{\theta}\left(\rho\, \dot{e} - \boldsymbol{\sigma} : \boldsymbol{D} + \operatorname{div}[\boldsymbol{q}]\right) \geq 0\,.$$

The introduction of the *specific free energy* ψ (also known as the *Helmholtz free energy per unit mass*) defined by

$$\psi := e - \theta\, s\,, \tag{5}$$

along with the identity

$$\operatorname{div}\left[\frac{\boldsymbol{q}}{\theta}\right] = \frac{1}{\theta} \operatorname{div}[\boldsymbol{q}] - \frac{1}{\theta^2}\, \boldsymbol{q} \cdot \nabla\theta\,,$$

into the fundamental inequality above results in the *Clausius-Duhem inequality*:

$$\boxed{\boldsymbol{\sigma}:\boldsymbol{D} - \rho\left(\dot{\psi} + s\,\dot{\theta}\right) - \frac{1}{\theta}\,\boldsymbol{q}\cdot\boldsymbol{g} \;\geq\; 0\,,} \tag{6}$$

where $\boldsymbol{g} := \nabla\theta$ is the temperature gradient.

2.2 Constitutive Axioms

The balance principles presented so far are valid for any continuum body. In order to distinguish between different types of material, a constitutive model must be introduced. This section presents three axioms which form the basis for the development of a rather general class of constitutive models of continua. In the present context, the principles laid down by those axioms must be followed regardless of the particular kind of material to be modelled.

Before going further, it is convenient to introduce the definitions of thermokinetic and calorodynamic processes (see Truesdell [111]). A *thermokinetic process* of $\mathscr{B}$ is the pair of fields

$$\boldsymbol{\varphi}(\boldsymbol{p}\,,t) \qquad \text{and} \qquad \theta(\boldsymbol{x},t)$$

A *calorodynamic process* is defined by the set

$$\{\boldsymbol{\sigma}(\boldsymbol{x},t),\, e(\boldsymbol{x},t),\, s(\boldsymbol{x},t),\, r(\boldsymbol{x},t),\, \boldsymbol{b}(\boldsymbol{x},t),\, \boldsymbol{q}(\boldsymbol{x},t)\}$$

of fields over $\mathscr{B}$ such that the balance of momentum, the first and the second principles of thermodynamics are satisfied.

Thermodynamic determinism

The *principle of thermodynamically compatible determinism* [111] postulates that "the history of the thermokinetic process to which a neighborhood of a point $\boldsymbol{p}$ of $\mathscr{B}$ has been subjected determines a calorodynamic process for $\mathscr{B}$ at $\boldsymbol{p}$". For a *simple material* the *local* history of $\boldsymbol{F}$, θ and $\boldsymbol{g}$ suffices to determine the history of the thermokinetic process for constitutive purposes. In that case, regarding the body force $\boldsymbol{b}$ and heat supply r as delivered, respectively, by the linear momentum balance $(2)_1$ and conservation of energy (3) and introducing the specific free energy, the principle of thermodynamic determinism implies the existence of functionals $\mathfrak{F}$, $\mathfrak{G}$, $\mathfrak{H}$ and $\mathfrak{I}$ such that, for a point $\boldsymbol{p}$,

$$\begin{aligned}\boldsymbol{\sigma}(t) &= \mathfrak{F}(\boldsymbol{F}^t,\theta^t,\boldsymbol{g}^t)\\ \psi(t) &= \mathfrak{G}(\boldsymbol{F}^t,\theta^t,\boldsymbol{g}^t)\\ s(t) &= \mathfrak{H}(\boldsymbol{F}^t,\theta^t,\boldsymbol{g}^t)\\ \boldsymbol{q}(t) &= \mathfrak{I}(\boldsymbol{F}^t,\theta^t,\boldsymbol{g}^t)\end{aligned} \tag{7}$$

and the Clausius-Duhem inequality (6) holds for every thermokinetic process of $\mathscr{B}$. The dependency on $\boldsymbol{p}$ is understood on both sides of (7) and $(\cdot)^t$ on the right hand sides denotes the *history* of $(\cdot)$ at $\boldsymbol{p}$ up to the present time t.

Material objectivity

Another important axiom of the constitutive theory is the *principle of material objectivity*. It states that "the material response is independent of the observer". The motion $\boldsymbol{\varphi}^*$ is related to the motion $\boldsymbol{\varphi}$ by a change in observer if

$$\boldsymbol{\varphi}^*(\boldsymbol{p}, t) = \boldsymbol{y}(t) + \boldsymbol{Q}(t)\ \boldsymbol{\varphi}(\boldsymbol{p}, t) \tag{8}$$

where $\boldsymbol{y}(t)$ is a point and $\boldsymbol{Q}(t)$ an orthogonal tensor. This relation corresponds to a rigid relative movement between the different observers and the deformation gradient corresponding to $\boldsymbol{\varphi}^*$ is given by

$$\boldsymbol{F}^* = \boldsymbol{Q}\,\boldsymbol{F} \tag{9}$$

Scalar fields (such as θ, ψ and s) are unaffected by a change in observer but the Cauchy stress $\boldsymbol{\sigma}(t)$, heat flux $\boldsymbol{q}(t)$ and the temperature gradient $\boldsymbol{g}(t)$ transform according to the rules

$$\begin{aligned} \boldsymbol{\sigma} &\longrightarrow \boldsymbol{\sigma}^* = \boldsymbol{Q}\,\boldsymbol{\sigma}\,\boldsymbol{Q}^T \\ \boldsymbol{q} &\longrightarrow \boldsymbol{q}^* = \boldsymbol{Q}\,\boldsymbol{q} \\ \boldsymbol{g} &\longrightarrow \boldsymbol{g}^* = \boldsymbol{Q}\,\boldsymbol{g} \end{aligned} \tag{10}$$

The principle of material objectivity places restrictions on the constitutive functionals (7). Formally, it requires that $\mathfrak{F}$, $\mathfrak{G}$, $\mathfrak{H}$ and $\mathfrak{I}$ satisfy

$$\begin{aligned} \boldsymbol{\sigma}^*(t) &= \mathfrak{F}\,(\boldsymbol{F}^{t*}, \theta^t, \boldsymbol{g}^{t*}) \\ \psi(t) &= \mathfrak{G}(\boldsymbol{F}^{t*}, \theta^t, \boldsymbol{g}^{t*}) \\ s(t) &= \mathfrak{H}(\boldsymbol{F}^{t*}, \theta^t, \boldsymbol{g}^{t*}) \\ \boldsymbol{q}^*(t) &= \mathfrak{I}\,(\boldsymbol{F}^{t*}, \theta^t, \boldsymbol{g}^{t*}) \end{aligned} \tag{11}$$

for any transformation of the form (9,10).

Material symmetry

The *symmetry group* of a material is the set of density preserving changes of reference configuration under which the material response functionals $\mathfrak{F}$, $\mathfrak{G}$, $\mathfrak{H}$ and $\mathfrak{I}$ are not affected. The symmetry group of a solid material is a subset of the orthogonal group $\mathscr{O}$. A subgroup $\mathscr{S}$ of $\mathscr{O}$ is said to be the symmetry group of the material defined by the constitutive functionals $\mathfrak{F}$, $\mathfrak{G}$, $\mathfrak{H}$ and $\mathfrak{I}$ if the relations

$$\begin{aligned} \mathfrak{F}\,(\boldsymbol{F}^t, \theta^t, \boldsymbol{g}^t) &= \mathfrak{F}\,([\boldsymbol{F}\boldsymbol{Q}]^t, \theta^t, \boldsymbol{g}^t) \\ \mathfrak{G}\,(\boldsymbol{F}^t, \theta^t, \boldsymbol{g}^t) &= \mathfrak{G}([\boldsymbol{F}\boldsymbol{Q}]^t, \theta^t, \boldsymbol{g}^t) \\ \mathfrak{H}\,(\boldsymbol{F}^t, \theta^t, \boldsymbol{g}^t) &= \mathfrak{H}([\boldsymbol{F}\boldsymbol{Q}]^t, \theta^t, \boldsymbol{g}^t) \\ \mathfrak{I}\,(\boldsymbol{F}^t, \theta^t, \boldsymbol{g}^t) &= \mathfrak{I}\,([\boldsymbol{F}\boldsymbol{Q}]^t, \theta^t, \boldsymbol{g}^t) \end{aligned} \tag{12}$$

hold for any *time independent* $\boldsymbol{Q} \in \mathscr{S}$. A solid is said to be *isotropic* if its symmetry group is the entire orthogonal group $\mathscr{O}$. In the development of any constitutive model, the constitutive functionals must comply with the restrictions imposed by the symmetries of the material in question.

2.3 Thermodynamics with Internal Variables

The constitutive equations (7) written in terms of functionals of the history of $\boldsymbol{F}$, θ and $\boldsymbol{g}$, in that format, are far too general to have practical utility in modelling real materials undergoing real a thermodynamical process. This is specially true if one has in mind the experimental identification of the constitutive functions and the solution of the corresponding boundary value problems. Therefore, it is imperative that simplifying assumptions are added to the general forms of the constitutive relations stated above.

An effective alternative to the general description based on history functionals is the adoption of the so called *thermodynamics with internal variables* The starting point of the thermodynamics with internal variables is the hypothesis that at any instant of a thermodynamical process the thermodynamic state (defined by $\boldsymbol{\sigma}$, ψ, s and $\boldsymbol{q}$) at a given point $\boldsymbol{p}$ can be completely determined by the knowledge of a finite number of *state variables*. The thermodynamic state depends only on the instantaneous value of the state variables and not on their past history. This very hypothesis is intimately connected with the assumption of existence of a (fictitious) state of thermodynamic equilibrium known as the *local accompanying state* [46] described by the current value of the state variables. In other words, every process is considered to be a succession of equilibrium states†.

From the mathematical point of view, the state variables can be seen as parameterizing the history of thermokinetic processes and replacing the complex constitutive description in terms of history functionals by an approximation involving a finite number of parameters. For the applications with which we are mostly concerned, it will be convenient to assume that at a certain time t, the thermodynamic state at a point is determined by the set

$$\{\boldsymbol{F},\, \theta,\, \boldsymbol{g},\, \boldsymbol{\alpha}\}$$

of state variables where $\boldsymbol{F}$, θ and $\boldsymbol{g}$ are the *instantaneous* values of deformation gradient, temperature and the temperature gradient and $\boldsymbol{\alpha}$ is a set:

$$\boldsymbol{\alpha} = \{\alpha_1, \alpha_2, ..., \alpha_k\}\,,$$

of k *internal variables* associated with dissipative mechanisms. Each element $\alpha_i \in \boldsymbol{\alpha}$ may be, in general, an entity of scalar, vectorial or tensorial nature.

Following the hypothesis above, the specific free energy is assumed to have the form‡

$$\psi \;=\; \psi(\boldsymbol{F},\, \theta,\, \boldsymbol{\alpha}) \tag{13}$$

so that its rate of change is given by

$$\dot{\psi} \;=\; \frac{\partial \psi}{\partial \boldsymbol{F}} : \dot{\boldsymbol{F}} \;+\; \frac{\partial \psi}{\partial \theta}\, \dot{\theta} \;+\; \frac{\partial \psi}{\partial \boldsymbol{\alpha}}\, \dot{\boldsymbol{\alpha}}\,. \tag{14}$$

In the last term on the r.h.s. of the expression above, the following convention has been adopted:

$$\frac{\partial \psi}{\partial \boldsymbol{\alpha}}\, \dot{\boldsymbol{\alpha}} \;=\; \sum_{i=1}^{k} \frac{\partial \psi}{\partial \alpha_i}\, \dot{\alpha}_i\,,$$

with the appropriate product implied. By introducing the connection:

$$\boldsymbol{\sigma} : \boldsymbol{D} = \frac{\rho}{\rho_0}\, \boldsymbol{P} : \dot{\boldsymbol{F}}\,, \tag{15}$$

where $\boldsymbol{P} := \det[\boldsymbol{F}]\, \boldsymbol{\sigma}\, \boldsymbol{F}^{-T}$ is the *first Piola-Kirchhoff* stress tensor and ρ_0 is the density in the reference configuration, one obtains for the Clausius-Duhem inequality:

$$\left(\boldsymbol{P} - \rho_0 \frac{\partial \psi}{\partial \boldsymbol{F}}\right) : \dot{\boldsymbol{F}} \;-\; \rho_0 \left(s + \frac{\partial \psi}{\partial \theta}\right) \dot{\theta} \;-\; \rho_0 \frac{\partial \psi}{\partial \boldsymbol{\alpha}}\, \dot{\boldsymbol{\alpha}} \;-\; \frac{\rho_0}{\rho\, \theta}\, \boldsymbol{q} \cdot \boldsymbol{g} \;\geq\; 0\,. \tag{16}$$

†Despite the success of the internal variable approach in numerous fields of continuum physics, phenomena induced by very fast external actions (at time scales compared to atomic vibrations) which involve states far from thermodynamic equilibrium are excluded from representation by internal variable theories.

‡The dependency of ψ on the temperature gradient is disregarded since it contradicts the second principle of thermodynamics (see reference [15]).

Since this inequality must hold for any thermokinetical process, a standard argument leads to the well known expressions:

$$\boldsymbol{P} = \rho_0 \frac{\partial \psi}{\partial \boldsymbol{F}}, \qquad s = -\frac{\partial \psi}{\partial \theta}, \tag{17}$$

for the first Piola-Kirchhoff stress, $\boldsymbol{P}$, and entropy, s.

Then, by defining

$$A_i := \rho_0 \frac{\partial \psi}{\partial \alpha_i} \tag{18}$$

as the *thermodynamical force* conjugate to each internal variable $\alpha_i \in \boldsymbol{\alpha}$, the Clausius-Duhem inequality can be rewritten as:

$$-A_i\, \dot{\alpha}_i - \frac{\rho_0}{\rho\,\theta}\, \boldsymbol{q} \cdot \boldsymbol{g} \geq 0\,, \tag{19}$$

with summation over i implied. For convenience, we shall define the set

$$\boldsymbol{A} = \{A_1, A_2, ..., A_k\}$$

of thermodynamical forces.

In order to completely characterize a constitutive model, complementary laws associated with the dissipative mechanisms are required. Namely, equations for the flux variables $\frac{1}{\theta}\boldsymbol{q}$ and $\dot{\alpha}$ must be derived. Recalling the principle of thermodynamic compatible determinism, the Clausius-Duhem inequality, now expressed by (19), must hold and that will evidently place restrictions on the possible constitutive relations. An effective way of ensuring that (19) is satisfied consists in postulating the existence of a scalar valued *dissipation* (pseudo) *potential* of the form

$$\Psi = \Psi(\boldsymbol{A}, \boldsymbol{g}) \tag{20}$$

possibly having the state variables as parameters, which is assumed to be convex with respect to each A_i and $\boldsymbol{g}$ and zero valued at the origin $\{\boldsymbol{A}, \boldsymbol{g}\} = \{\boldsymbol{0}, \boldsymbol{0}\}$. In addition, the hypothesis of *normal dissipativity* is introduced, i.e, the flux variables are assumed to be determined by the laws

$$\dot{\alpha}_i = -\frac{\partial \Psi}{\partial A_i}, \qquad \frac{1}{\theta}\boldsymbol{q} = -\frac{\partial \Psi}{\partial \boldsymbol{g}} \tag{21}$$

It should be noted that the constitutive description by means of convex potentials as described above is *not* a consequence of thermodynamics but, rather, a tool for formulating constitutive equations without violating thermodynamics. Indeed, it is obvious that a constitutive model defined by (13), (17) and (21) satisfies "a priori" the dissipation inequality. Some examples of constitutive models supported by experimental evidence which do not admit representation by means of dissipation potentials are discussed by Onat and Leckie [79].

2.3.1 The Phenomenological approach

Undoubtedly, the success of a constitutive model intended to describe the behaviour of a particular material lies in the choice of an appropriate set of internal variables. Since no plausible model will be general enough to describe the response of a material under all processes, the definition of the internal variables must be guided not only by the specific material in question but, rather, by the combined consideration of the material *and* the range of processes under which it will be analysed. In general, due to the difficulty involved in the identification of the underlying dissipative mechanisms, the choice of the appropriate set of internal variables is somewhat subtle and will obviously be biased by the preference of the investigator.

Basically, constitutive modelling by means of internal variables relies either on a micromechanical or on a phenomenological approach. The micromechanical approach involves the determination of mechanisms and related variables at the atomic, molecular or crystalline levels. In general, these variables are discrete quantities and their continuum (macroscopic) counterparts are determined by means of homogenization techniques. The phenomenological approach, on the other hand, bypasses the need for measurements of microscopic quantities. It is based on the study of the response of the *representative volume element*, i.e., the element of matter large enough to be regarded as a continuum. The internal variables in this case will be directly associated with the dissipative behaviour observed at the *macroscopic* level in terms of continuum quantities (such as strain, stress, temperature, etc.). Despite the macroscopic nature of theories derived on the basis of the phenomenological methodology, it should be expected that "good" phenomenological internal variables will be somehow related to the underlying microscopic dissipation mechanisms.

The phenomenological approach to irreversible thermodynamics has been particularly successful in the field of solid mechanics. Numerous well established models of solids, such as classical elastoplasticity [39], have been developed on a purely phenomenological basis providing evidence of how powerful such an approach to irreversible thermodynamics can be when the major concern is the description of the essentially macroscopic behaviour. Direct application of phenomenological thermodynamics with internal variables will be discussed in Sections 6 and 7, where the formulation of continuum models for internal damage in rubbers and metals undergoing finite strains is addressed.

3 PHYSICAL ASPECTS OF INTERNAL DAMAGE IN SOLIDS

Basically, internal damage can be defined by the presence and evolution of cracks and cavities at the microscopic level which may, eventually, lead to a complete loss of load carrying capability of the material. The characterization of internal damage as well as the scale at which it occurs in common engineering materials depend crucially upon the specific type of material considered. In addition, for the same material, damage evolution may take place triggered by very different physical mechanisms which depend fundamentally on the type, rate of loading, temperature as well as environmental factors such as exposure to corrosive substances or nuclear radiation. Therefore, rather than the material alone, the material-process-environment triad must be considered in the study of internal damage. To illustrate the diversity of phenomena which may be involved in the process of internal degradation of solids, some basic physical mechanisms underlying damage evolution in metals and rubbery polymers are outlined below.

3.1 Metals

In metals, the primary mechanisms which characterize the phenomenon of mechanical degradation may be divided into two distinct classes: *brittle* and *ductile* damage. Brittle damaging occurs mainly in the form of cleavage of crystallographic planes in the presence of negligible inelastic deformations. This behaviour is observed for many metallic materials usually at low temperatures. At high temperatures, brittle damage can also be observed associated with creep processes. In that case, the decohesion of interatomic bonds is concentrated at grain boundaries. At low stresses they are accompanied by relatively small strains. Ductile damage, on the other hand, is normally associated with the presence of large plastic deformations in the neighbourhood of crystalline defects. The decohesion of interatomic bonds is initiated at the boundary interface of inclusions, precipitates and particles of alloy

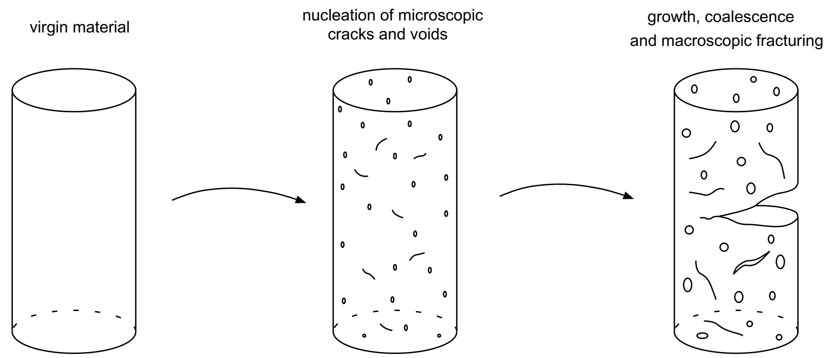

Figure 1. Ductile damage in metals. Schematic illustration

elements leading to the formation of microscopic cracks and cavities. Further evolution of local plastic deformation may cause the cavities to coalesce resulting in final rupture. This mechanism is schematically illustrated in Figure 1. For most metallic materials, the damage behaviour is a combination of brittle and ductile response and the contribution of each mode is, to a significant extent, dependent on the temperature, loading rate, etc.

Another important mode of material deterioration in metals is *fatigue damage*. It is normally observed in mechanical components subjected to a large number of load and/or temperature cycles. Although fatigue damage occurs at overall stress amplitudes below the plastic yield limit, the nucleation of microcracks is attributed to the accumulation of dislocations observed in connection with cyclic plastic deformation due to stress concentration near microscopic defects. A large number of complex interactive physical mechanisms take place from the nucleation of cracks to the complete failure of the material and the understanding of fatigue degradation processes in metals remains a challenging issue in the field of materials science. Some of the most important mechanisms of material damage are described by Engel and Klingele [24].

3.2 Rubbery Polymers

Rubbery polymers are widely employed in engineering applications. Essentially, these materials are made of long cross-linked molecular chains which differ radically from the structure of crystalline metals [2]. Although rubbery polymers exhibit a behaviour which, under a variety of circumstances, may be regarded as purely elastic, damaging does take place due to straining and/or thermal activation. The internal degradation in this case is mainly characterized by the rupture of molecular bonds concentrated in regions containing impurities and defects. In general, the damage response of such materials is predominantly *brittle* (in the sense that permanent deformations are small).

Filled rubbers are particularly susceptible to internal damaging. Those materials are obtained by addition of a filler in order to enhance the strength properties of the original rubber. In that case, even at very small overall straining, damage can occur in the form of progressive breakage of shorter polymer chains attached between filler particles. This phenomenon, as described by Bueche [7], is schematically illustrated in Figure 2.

4 CONTINUUM DAMAGE MECHANICS

Since the pioneering work by Kachanov [44], a considerable body of the literature on applied mechanics has been devoted to the formulation of constitutive models to describe internal

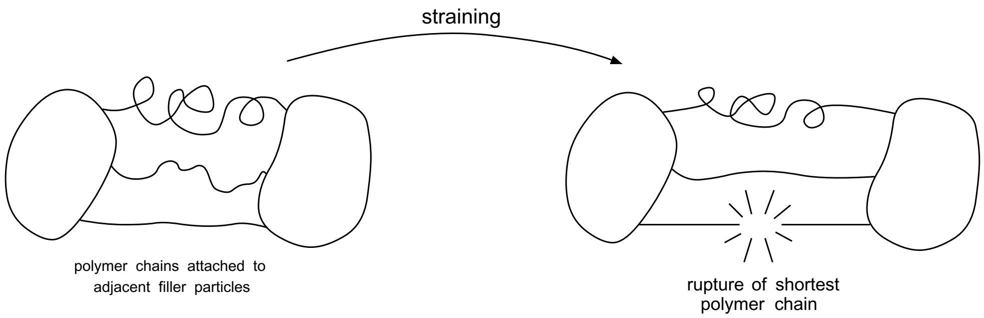

Figure 2. Damage in filled rubbery polymers. Schematic representation

degradation of solids within the framework of continuum mechanics. After over two decades of uninterrupted development, significant progress has been achieved and such theories have merged into what is currently known as *Continuum Damage Mechanics* (*CDM* for short). The concepts underlying the development of *CDM* models along with a brief historical review of this new branch of continuum mechanics are presented below.

In the previous section, some basic microscopic mechanisms associated with internal damage evolution in solids have been reviewed. It is clear that the underlying phenomena which characterize damage are essentially different from those characterizing deformation. While damage manifests itself in the form of irreversible rupture of atomic bonds, deformation can be associated with reversible variations of interatomic spacing (in purely elastic processes) and movement and accumulation of dislocations (in permanent deformations of metals). Therefore, it should be expected that in order to describe the internal degradation of solids within the framework of the continuum mechanics theory, new variables intrinsically connected with the internal damage process will have to be introduced in addition to the standard variables (such as the strain tensor, plastic strain, etc.) employed in the description of deformation. In this context, we shall refer to as a *Continuum Damage Mechanics Model* any continuum constitutive model which features special internal variables representing, directly or indirectly, the density and/or distribution of the microscopic defects that characterize damage.

4.1 Original Development. Creep-damage

The first continuum damage mechanics model was proposed by Kachanov [44] in 1958. Without a clear physical meaning for damage, Kachanov introduced a scalar internal variable to model the creep failure of metals under *uniaxial* loads. A physical significance for the damage variable was given later by Rabotnov [86] who proposed the reduction of the cross-sectional area due to microcracking as a suitable measure of the state of internal damage. In this context, denoting respectively by A and A_0 the effective load bearing areas of the virgin and damaged materials, the damage variable D was introduced as

$$D = \frac{A - A_0}{A} \tag{22}$$

with $D = 0$ corresponding to the virgin material and $D = 1$ representing the total loss of load bearing capacity[§]. In order to describe the strain rate increase which characterizes tertiary

[§]Kachanov has in fact used the *material continuity* or *integrity*, $\Omega = 1 - D$, as the variable associated with the internal deterioration process.

creep, Kachanov has replaced the observed uniaxial stress σ with the *effective stress*

$$\sigma^* := \frac{\sigma}{1-D} \tag{23}$$

in the standard Norton Law.

Since Kachanov-Rabotnov's original developments, it did not take long before the concept of internal damage variable was extended to three-dimensional situations by a number of authors. Leckie and Hayhurst [51] have exploited the idea of the effective load bearing area reduction as a scalar measure of material deterioration to define a model for creep-rupture under multiaxial stresses. The theories derived later by Chaboche [9, 10, 11] and Murakami and Ohno [71] deserve special mention. Based on rigorous thermodynamic foundations, Chaboche has proposed a phenomenological theory for creep-damage in which, as a consequence of the hypothesis of *strain equivalence*, the damage variable appears as a *fourth order* non-symmetric tensor in the most general anisotropic case. In the theory derived by Murakami and Ohno, the anisotropic damage variable is represented by a *second rank* symmetric tensor. In that case, the definition of the damage variable follows from the extension of the effective stress concept to three dimensions by means of the hypothesis of the existence of a mechanically equivalent *fictitious undamaged configuration*. Murakami's fictitious undamaged configuration concept was later extended to describe general anisotropic states of internal damage in solids with particular reference to the analysis of elastic-brittle materials [69]. Still within the context of creep-rupture, Saanouni *et al.* [91] have used a non-local formulation to predict the nucleation and growth of cracks.

4.2 Other Theories

Despite its origin in the description of creep rupture, Continuum Damage Mechanics was shown to provide an effective tool to describe the phenomenon of internal degradation in other areas of solid mechanics.

Within the theory of elastoplasticity, Gurson [32] has proposed a model for ductile damage where the (scalar) damage variable is obtained from the consideration of microscopic spherical voids embedded in an elastoplastic matrix. Gurson's void growth theory was shown to be particularly suitable for the representation of the behaviour of porous materials. A scalar damage variable was also considered by Lemaitre [54] in the definition of a purely phenomenological model for ductile isotropic damage in metals. By appealing to the hypothesis of strain equivalence, which states that *"the deformation behaviour of the damaged material is represented by the constitutive laws of the virgin material with the true stress replaced by the effective stress"*, the standard definition of damage in terms of reduction of the (neither well defined nor easily measurable) load carrying area is replaced in Lemaitre's model by the reduction of the Young's modulus in the ideally isotropic case. Thus, with E_0 and E denoting respectively the Young's moduli of the virgin and damaged materials, the damage variable (22) is redefined as:

$$D = \frac{E - E_0}{E} \,. \tag{24}$$

Lemaitre's ductile damage theory was further elaborated in references [56, 57] and ageing effects were later incorporated by Marquis and Lemaitre [63]. Based on the the concept of *energy* equivalence (as opposed to Lemaitre's strain equivalence) another model for elastoplastic damage worth mentioning was proposed by Cordebois and Sidoroff [19]. The damage variable in this case takes the form of a second order tensor under general anisotropy. Also within the theory of elastoplasticity, Simo and Ju [97] proposed a framework for the development of (generally anisotropic) strain- and stress-based damage models. In this case, Lemaitre's hypothesis of strain equivalence and its dual *hypothesis of stress equivalence* are used, respectively, in the formulation of models in stress and strain spaces. Application of the proposed framework was made in the description of brittle damage in concrete.

A somewhat different approach was followed by Krajčinović and Fonseka [50] (see also Fonseka and Krajčinović [26]) in the derivation of a continuum damage theory for brittle materials. Assuming that damage in this case is characterized mainly by planar penny-shaped microcracks, a *vectorial* variable was proposed as the local measure of internal deterioration. Later, in reference [47], the model was endowed with a thermodynamical structure and extended to account for ductile damage. Further developments were introduced in reference [48] with the distinction between active and passive systems of microcracks. Other vectorial models are described by Kachanov [45] and Mitchell [65].

Continuum damage mechanics has also been applied to the description of fatigue processes. Janson [43] developed a continuum theory to model fatigue crack propagation which showed good agreement with simple uniaxial experiments. A general formulation incorporating low and high-cycle fatigue as well as creep-fatigue interaction at arbitrary stress states is presented by Lemaitre [58]. Further discussion on these models is provided by Chaboche [12] and Lemaitre and Chaboche [60]. In order to model the effects of fatigue, the evolution law for the damage variable is usually formulated in terms of a differential equation which relates damage growth with the mean stress, maximum stress and number of cycles.

4.3 Remarks on the Nature of the Damage Variable

As pointed out in Section 2.3.1, the appropriate definition of internal variables associated with a specific phenomenon is one of the most important factors determining the success or failure of the continuum model intended for its description.

Due to the diversity of forms in which internal damage manifests itself at the microscopic level, the definition of adequate damage variables is certainly not an easy task. During the development of *CDM*, briefly reviewed above, variables of different mathematical nature (scalars, vectors, tensors) possessing different physical meaning (reduction of load bearing area, loss of stiffness, distribution of voids) have been employed in the description of damage under various circumstances.

4.3.1 Physical significance

With regard to the physical significance of damage variables, it is convenient to separate the *CDM* theories into two main categories: *micromechanical* and *phenomenological* models.

In micromechanical models, the damage internal variable must represent some average of the microscopic defects which characterize the state of internal deterioration. Despite the physical appeal of internal variables such as the reduction of load bearing area, as suggested by Rabotnov [86], or distribution of microcracks, as adopted by Krajčinović [47, 48] in his vectorial model, the enormous amount of bookkeeping required in conjunction with the serious difficulties involved in the experimental identification of damaged states and evolution laws preclude most micromechanical theories from practical applications. This is especially true if the final objective is the analysis of large scale problems for engineering design purposes.

Phenomenological damage variables, on the other hand, can be defined on the basis of the influence that internal degradation exerts on the macroscopic properties of the material. In particular, properties such as the elastic moduli [18, 42], yield stress, density and electric resistance can be strongly affected by the presence of damage in the form of microscopic cavities. Needless to say, the measurement of such quantities is in general far easier than the determination of the geometry or distribution of micro-defects. Based on such concepts and supported by experimental evidence, the class of models presented by

Lemaitre and Chaboche [60] rely mostly on the use of the degradation of the elastic moduli as the macroscopic measure of damage. In its simplest form, i.e., under ideally isotropic conditions, the damage variable is the scalar defined by expression (24). A similar definition for the damage variable is employed by Cordebois and Sidoroff [19]. A model relying on the volume changes due to void growth as a measure of internal degradation is described by Gelin and Mrichcha [28].

Current methods of experimental identification of damage, comprising direct as well as indirect techniques, are described in detail by Lemaitre and Dufailly [61]. Such techniques range from the direct observation of microscopic pictures to the measurement of the degradation of the elastic moduli by means of ultrasonic emissions and micro-hardness tests. The potentialities and limitations of both micromechanical and phenomenological approaches to damage mechanics are discussed by Basista *et al.* [3]. In the present state of development of *CDM* it has been verified that, in general, the loss of microscopic information resulting from a phenomenological approach is compensated by the gain in analytical, experimental and computational tractability of the model.

4.3.2 Mathematical representation

In view of the many possibilities with regard to the choice of the damage internal variable, Leckie and Onat [52] have shown that the distribution of voids on the grain boundaries can be mathematically represented by a sequence of *even* rank irreducible tensors. Although this result has been obtained in the context of creep-damage theories, Onat [78] has later shown that the same phenomenological representation for the damage variable applies to general micro-cracked continua regardless of the underlying deformation processes.

The conclusions drawn by Onat were based on the use of averaging techniques to transform the distribution of micro-defects into a mathematically well defined continuum measure of damage. In spite of the micromechanic nature of Onat's argument, it is desirable that, in purely phenomenological theories, such restriction on the mathematical representation of the internal variables related to damage be also satisfied. This is obviously an expression of the requirement, stated in Section 2.3.1, that "good" phenomenological internal variables be somehow connected to the underlying physical mechanisms they are intended to represent.

5 THE NUMERICAL SIMULATION OF FINITE STRAIN PROBLEMS

Let us assume that a particular material model has been defined within the framework of continuum thermodynamics with internal variables. The next step towards the prediction of the behaviour of this material in situations of practical interest is the establishment of the corresponding mathematical problem along with a numerical framework capable of producing accurate solutions over a wide range of conditions. In this section, a general framework for the efficient *implicit* finite element simulation of large strain problems involving dissipative materials is described. Its basic ingredients comprise:

- An algorithm for numerical integration of the rate constitutive equations, leading to an incremental version of the original constitutive law;

- A finite element discretization of the corresponding incremental (equilibrium) boundary value problem stated in the *spatial* configuration; and

- Use of the full Newton-Raphson scheme for iterative solution of the resulting nonlinear algebraic systems of equations to be solved at each increment.

5.1 Numerical Integration Algorithm. The Incremental Constitutive Law

Given a generic dissipative material model, the solution of the evolution problem defined by the corresponding rate constitutive equations and a set of initial conditions (initial values for the internal variables) is usually not known for complex deformation (and temperature) paths. Therefore, the use of an appropriate numerical algorithm for integration of the rate constitutive equations is an essential requirement in the numerical simulation of problems of interest. The choice of a particular technique for integration of a constitutive law will be obviously dependent on the characteristics of the model considered. In general, algorithms for integration of rate constitutive equations are obtained by adopting some kind of time (or pseudo-time) discretization along with some hypothesis on the deformation path between adjacent time stations. Within the context of the purely mechanical theory, considering the time increment $[t_n, t_{n+1}]$ and given the set $\boldsymbol{\alpha}_n$ of internal variables at t_n, the deformation gradient $\boldsymbol{F}_{n+1}$ at time t_{n+1} must determine the stress $\boldsymbol{\sigma}_{n+1}$ uniquely through the integration algorithm. One may regard this requirement as the numerical counterpart of the principle of thermodynamic determinism stated in Section 2.2. Such an algorithm defines an (approximate) incremental constitutive functional, $\hat{\boldsymbol{\sigma}}$, for the stress tensor:

$$\boxed{\boldsymbol{\sigma}_{n+1} = \hat{\boldsymbol{\sigma}}\,(\boldsymbol{\alpha}_n, \boldsymbol{F}_{n+1})\,,} \tag{25}$$

which is path-*independent* within one increment and whose outcome $\boldsymbol{\sigma}_{n+1}$ must tend to the exact solution to the actual evolution problem with vanishingly small deformation increments. Equivalently, an algorithmic functional, $\hat{\boldsymbol{\tau}}$ for the Kirchhoff stress, $\boldsymbol{\tau}$, can be defined:

$$\boxed{\boldsymbol{\tau}_{n+1} = \hat{\boldsymbol{\tau}}\,(\boldsymbol{\alpha}_n, \boldsymbol{F}_{n+1}) \;=\; \det[\boldsymbol{F}_{n+1}]\,\hat{\boldsymbol{\sigma}}\,(\boldsymbol{\alpha}_n, \boldsymbol{F}_{n+1})\,.} \tag{26}$$

Within the small strain elasto-plasticity theory, procedures such as the classical return mappings [80, 96] provide concrete examples of numerical integration schemes for path-dependent constitutive laws.

Another important aspect concerning integration algorithms for general dissipative materials is the requirement of *incremental objectivity*. As a numerical version of the principle of material objectivity stated in Section 2.2, incremental objectivity demands that the algorithmic constitutive law be invariant with respect to rigid rotations. If this principle is violated, an undesirable dependency of stresses on rotations exits and meaningless results may be obtained with the application of the integration algorithm. In cases such as hypo-elastic formulations (including hypo-elastic based finite elasto-plasticity), incremental objectivity may not be easily imposed [90] and, in some instances, its enforcement may result in rather cumbersome algorithms. We remark, however, that since the finite strain damage models described in this paper are based on hyperelasticity, i.e., the stress tensor is the derivative of a (history dependent) free energy potential, incremental objectivity can be trivially ensured.

5.2 The Incremental Boundary Value Problem. Finite Element Discretization

The strong form of the momentum balance has been stated in Section 2 by expression (2). Its weak counterpart, the *principle of virtual work*, is the starting point of displacement based finite element solution procedures [4, 75, 120, 121]. Consider the body $\mathscr{B}$ subjected to body forces in its interior Ω and surface tractions prescribed on the portion $\partial\Omega_f$ of its boundary $\partial\Omega$. In addition, let the motion be prescribed by a given function $\bar{\boldsymbol{\varphi}}$ on the remaining portion $\partial\Omega_u$ of $\partial\Omega$:

$$\boldsymbol{\varphi}_t(\boldsymbol{p}) = \bar{\boldsymbol{\varphi}}_t(\boldsymbol{p}) \qquad \forall \;\; \boldsymbol{p} \in \partial\Omega_u \,,$$

so that at a time t the set of *kinematically admissible* deformations of $\mathscr{B}$ (often referred to as the *trial solution* set) is defined by:

$$\mathscr{K} = \{\boldsymbol{\varphi}_t(\cdot) \mid \boldsymbol{\varphi} = \bar{\boldsymbol{\varphi}} \quad \text{on} \quad \partial\Omega_u\} \,,$$

where, for simplicity, the notation $\boldsymbol{\varphi}_t(\cdot) \equiv \boldsymbol{\varphi}(\cdot, t)$ has been used.

The principle of virtual work, in its *spatial* version, states that $\mathscr{B}$ is in equilibrium at t if and only if its Cauchy stress field, $\boldsymbol{\sigma}$, satisfies the variational equation:

$$G(\boldsymbol{\varphi}, \boldsymbol{\eta}) := \int_{\varphi_t(\Omega)} (\boldsymbol{\sigma} : \nabla\boldsymbol{\eta} - \boldsymbol{b} \cdot \boldsymbol{\eta}) \, dv - \int_{\varphi_t(\partial\Omega_f)} \boldsymbol{f} \cdot \boldsymbol{\eta} \, da = 0 \qquad \forall \; \boldsymbol{\eta} \in \mathscr{V}, \tag{27}$$

where $\boldsymbol{b}$ and $\boldsymbol{f}$ are respectively the body force and surface traction fields referred to the current configuration and $\mathscr{V}$ is the space of virtual displacements of $\mathscr{B}$

$$\mathscr{V} = \{\boldsymbol{\eta} : \boldsymbol{\varphi}_t(\Omega) \rightarrow \mathscr{U} \mid \boldsymbol{\eta} = \boldsymbol{0} \quad \text{on} \quad \partial\Omega_u\} \,.$$

With the introduction of the algorithmic constitutive function $\hat{\boldsymbol{\sigma}}$ in the weak form of the equilibrium, the *incremental* boundary value problem can be stated as follows: "Given the set $\boldsymbol{\alpha}_n$ of internal variables at time t_n and given the body forces and surface traction fields at t_{n+1}, find a kinematically admissible configuration $\boldsymbol{\varphi}_{n+1}(\Omega)$ such that

$$\int_{\varphi_{n+1}(\Omega)} (\hat{\boldsymbol{\sigma}} : \nabla\boldsymbol{\eta} - \boldsymbol{b}_{n+1} \cdot \boldsymbol{\eta}) \, dv - \int_{\varphi_{n+1}(\partial\Omega_f)} \boldsymbol{f}_{n+1} \cdot \boldsymbol{\eta} \, da = 0 \qquad \forall \;\; \boldsymbol{\eta} \in \mathscr{V} \tag{28}$$

holds". Note that due to the introduction of $\hat{\boldsymbol{\sigma}}$, the constitutive relations are satisfied only approximately.

Approximations to the incremental boundary value problem above can be obtained by replacing the functional sets $\mathscr{V}$ and $\mathscr{K}$ with discrete subsets generated through a finite element discretization on the configuration $\boldsymbol{\varphi}_{n+1}(\Omega)$ (references [4, 75, 120, 121] provide a detailed account of the finite element method). Thus, the discrete counterpart of (28) reads: Find a vector $\mathbb{U}_{n+1}$ of global nodal displacements at t_{n+1} such that the following non-linear algebraic system:

$$\mathbb{R}(\mathbb{U}_{n+1}) := \;\; \mathbb{F}^{\text{INT}} - \;\; \mathbb{F}^{\text{EXT}} \; = \; 0 \tag{29}$$

is satisfied, where $\mathbb{F}^{\text{INT}}_{n+1}$ and $\mathbb{F}^{\text{EXT}}_{n+1}$ are, respectively, internal and external global force vectors resulting from the assemblage of the element vectors

$$\begin{aligned} \mathbb{F}^{\text{INT}}_e &= \int_{\varphi(\Omega^e)} \mathbb{B}^T \, \{\boldsymbol{\sigma}_{n+1}\} \, dv \\ \mathbb{F}^{\text{EXT}}_e &= \int_{\varphi(\Omega^e)} \mathbb{N}^T \, \boldsymbol{b}_{n+1} \, dv + \int_{\varphi(\partial\Omega^e \bigcap \partial\Omega_f)} \mathbb{N}^T \, \boldsymbol{f}_{n+1} \, da \end{aligned} \tag{30}$$

with $\mathbb{B}$ and $\mathbb{N}$ being, respectively, the standard discrete symmetric gradient operator and the interpolation matrix of the element e in the configuration defined by $\mathbb{U}_{n+1}$ and $\{\boldsymbol{\sigma}_{n+1}\}$ is the vector containing the Cauchy stress components delivered by the algorithmic function (25).

5.3 The Newton-Raphson Scheme. Linearization

An effective and efficient way to find a solution $\mathbb{U}_{n+1}$ to the non-linear system above is to use the standard Newton-Raphson iterative procedure, obtained from the exact linearization of (29). During a typical Newton-Raphson iteration (k), the following linear system is solved for the iterative displacement $\Delta\mathbb{U}^{(k)}$:

$$\mathbb{K}(\mathbb{U}_{n+1}^{(k)})\,[\Delta\mathbb{U}^{(k)}] = -\mathbb{R}(\mathbb{U}_{n+1}^{(k)})\,, \tag{31}$$

and the new guess for the solution $\mathbb{U}_{n+1}$ is updated as:

$$\mathbb{U}_{n+1}^{(k+1)} = \mathbb{U}_{n+1}^{(k)} + \Delta\mathbb{U}^{(k)}\,. \tag{32}$$

The *tangent stiffness* $\mathbb{K}$ is defined by the directional derivative formula:

$$\mathbb{K}(\mathbb{U})\,[\Delta\mathbb{U}] = \left.\frac{d}{d\varepsilon}\right|_{\varepsilon=0} \mathbb{R}(\mathbb{U} + \varepsilon\,\Delta\mathbb{U})\;. \tag{33}$$

If the external loads are assumed independent of $\mathbb{U}$, then the element tangent stiffness is given by the formula:

$$\mathbb{K}_e = \int_{\varphi(\Omega_e)} \mathbb{G}^T\,[\boldsymbol{a}]\,\mathbb{G}\,dv \tag{34}$$

where $\mathbb{G}$ is the standard discrete spatial gradient operator and $[\boldsymbol{a}]$ denotes the matrix form of the *spatial elasticity tensor* given, in cartesian components, by:

$$a_{ijkl} = \frac{1}{J}\,\frac{\partial\tau_{ij}}{\partial F_{kq}}\,F_{lq} - \sigma_{il}\,\delta_{jk} \tag{35}$$

Note that, since the Kirchhoff stress tensor is the outcome of the algorithmic function (26), its derivative appearing in the expression above is, in fact, the derivative

$$\left.\frac{\partial\hat{\boldsymbol{\tau}}}{\partial\boldsymbol{F}}\right|_{\boldsymbol{\alpha}_n,\boldsymbol{F}_{n+1}^{(k)}}$$

of the *incremental* (rather than the actual) constitutive functional. The need for such a consistency between the tangent stiffness and the local algorithm for integration of the rate constitutive equations was first addressed by Nagtegaal[72], in the context of hypo-elastic based finite strain plasticity, and later formalised by Simo and Taylor [99] who, within the context of infinitesimal J_2 elastoplasticity, derived a closed formula for the so-called *consistent tangent operators* associated to classical return mapping schemes. It is worth mentioning here that whenever more complex integration algorithms and/or material models (particularly in the finite strain range) are involved, consistent tangent operators may not be easily derived. Issues associated with consistent linearization aspects in finite multiplicative plasticity are discussed in detail by Simo [95] and Cuitiño and Ortiz[21]. We remark that, within the present framework, consistent linearization is regarded as a crucial aspect of the formulations presented and will receive particular attention in Sections 6 and 7 where models for elastic and elasto-plastic damage are described. The asymptotically quadratic rates of convergence resulting from the exact linearization of the field equations more than justify the importance given to such an issue in this paper.

6 FINITE STRAIN ELASTIC DAMAGE: FILLED POLYMERS

One of the main drawbacks of hyperelastic material models [77] in the description of the behaviour of filled polymers arises from the fact that such theories are not able to predict the strain induced loss of stiffness to which these materials are subject. This dissipative phenomenon, known as the *Mullins effect* originates from internal damage in the form of debonding of polymer chains attached between filler particles as alluded to in Section 3. In a uniaxial cyclic extension experiment, the Mullins effect is phenomenologically characterized by the degradation of the elastic properties at strain levels below the maximum strain attained in the history of deformation [67, 108]. This fact is schematically illustrated in Figure 3. During a typical (quasi-static) uniaxial experiment with a filled polymer, the initial stretching up to ε_1 follows the stress-strain path A with unloading from ε_1 via curve B. A subsequent stretching up to ε_2 will follow path BC. Then, unloading will follow curve D with a third stretch occurring via DE and so on. It is obvious that a hyperelastic theory cannot represent such a behaviour.

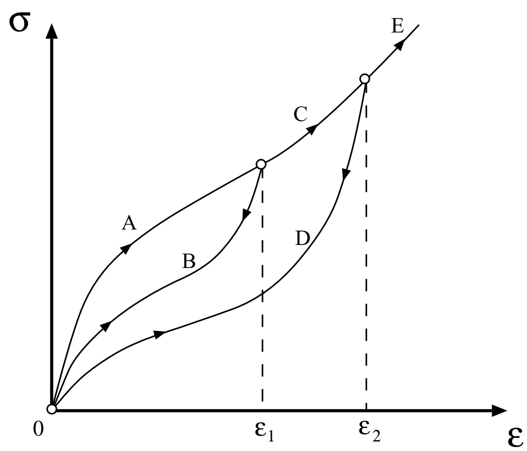

Figure 3. Mullins effect. Schematic representation

The microscopic mechanisms which give rise to the Mullins effect have long been the subject of intensive research by a number of authors [7, 8, 67]. Nevertheless, only few attempts seem to have been made to formulate continuum models suitable for incorporation into numerical procedures for simulation of large scale problems. As a pioneering development in this direction, we cite Simo [94] who, invoking the principle of strain equivalence [60], introduced continuous damage in a three-dimensional model for finite-strain viscoelasticity. More recently Govindjee and Simo [30] derived a continuum rate-independent theory for carbon black-filled rubbers based on micromechanical considerations. The model was later extended to account for viscous effects [31].

In this section, a simple three-dimensional rate-independent continuum damage model for highly filled polymers is described. The model has been recently proposed by de Souza Neto *et al.* [105] and provides an effective framework for the simulation of the Mullins effect in large scale problems. Based on thermodynamics with internal variables, it generalizes to three dimensions the 1-D phenomenological theory proposed by Gurtin and Francis [34] to describe internal damage in highly filled solid propellants. Viscous effects are not accounted for so that the applicability of the model is limited to very slow and very fast processes – conditions met in a vast number of engineering applications.

From the experimental standpoint, the theory is relatively simple. Since it relies on purely phenomenological considerations, the identification of the material parameters does not require the measurement of any microscopic quantities. Indeed, the behaviour of the material at damaged states is characterized by one single curve determined from loading/unloading experiments.

On the computational side, due to the particular features of the model, the algorithm for integration of the constitutive equations assumes an extremely simple format allowing for a straightforward computational implementation.

6.1 The Gurtin and Francis 1-D Model

Focusing attention on uniaxial tension experiments with highly filled solid propellants, Gurtin and Francis [34] proposed a simple unidimensional theory in which the current state of internal damage is characterized by the maximum axial strain, ε^m, attained up to the present time t

$$\varepsilon^m(t) \quad = \quad \max_{0 \le s \le t} \{\varepsilon(s)\} \tag{36}$$

In their model, Gurtin and Francis adopted a constitutive equation expressing the uniaxial stress, σ, as a function of the current strain and damage:

$$\sigma = \bar{f}(\zeta)\, \bar{g}(\varepsilon^m)\,, \tag{37}$$

where $\bar{g}$ is called the *virgin curve* and ζ is the *relative strain*

$$\zeta := \frac{\varepsilon}{\varepsilon^m}\,. \tag{38}$$

The function $\bar{f}(\zeta)$, named the *master damage curve*, defines the loss of stiffness experienced by highly filled polymers at strain levels below the maximum previously attained strain ε^m. It satisfies

$$\bar{f}(1) = 1\,, \tag{39}$$

so that when the maximum strain occurs at the current time ($\varepsilon^m = \varepsilon$), the uniaxial stress is given by

$$\sigma = \bar{g}(\varepsilon^m)\,, \tag{40}$$

that is, the function $\bar{g}$ defines the uniaxial stress-strain curve obtained from an experiment with monotonically increasing/decreasing strain. In Figure 3, the function $\bar{g}$ is identified with the path ACE.

To completely characterize the material parameters for this model, one needs, in addition to the virgin curve, to determine the master damage curve $\bar{f}(\zeta)$. This curve is obtained from loading/unloading experiments [34].

6.2 The 3-D Rate-independent Model for Elastic Damage

Based on similar concepts employed by Gurtin and Francis in the definition of their unidimensional theory, the finite strain elastic damage model proposed in reference [105] is applicable to general three-dimensional situations. The 3-D model is described below in detail.

Let us consider a general isotropic hyperelastic material governed by the free energy ψ^0 described as a function of the principal stretches $\{\lambda_{(1)}, \lambda_{(2)}, \lambda_{(3)}\}$ [77]. The principal Kirchhoff stresses are expressed as

$$\tau_{(i)} = \lambda_{(i)}\, \frac{\partial \psi^0}{\partial \lambda_{(i)}} =: g_i(\lambda_{(1)}, \lambda_{(2)}, \lambda_{(3)})\,. \tag{41}$$

The crucial idea in the definition of the 3-D model for elastic damage, is to assume that the constitutive equation (41) above is valid *only* upon loading. In addition, similarly to (37), a general stress constitutive function of the form:

$$\tau_{(i)} = f(\xi)\ g_i(\lambda_{(1)}, \lambda_{(2)}, \lambda_{(3)}) \tag{42}$$

is postulated. Analogously to its one-dimensional counterpart $\bar{f}$, the function $f : [0,1] \rightarrow [0,1]$ is expressed in terms of a, as yet not defined, three-dimensional measure of relative strain ξ. It also satisfies

$$f(1) = 1\,. \tag{43}$$

6.2.1 The damage variable – damage evolution

Generalizing the notion of maximum attained strain used by Francis and Gurtin [see expression (36)], the new internal variable, D, is defined as a history recording parameter for the phenomenon of material damage in general 3-D situations:

$$D(t) \;=\; \max_{0\,\leq\, s\,\leq\, t} \{\psi^0(s)\}\,, \tag{44}$$

and the uniaxial *relative strain*, ζ, defined in (38) may be immediately generalized as:

$$\xi := \frac{\psi^0}{D}\,. \tag{45}$$

REMARK 6.1 By its very definition, the damage variable D can only increase whenever there is damage evolution. Therefore, the phenomenon of recovery of elastic modulus observed when filled rubbers are exposed to higher temperatures is excluded from representation by the present model. □

Following the definition (44) for the damage internal variable, a straightforward analogy between classical elastoplasticity and the present model for elastic damage may be established by introducing the *damage surface* (*cf.* yield surface) in the space of principal stretches:

$$\Phi(\lambda_{(1)}, \lambda_{(2)}, \lambda_{(3)}, D) := \psi^0(\lambda_{(1)}, \lambda_{(2)}, \lambda_{(3)}) - D = 0\,. \tag{46}$$

For a fixed D, the damage surface delimits the region of the principal stretches space in which the behaviour of the material is purely elastic without evolution of damage. Correspondingly, the criterion for damage evolution (loading/unloading) can be characterized by means of the complementarity law

$$\Phi \leq 0 \qquad\qquad \dot{D} \geq 0 \qquad\qquad \dot{D}\Phi = 0 \tag{47}$$

For convenience, the three-dimensional constitutive model for elastic damage is summarized in Box 6.1.

6.2.2 Thermodynamical aspects

Alternatively to the arguments above, the present theory for damage in filled polymers can be obtained by postulating the existence of a specific free energy of the form

$$\psi(\lambda_{(1)}, \lambda_{(2)}, \lambda_{(3)}, D) \;=\; \psi(\psi^0(\lambda_{(1)}, \lambda_{(2)}, \lambda_{(3)}), D) \;=\; \int_0^{\psi^0} f\left(\frac{\kappa}{D}\right)\, d\kappa \tag{48}$$

(i) Damage variable

$$D(t) \;=\; \max_{0\,\leq\,s\,\leq\,t} \{\psi^0(s)\}$$

(ii) Stress constitutive relation

$$\tau_{(i)} = f(\xi)\;\lambda_{(i)}\,\frac{\partial\psi^0}{\partial\lambda_{(i)}}$$

$$\xi := \frac{\psi^0}{D}$$

(iii) Damage surface

$$\Phi(\lambda_{(1)},\lambda_{(2)},\lambda_{(3)},D) := \psi^0(\lambda_{(1)},\lambda_{(2)},\lambda_{(3)}) - D = 0$$

(iv) Loading/unloading criterion

$$\Phi \leq 0 \qquad\qquad \dot{D} \geq 0 \qquad\qquad \dot{D}\Phi = 0$$

Box 6.1 3-D constitutive model for damage in highly filled polymers

recalling that ψ^0 is the free energy of the hypothetical hyperelastic (non-damageable) rubber which governs the behaviour of the material upon loading and f is the master damage function. Indeed, with the free energy defined by (48), the principal Kirchhoff stresses are given by

$$\tau_{(i)} \;=\; \lambda_{(i)}\,\frac{\partial\psi}{\partial\lambda_{(i)}} \;=\; f\left(\frac{\psi^0}{D}\right)\;\lambda_{(i)}\,\frac{\partial\psi^0}{\partial\lambda_{(i)}} \tag{49}$$

which is precisely the constitutive function (42). Note that within the elastic domain, i.e., in the region of the principal stretches space delimited by the damage surface (with fixed D), the expression above defines an essentially *hyperelastic* behaviour characterized by the strain energy function ψ.

REMARK 6.2 A definition similar to (44) for the damage variable in conjunction with the concept of equivalent stress described in Section 4.1 has been employed by Simo [94] in the derivation of a three-dimensional model for viscoelastic damage. In the present theory, the damage internal variable, D, represents the maximum energy supplied to the material during the entire history of deformation. Part of this energy has been stored in the form of elastic potential energy, ψ, and will be recovered during elastic unloading following constitutive relation (42). The remaining energy has been consumed by micromechanisms related to the internal degradation of the material. □

REMARK 6.3 With the free energy defined by (48) and disregarding effects of thermal dissipation, the Clausius-Duhem inequality (19) reads:

$$-\frac{\partial\psi}{\partial D}\;\dot{D} \;\geq\; 0\,. \tag{50}$$

It has been shown in reference [105] that a sufficient condition for (50) to hold is that f be a differentiable and non-decreasing function of ξ. □

REMARK 6.4 If ψ^0 is convex in $\lambda_{(i)}$, some restrictions on the master damage function f can guarantee that this convexity is transferred to the potential ψ. Indeed, it has been proved in reference [105] that if the master damage function $f(\xi)$ is a non-negative and non-decreasing function of ξ, then the free energy ψ is also convex in $\lambda_{(i)}$. □

6.3 Integration Algorithm

The damage variable for the present model has been chosen as the maximum value of $\psi^0(\lambda_{(1)}, \lambda_{(2)}, \lambda_{(3)})$ recorded during the history of deformation. This choice allows the formulation of an extremely simple algorithm for numerical integration of the constitutive equations of the model based solely on a hypothesis on the deformation path between adjacent time stations. The algorithm is described in the following.

Assume that within a generic (pseudo) time increment $[t_n, t_{n+1}]$ the evolution of the deformation is such that the value of ψ^0 is either monotonically increasing or monotonically decreasing. Under such conditions, the update formula for D is immediately given as follows:

1. Given the damage variable D_n at t_n and the stretches $\lambda_{(i)_{n+1}}$ at time t_{n+1}, compute $\psi^0_{n+1} := \psi^0(\lambda_{(1)_{n+1}}, \lambda_{(2)_{n+1}}, \lambda_{(3)_{n+1}})$.
2. If $\psi^0_{n+1} > D_n$ then there is damage evolution and D is updated as $D_{n+1} := \psi^0_{n+1}$. Otherwise, no damage evolution takes place within the increment and $D_{n+1} := D_n$.

With the current value, D_{n+1}, of the damage internal variable at hand, the principal Kirchhoff stresses are updated as:

$$\tau_{(i)_{n+1}} := f(\xi_{n+1})\, \lambda_{(i)_{n+1}} \left. \frac{\partial \psi^0}{\partial \lambda_{(i)}} \right|_{n+1}, \tag{51}$$

with the relative strain ξ_{n+1} computed as:

$$\xi_{n+1} := \frac{\psi^0_{n+1}}{D_{n+1}}. \tag{52}$$

The Kirchhoff stress tensor can then be assembled by referring to the spectral decomposition formula:

$$\boldsymbol{\tau}_{n+1} = \sum_{i=1}^{3} \tau_{(i)_{n+1}}\, \boldsymbol{M}_{(i)_{n+1}}, \tag{53}$$

where, due to the assumed material isotropy, the *eigenprojection tensors*, $\boldsymbol{M}_{(i)_{n+1}}$, of $\boldsymbol{\tau}_{n+1}$ coincide with the eigenprojections of the current *left Cauchy-Green* strain tensor:

$$\boldsymbol{B}_{n+1} = \sum_{i=1}^{3} b_{(i)_{n+1}}\, \boldsymbol{M}_{(i)_{n+1}}, \tag{54}$$

whose eigenvalues $b_{(i)\,n+1}$ are given by:

$$b_{(i)\,n+1} = \lambda^2_{(i)_{n+1}}. \tag{55}$$

The overall integration algorithm for the elastic damage constitutive equations is conveniently described in Box 6.2 where the typical time interval $[t_n, t_{n+1}]$ is considered. It defines an incremental constitutive rule that can be written in the form:

$$\boldsymbol{\tau}_{n+1} = \tilde{\boldsymbol{\tau}}(D_n, \boldsymbol{B}_{n+1}(\boldsymbol{F}_{n+1})) = \hat{\boldsymbol{\tau}}(D_n, \boldsymbol{F}_{n+1}), \tag{56}$$

(i) Given the deformation gradient $\boldsymbol{F}_{n+1}$, compute

$$\boldsymbol{B}_{n+1} := \boldsymbol{F}_{n+1}\boldsymbol{F}^T_{n+1}$$

(ii) Perform the spectral decomposition of $\boldsymbol{B}_{n+1}$ (using closed formulae given in the appendix)

$$\boldsymbol{B}_{n+1} = \sum_{i=1}^{n_{\dim}} b_{(i)\,n+1}\ \boldsymbol{M}_{(i)\,n+1}$$

compute principal stretches

$$\lambda_{(i)\,n+1} := \sqrt{b_{(i)\,n+1}}$$

and

$$\psi^0_{n+1} := \psi^0(\lambda_{(1)\,n+1}, \lambda_{(2)\,n+1}, \lambda_{(3)\,n+1})$$

(iii) Check evolution of damage and update D

IF $\Phi^{\text{trial}}_{n+1} := \psi^0_{n+1} - D_n \leq 0$ THEN

no damage evolution $\Rightarrow D_{n+1} := D_n$

ELSE

damage evolution $\Rightarrow D_{n+1} := \psi^0_{n+1}$

ENDIF

(iv) Update principal Kirchhoff stresses

$$\xi := \frac{\psi^0_{n+1}}{D_{n+1}}$$

$$\tau_{(i)\,n+1} := f(\xi)\ \lambda_{(i)\,n+1}\ \frac{\partial\psi^0}{\partial\lambda_{(i)}}\bigg|_{n+1}$$

(v) Compute the Kirchhoff stress tensor

$$\boldsymbol{\tau}_{n+1} := \sum_{i=1}^{n_{\dim}} \tau_{(i)\,n+1}\ \boldsymbol{M}_{(i)\,n+1}$$

Box 6.2 Algorithm for integration of elastic damage constitutive equations

i.e, it is a particular case of the general algorithmic functional (26).

REMARK 6.5 In contrast to integration procedures usually employed in classical elasto-plasticity the algorithm described in Box 6.2 is *exact*, independently of the increment size, provided that in the actual deformation path, the material is being loaded or unloaded monotonically between times t_n and t_{n+1}. □

REMARK 6.6 Note that, effectively, only the principal stresses are updated by the algorithm of Box 6.2. The eigenprojections of the Kirchhoff stress tensor coincide with the eigenprojections of $\boldsymbol{B}$ and do not depend on damage evolution so that, from (56), we may write:

$$\tilde{\boldsymbol{\tau}}(D_n, \boldsymbol{B}) = \sum_{i=1}^{3} \tau_{(i)}\, \boldsymbol{M}_{(i)}(\boldsymbol{B}) \ . \tag{57}$$

where, for each principal direction i, the corresponding principal Kirchhoff stress, $\tau_{(i)}$, is obtained from an algorithmic (scalar) function:

$$\begin{aligned} \tau_{(i)} &:= \tilde{\tau}(D_n, b_{(i)}, b_{(j)}, b_{(k)}) \\ &= \bar{\tau}(D_n, \lambda_{(i)}, \lambda_{(j)}, \lambda_{(k)}) \ = \ f(\xi(D_n, \lambda_{(1)}, \lambda_{(2)}, \lambda_{(3)}))\ g_i(\lambda_{(1)}, \lambda_{(2)}, \lambda_{(3)}) \end{aligned} \tag{58}$$

with (i,j,k) being cyclic permutations of $(1,2,3)$. Expressions (57,58) define an isotropic tensor-valued function of $\boldsymbol{B}$ – a member of the class of general isotropic functions described in Section A.1 of the Appendix. The computation of $\boldsymbol{\tau}_{n+1}$ in the integration algorithm of Box 6.2 corresponds to a specialization of the general procedure of Box A.1, in which $\boldsymbol{Y} \equiv \tilde{\boldsymbol{\tau}}$, $y \equiv \tilde{\tau}$ and $\boldsymbol{X} \equiv \boldsymbol{B}$ □

6.4 The Spatial Tangent Modulus

Having defined the continuum constitutive law for finite elastic damage along with an appropriate numerical integration algorithm, the incorporation of the model within the numerical framework of Section 5 is accomplished with the derivation of a closed formula for the *consistent* spatial tangent modulus given by expression (35). In the present context, the expression:

$$\mathsf{a}_{ijkl} \ = \ \frac{1}{J}\left(2\ \left[\frac{\partial \tilde{\boldsymbol{\tau}}}{\partial \boldsymbol{B}}\right]_{ijkm} B_{ml} \ - \ \tau_{il}\,\delta_{jk}\right)\,, \tag{59}$$

is found more convenient for derivation of the closed form of the tangent modulus. It can be obtained from (35) by a straightforward manipulation. For notational convenience, the subscript $n+1$, where applicable, is ommited in (59) and in what follows.

Since, as pointed out in Remark 6.6, $\tilde{\boldsymbol{\tau}}$ belongs to the class of isotropic functions discussed in Section A.1, the derivative $\partial\tilde{\boldsymbol{\tau}}/\partial\boldsymbol{B}$ can be computed in closed form by following the procedure described in Box A.3. In this case, the partial derivatives $\partial\tau_{(i)}/\partial b_{(l)}$, that will take part in the assemblage of $\partial\tilde{\boldsymbol{\tau}}/\partial\boldsymbol{B}$ [refer to item (ii) of Box A.3], are given by:

$$\frac{\partial \tau_{(i)}}{\partial b_{(l)}} = \frac{1}{2\,\lambda_{(l)}}\ \frac{\partial}{\partial \lambda_{(l)}}\bar{\tau}(D_n, \lambda_{(i)}, \lambda_{(j)}, \lambda_{(k)})\,. \tag{60}$$

Note that if f and g in expression (42) are differentiable and the strain state is inside the elastic domain, i.e., $\psi^0 < D$, then the algorithmic function $\tilde{\boldsymbol{\tau}}$ is differentiable. On the other hand, if the strain state lies on the damage surface (defined by $\psi^0 = D$) then loading which rejoins the virgin curve as well as unloading via the softer stress-strain path are possible and $\tilde{\boldsymbol{\tau}}$ is not differentiable in general. In this case, the term $\partial\tau_{(i)}/\partial b_{(l)}$ above is rather a *one-sided derivative* [89]. Therefore, $\partial\tau_{(i)}/\partial b_{(l)}$ will be computed as follows:

- If the strain state is inside the elastic domain or if it lies on the damage surface and *unloading* is assumed to occur, then

$$\begin{aligned} \frac{\partial \tau_{(i)}}{\partial b_{(l)}} \ &= \ \frac{1}{2\,\lambda_{(l)}}\left[f(\xi)\ \frac{\partial g_i}{\partial \lambda_{(l)}} + g_i\ \frac{\partial f}{\partial \lambda_{(l)}}\right] \\ &= \ \frac{1}{2\,\lambda_{(l)}}\left[f(\xi)\ \frac{\partial g_i}{\partial \lambda_{(l)}} + \frac{f'\ g_i^2}{D\ \lambda_{(l)}}\right]\ , \end{aligned} \tag{61}$$

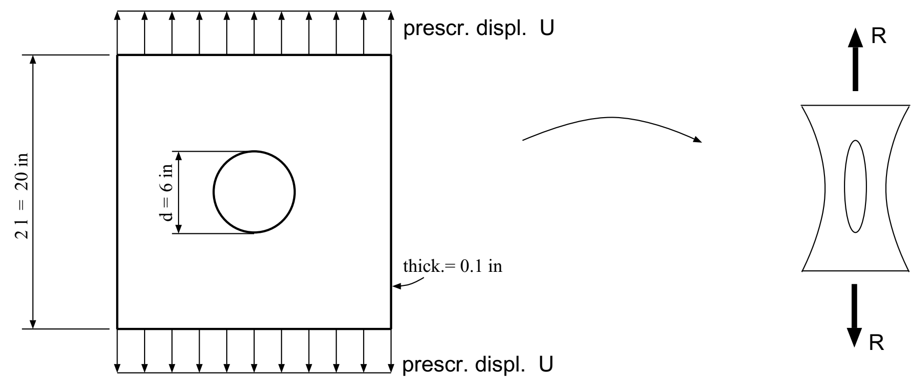

Figure 4. Square perforated sheet. Geometry and boundary conditions

- Otherwise, damage evolution occurs and $f(\xi) = 1$ and $\frac{\partial f}{\partial \lambda_{(l)}} = 0$ so that

$$\frac{\partial \tau_{(i)}}{\partial b_{(l)}} = \frac{1}{2\,\lambda_{(l)}} \frac{\partial g_i}{\partial \lambda_{(l)}} . \tag{62}$$

Finally, with $\partial \tilde{\boldsymbol{\tau}}/\partial \boldsymbol{B}$ at hand, the spatial tangent modulus $\boldsymbol{a}$ is computed exactly from expression (59).

6.5 Numerical Examples

EXAMPLE 6.1 Square perforated sheet subjected to cyclic stretching. The problem consists of a square sheet containing a circular hole subjected to cyclic stretching. The geometry and the boundary conditions are shown in Figure 4. The particular form of the function ψ^0 employed to describe the stress-strain behaviour during loading [see expressions (41,42)] corresponds to a neo-hookean material, i.e,

$$\psi^0 = C(\lambda_{(1)}^2 + \lambda_{(2)}^2 + \lambda_{(3)}^2 - 3)\,, \tag{63}$$

with the constant C chosen as

$$C = 135\,\text{psi}\,.$$

The master damage curve adopted is plotted in Figure 5. The non-dimensional load factor γ is defined as

$$\gamma = \frac{U}{l}$$

and the cyclic load with increasing amplitude shown in Figure 6.a is applied to the sheet. Due to the symmetry of the problem, only one quarter of the sheet is considered in the finite element simulation. A mesh of 660 three-noded triangular membrane elements is used to discretize the sheet. As a result of the plane stress assumption associated with the membrane elements, incompressibility can be enforced in a trivial manner by the appropriate update of the membrane thickness as described in reference [106]. The finite element meshes corresponding to the initial configuration ($\gamma = 0$) and to the configuration defined by $\gamma = 1$ are shown in Figure 7.

The reaction force R on the restrained edge of the sheet obtained in the computations is plotted in Figure 6.b. It shows the influence of the Mullins effect on the global behaviour of the structure. In an uniaxial cyclic test (see reference [105]), the material parameters

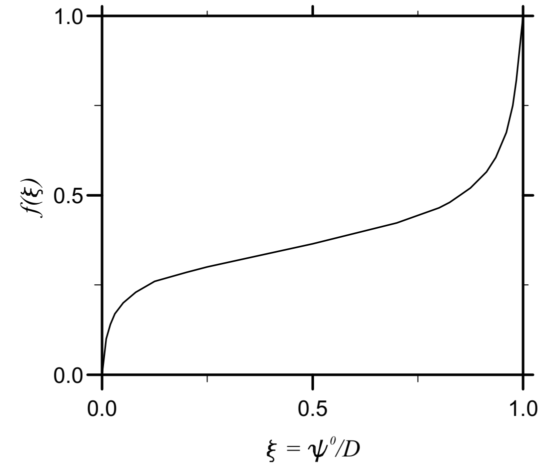

Figure 5. Master damage curve

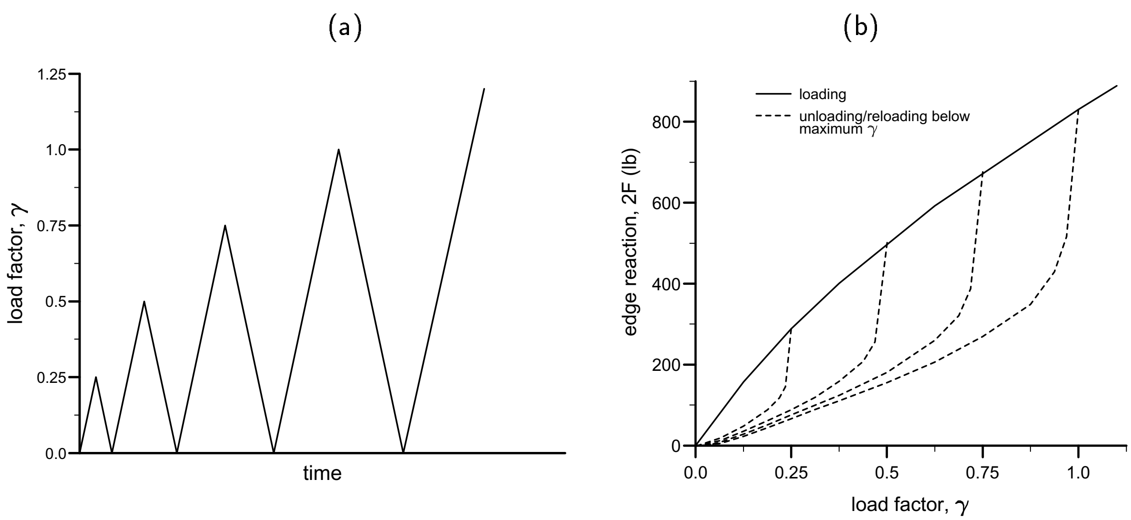

Figure 6. Square perforated sheet. (a) Load history, and (b) Reaction on restrained edge

chosen in this example produce a good qualitative agreement with the experiment with a highly filled solid propellant (TP-H1011-86% solids) reported by Gurtin and Francis [34]. As far as the specific material tested by Gurtin and Francis [34] is concerned, the strain levels attained in this simulation are unrealistic (the specimen tested by Gurtin and Francis debonded at 11.22% of axial strain). Nevertheless, the present example serves as an illustration of the effectiveness of the adopted framework in simulating the Mullins effect in large scale problems. Due to the use of the exact tangent modulus, shown in Section 6.4, asymptotically quadratic rates of convergence are achieved in the Newton-Raphson procedure employed to solve the implicit incremental boundary value problem. This fact is illustrated in Figure 8. Figure 8.a shows the convergence table of the Newton-Raphson algorithm during a typical load step. In the graph of Figure 8.b we plot, for two typical load increments, the residual norm $||r_k||$, of iteration k, against the residual norm $||r_{k+1}||$ of the subsequent iteration $k+1$. Note that the slope 2:1 indicated in the graph corresponds to quadratic convergence. We remark that, considering the case of monotonic

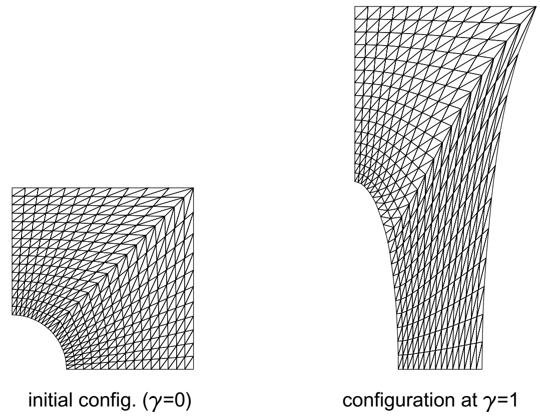

Figure 7. Square perforated sheet. Finite element discretization

(a)

N-R algorithm. Convergence table

k	$\|\|r_k\|\|$
1	0.160066E+01
2	0.207231E-01
3	0.664932E-05
4	0.309021E-11

(b)

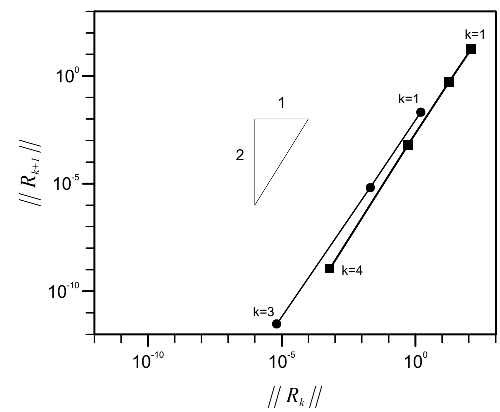

Figure 8. Square perforated sheet. Newton-Raphson behaviour. (a) Convergence table: $||r_k|| \rightarrow$ norm of residual at iteration k. (b) Graph of convergence

loading and starting from the initial configuration with the virgin sheet, the configuration defined by $\gamma = 1$ may be reached in 2 load increments only.

EXAMPLE 6.2 Inflation and deflation of a damageable rubber balloon. In this problem, we consider the simulation of a spherical membrane made of a damageable rubber inflated and deflated under internal pressure. A mesh of 675 isoparametric three-noded membrane elements, shown in Figure 11.a, discretizes one octant of the sphere with symmetry boundary conditions imposed along the edges. The function ψ^0 is chosen as the three-term Ogden strain energy function [76, 77], i.e.,

$$\psi^0(\lambda_{(1)}, \lambda_{(2)}, \lambda_{(3)}) = \sum_{p=1}^{3} \frac{\mu_p}{\alpha_p} \left(\lambda_{(1)}^{\alpha_p} + \lambda_{(2)}^{\alpha_p} + \lambda_{(3)}^{\alpha_p} - 3\right), \tag{64}$$

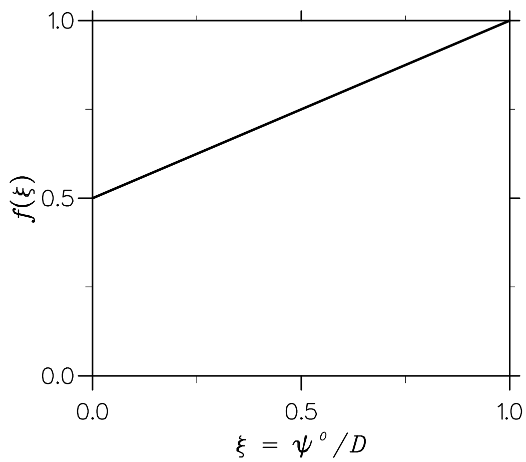

Figure 9. Rubber balloon. Master damage curve

where the material constants are taken as:

$$\begin{array}{lll} \alpha_1 = 1.3 & \alpha_2 = 5.0 & \alpha_3 = -2.0 \\ \mu_1 = 6.3 & \mu_2 = 0.012 & \mu_3 = -0.1\text{kg/cm}^2 . \end{array}$$

The master damage curve adopted is shown in Figure 9.

Within the context of hyperelasticity, the stability in this problem is known to be crucially dependent on the specific strain energy function adopted [76, 5]. Pressure instability is detected, in particular, for the three-term Ogden function, ψ^0, with the constants chosen above which describes the behaviour of the material upon continuous loading. For this reason, the *arc-length method* [20] will be employed in conjunction with the Newton-Raphson algorithm to allow equilibrium to be found beyond the instability point. For convenience, we define the normalized internal pressure,

$$p^* = \frac{p\, r_0}{2\, t_0} ,$$

and the expansion ratio of the balloon,

$$\lambda = \frac{r}{r_0} ,$$

where r and r_0 are, respectively, the current and initial radii of the balloon, t_0 is the initial thickness of the rubber membrane and p is the current internal pressure. By means of arc-length control, starting from the initial configuration ($\lambda = 1$), the internal pressure is applied gradually and the membrane is inflated until the configuration defined by $\lambda = 5.182$ (point A of Figure 11.b) is reached. At this stage, the load is reversed and the balloon is deflated returning to its initial configuration. Figure 10 shows the convergence behaviour of the Newton-Raphson scheme during a typical increment. As in the previous example, a quadratic rate of convergence is observed. The pressure-expansion curve obtained in the simulation is presented in Figure 11.b. Since inflation occurs under monotonically increasing circumferential stretching, the inflation branch of the pressure-expansion diagram corresponds to the behaviour governed by the strain energy function ψ^0. Indeed, it matches nearly exactly the analytical hyperelastic solution obtained by Ogden [76, 77]. The deflation branch of the curve shows clearly the softening effect of material damage at the global

N-R algorithm. Convergence table

k	$\|\|r_k\|\|$
1	0.182859E+01
2	0.778551E-04
3	0.371668E-09

Figure 10. Rubber balloon. Convergence table: $||r_k|| \rightarrow$ norm of residual at iteration k

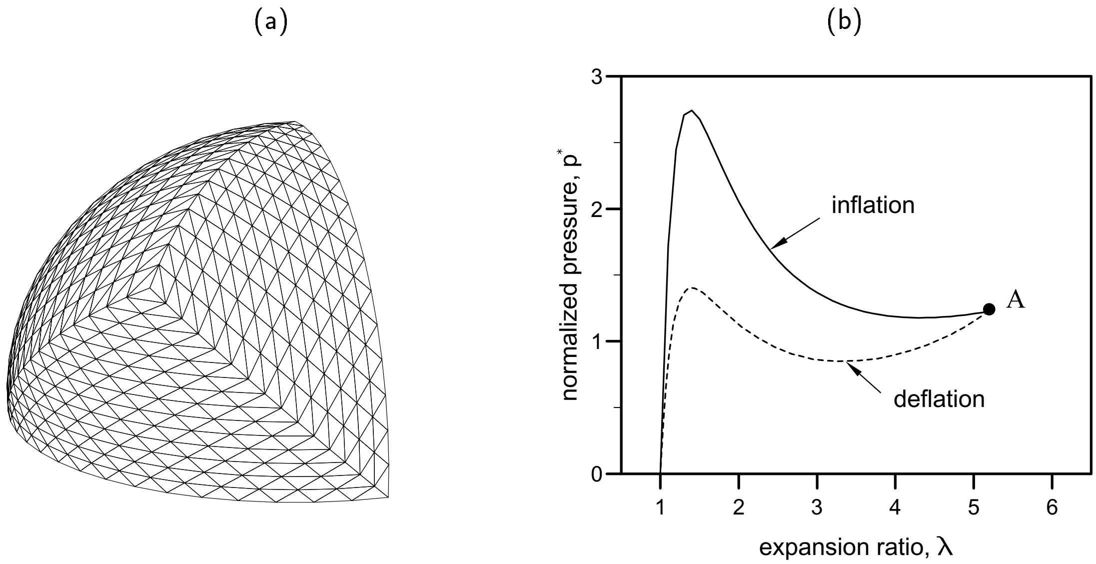

Figure 11. Rubber balloon. (a) Finite element mesh, and (b) Pressure-Expansion diagram

level. Interestingly, the pressure-expansion curve obtained in the present simulation has a good qualitative agreement with the balloon inflation experiment discussed by Beatty [5] which, obviously, can not be reproduced by hyperelastic theories. In the experiment studied by Beatty [5], a residual circumferential strain was observed after complete deflation of the balloon (null pressure). Incorporation of this effect would require the consideration of additional internal variables leading to a theory which allows for description of irreversible deformations with possible inclusion of viscous effects. The representation of such a phenomenon is outside the scope of the present model.

7 FINITE ELASTO-PLASTIC DAMAGE: DUCTILE METALS

Over the past fifteen years or so, considerable effort has been concentrated on modelling the gradual internal deterioration which frequently precipitates the occurence of macroscopic failure in ductile metals undergoing plastic deformations.

Early attempts to describe this phenomenon have been mainly restricted to micromechanical analysis (see references [64] and [88]) and the inherent complexity of such an approach has prevented the inclusion of the effect of internal damage in the analysis of large scale problems of industrial interest. More recently, as pointed out in Section 4, with the rapid progress of continuum damage mechanics, several continuum damage models to

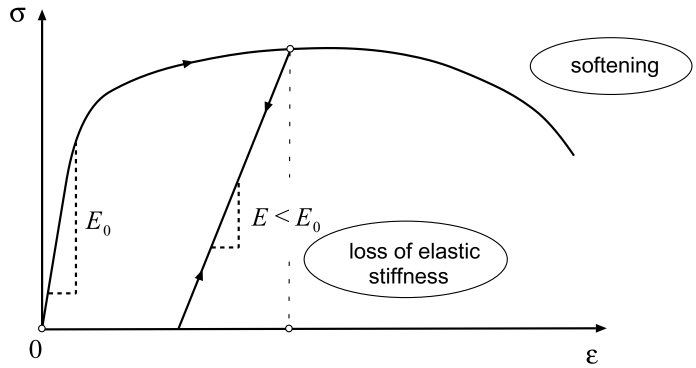

Figure 12. Ductile damage in metals. Phenomenological effects

describe internal degradation in ductile materials have been developed [19, 27, 28, 32, 56, 97, 109, 119].

Such interest in the development of continuum theories for ductile damage may be attributed in part to the increasing industrial requirement for models capable of simulating the behaviour of metals under conditions in which internal deterioration plays a significant role. A typical situation in which the effects of internal damage are not negligible occurs frequently in metal forming processes [54, 74]. As experimentally observed for many ductile metals [56, 57], the nucleation and growth of voids and microcracks which accompany large plastic flow causes considerable reduction of the elastic modulus as well as material softening and is highly influenced by the triaxiality of the stress state (a schematic illustration of typical uniaxial tests with ductile metals is shown in Figure 12). Close to material failure, such mechanisms have a dominant effect on the behaviour of metals and classical elasto-plasticity theories frequently fail to predict forming limits with reasonable accuracy Also, in many circumstances, due to the strong coupling between internal damage and macroscopic material properties, it is well accepted that "a posteriori" damage calculations based on the assumption of damage localization (as described by Lemaitre in reference [59]) would lead to inaccurate results. In such cases, the formulation of finite strain coupled elasto-plasticity-damage models seems to be an essential step towards more accurate predictions of failure in industrial forming operations.

This section describes in detail the extension, to the finite strain range, of two well known (small strain) ductile damage theories: The model proposed by Lemaitre [57] and the model introduced by Gurson [32]. Despite their original formulation within the realm of infinitesimal deformations, important phenomena such as the loss of elastic stiffness predicted by Lemaitre's theory, the increasing plastic compressibility predicted by Gurson's model and the general material softening predicted by both theories as a result of damage growth, are also experimentally observed in the finite strain range. This makes extensions of these theories strong candidates for the phenomenological description of ductile damage at large strains. Obviously, it is desirable that the most important features of the infinitesimal models be preserved by their finite strain extensions.

The extensions to Lemaitre's and Gurson's damage models described in this section have been introduced, respectively by de Souza Neto *et al.* [103, 104, 100] and Steinmann *et al.* [107]. They rely on a general framework for the treatment of multiplicative large strain elasto-plasticity based on the hyperelastic description of the reversible behaviour and the use of a logarithmic strain measure. This framework has been successfully employed by a number of authors [25, 84, 85, 95, 98, 118] in the formulation of finite strain elasto-plasticity models and has been enjoying growing acceptance within the computational mechanics community over the last few years. Some features of the present approach to large strain plasticity are particularly important. For instance, it carries over *exactly*, to the finite range, the (in)compressiblity of the plastic flow associated with pressure (in)sensitive criteria in small strain theory. In addition, by employing an exponential map in the discretization of the plastic flow rule, an algorithm for integration of the constitutive equations is obtained in which the essential stress updating procedure retains the same format of the classical return mapping algorithms of the infinitesimal theory with all finite strain effects appearing only at the kinematic level. The general form of the resulting spatial consistent tangent moduli is particularly simple and allows a relatively straightforward computational implementation within the context of the implicit finite element scheme described in Section 5. Another important property is that, due to the hyperelastic description of reversible phenomena, the algorithm satisfies trivially the requirement of incremental objectivity.

7.1 Hyperelastic Based Finite Strain Elasto-plasticity

7.1.1 Multiplicative elasto-plasticity kinematics

The main hypothesis underlying the present approach to finite strain elasto-plastic damage is the *multiplicative split* of the deformation gradient, $\boldsymbol{F}$, into elastic and plastic parts [53, 73]:

$$\boldsymbol{F} = \boldsymbol{F}^e \boldsymbol{F}^p . \tag{65}$$

This assumption, firstly introduced by Lee [53], admits the existence of a local unstressed *intermediate configuration* obtained from the current configuration by a purely elastic unloading of the neighbourhood of a material point as schematically shown in Figure 13. Due to its suitability for the computational treatment of finite strain elasto-plasticity, the hypothesis of multiplicative decomposition is currently widely employed in the computational mechanics literature [21, 25, 66, 85, 93, 95].

Following the multiplicative split of $\boldsymbol{F}$, the *velocity gradient*, $\boldsymbol{L} \equiv \dot{\boldsymbol{F}}\,\boldsymbol{F}^{-1}$, can be decomposed additively as:

$$\boldsymbol{L} = \boldsymbol{L}^e + \boldsymbol{L}^p , \tag{66}$$

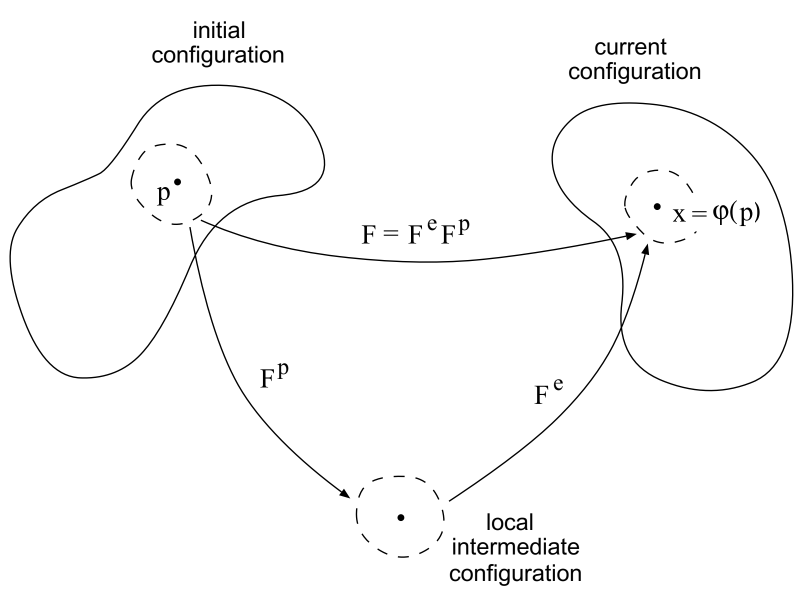

Figure 13. Multiplicative decomposition of the deformation gradient

where $\boldsymbol{L}^e$ and $\boldsymbol{L}^p$ are, respectively, the elastic and plastic contributions [73] *defined* by

$$\boldsymbol{L}^e := \dot{\boldsymbol{F}}^e \boldsymbol{F}^{e-1}, \qquad \boldsymbol{L}^p := \boldsymbol{F}^e \dot{\boldsymbol{F}}^p \boldsymbol{F}^{p-1} \boldsymbol{F}^{e-1}. \tag{67}$$

Similarly, the *stretching* (or *rate of deformation*) tensor, $\boldsymbol{D} \equiv \mathrm{sym}[\boldsymbol{L}]$, can be decomposed as:

$$\boldsymbol{D} = \boldsymbol{D}^e + \boldsymbol{D}^p, \tag{68}$$

with the elastic and plastic stretchings given by

$$\boldsymbol{D}^e := \mathrm{sym}[\boldsymbol{L}^e], \qquad \boldsymbol{D}^p := \mathrm{sym}[\boldsymbol{L}^p]. \tag{69}$$

It will be convenient to introduce the *modified* plastic contribution, to the velocity gradient†:

$$\bar{\boldsymbol{L}}^p := \dot{\boldsymbol{F}}^p \boldsymbol{F}^{p-1}, \tag{70}$$

along with the *modified plastic stretching*:

$$\bar{\boldsymbol{D}}^p := \mathrm{sym}\left[\bar{\boldsymbol{L}}^p\right]. \tag{71}$$

Note that $\bar{\boldsymbol{D}}^p$ measures the rate of plastic deformation on the *intermediate* configuration. Since the *spatial* configuration will be used to formulate constitutive equations in the following sections, the rotation of $\bar{\boldsymbol{D}}^p$, defined by:

$$\tilde{\boldsymbol{D}}^p := \boldsymbol{R}^e \, \bar{\boldsymbol{D}}^p \, \boldsymbol{R}^{eT} = \boldsymbol{R}^e \, \mathrm{sym}\left[\dot{\boldsymbol{F}}^p \boldsymbol{F}^{p-1}\right] \boldsymbol{R}^{eT}, \tag{72}$$

will be adopted in the definition of the plastic flow rule. The *elastic rotation*, $\boldsymbol{R}^e$, results from the polar decomposition of $\boldsymbol{F}^e$:

$$\boldsymbol{F}^e = \boldsymbol{R}^e \boldsymbol{U}^e = \boldsymbol{V}^e \boldsymbol{R}^e, \tag{73}$$

where $\boldsymbol{U}^e$ and $\boldsymbol{V}^e$ denote, respectively, the *right* and *left stretch tensors*.

7.1.2 The logarithmic strain measure

Eulerian (or spatial) elastic strain measures can be defined by using $\boldsymbol{V}^e$. The use of the *logarithmic* (or *natural*) strain measure is particularly convenient for the description of the elastic behaviour. In addition to its physical appeal, the use of logarithmic strains results, as we shall see in what follows, in substantial simplifications in the stress integration algorithm and allows a natural extension, to the finite strain range, of the now classical return mapping algorithms of infinitesimal elasto-plasticity. The Eulerian logarithmic elastic strain is defined by:

$$\boldsymbol{\varepsilon}^e := \ln[\boldsymbol{V}^e] = \tfrac{1}{2} \ln[\boldsymbol{B}^e], \tag{74}$$

where $\ln[\cdot]$ above denotes the *tensor logarithm* of $(\cdot)$ and $\boldsymbol{B}^e = \boldsymbol{F}^e \boldsymbol{F}^{eT} = \boldsymbol{V}^{e2}$ is the elastic left Cauchy-Green strain tensor.

The deviatoric/volumetric split of the elastic logarithmic strain gives:

$$\boldsymbol{\varepsilon}^e = \boldsymbol{\varepsilon}^e_d + \varepsilon^e_v \boldsymbol{I}, \tag{75}$$

†In [53], Lee has regarded $\bar{\boldsymbol{L}}^p$ as the velocity gradient of the *purely plastic* deformation and concluded that the additive decomposition (66) was valid only if the elastic strains were infinitesimal. This conclusion has been later contested by Nemat-Nasser [73] who showed that (67)₂ is an equally acceptable definition for the plastic contribution to the velocity gradient.

where

$$\boldsymbol{\varepsilon}_d^e := \boldsymbol{\varepsilon}^e - \mathrm{tr}[\boldsymbol{\varepsilon}^e]\,\boldsymbol{I}\,, \tag{76}$$

and the volumetric elastic strain is given by

$$\varepsilon_v^e := \mathrm{tr}[\boldsymbol{\varepsilon}^e] = \ln J^e\,, \tag{77}$$

with

$$J^e := \det[\boldsymbol{F}^e]\,. \tag{78}$$

Note that, due to the properties of the logarithmic strain measure, as in the infinitesimal theory, a traceless $\boldsymbol{\varepsilon}^e$ corresponds to a volume preserving elastic deformation.

7.1.3 General hyperelastic based elasto-plastic constitutive model

Following the formalism of thermodynamics with internal variables described in Section 2 and restricted to isothermal processes, a rather general class of isotropic hyperelastic-based finite strain elasto-plastic constitutive models, formulated in the spatial configuration, can be defined by postulating:

1. The existence of a *free energy potential*:

$$\psi(\boldsymbol{\varepsilon}^e, \boldsymbol{\alpha})\,, \tag{79}$$

   expressed as a function of the elastic logarithmic strain and a generic set $\boldsymbol{\alpha} \equiv \{\alpha_1, \alpha_2, \cdots, \alpha_k\}$ of k internal variables.

2. A *yield function* $\Phi(\boldsymbol{\tau}, \boldsymbol{A}, \boldsymbol{\alpha})$ that, for fixed $\boldsymbol{\alpha}$, defines the *elastic domain*, where only reversible phenomena take place, as the set of all points $\{\boldsymbol{\tau}, \boldsymbol{A}\}$ in the space of thermodynamical forces for which

$$\Phi(\boldsymbol{\tau}, \boldsymbol{A}, \boldsymbol{\alpha}) \leq 0\,. \tag{80}$$

   The yield surface is defined by $\Phi(\boldsymbol{\tau}, \boldsymbol{A}, \boldsymbol{\alpha}) = 0$.

3. A *dissipation potential* $\Psi(\boldsymbol{\tau}, \boldsymbol{A}, \boldsymbol{\alpha})$, from which the evolution laws for the plastic flow and internal variables are derived, respectively, as:

$$\tilde{\boldsymbol{D}}^p = \dot{\gamma}\,\frac{\partial}{\partial \boldsymbol{\tau}}\Psi(\boldsymbol{\tau}, \boldsymbol{A}, \boldsymbol{\alpha}) \tag{81}$$

   and

$$\dot{\alpha}_i = -\dot{\gamma}\,\frac{\partial}{\partial A_i}\Psi(\boldsymbol{\tau}, \boldsymbol{A}, \boldsymbol{\alpha}) \qquad (i = 1, ..., k)\,, \tag{82}$$

   where the *plastic multiplier* $\dot{\gamma}$ satisfies the *loading/unloading criterion*:

$$\Phi \leq 0 \qquad\qquad \dot{\gamma} \geq 0 \qquad\qquad \dot{\gamma}\Phi = 0\,. \tag{83}$$

The dissipation inequality
Following assumption (79), the time derivative of the free energy reads:

$$\dot{\psi} = \frac{\partial \psi}{\partial \boldsymbol{\varepsilon}^e} : \dot{\boldsymbol{\varepsilon}}^e + \frac{1}{\rho_0}\,\boldsymbol{A}\,\dot{\boldsymbol{\alpha}}\,, \tag{84}$$

where the notation:

$$\boldsymbol{A}\,\dot{\boldsymbol{\alpha}} = \sum_{i=1}^{k} A_i\,\dot{\alpha}_i\,,$$

with the appropriate product implied, has been adopted. Equivalently by applying the chain rule to the definition (74) of $\boldsymbol{\varepsilon}^e$,

$$\begin{aligned}\dot{\psi} &= \frac{1}{2}\,\frac{\partial\psi}{\partial\boldsymbol{\varepsilon}^e} : \frac{\partial(\ln \boldsymbol{B}^e)}{\partial\boldsymbol{B}^e} : \dot{\boldsymbol{B}}^e + \frac{1}{\rho_0}\,\boldsymbol{A}\,\dot{\boldsymbol{\alpha}} \\ &= \frac{1}{2}\left[\frac{\partial\psi}{\partial\boldsymbol{\varepsilon}^e} : \frac{\partial(\ln \boldsymbol{B}^e)}{\partial\boldsymbol{B}^e}\,\boldsymbol{B}^e\right] : \dot{\boldsymbol{B}}^e\,\boldsymbol{B}^{e-1} + \frac{1}{\rho_0}\,\boldsymbol{A}\,\dot{\boldsymbol{\alpha}}\,.\end{aligned} \tag{85}$$

It should be noted that in the expression above, the tensors $\boldsymbol{\varepsilon}^e$, $\boldsymbol{B}^e$ and $\partial\psi/\partial\boldsymbol{\varepsilon}^e$ share the same principal axes. Also, the tensor logarithm is a member of the class of isotropic tensor functions discussed in Section A of the appendix. These observations in conjunction with the particularization of the formulae given in item (iii) of Box A.4 of the appendix to the derivative $\partial(\ln \boldsymbol{B}^e)/\partial\boldsymbol{B}^e$ lead to the identity:

$$\frac{\partial\psi}{\partial\boldsymbol{\varepsilon}^e} : \frac{\partial(\ln \boldsymbol{B}^e)}{\partial\boldsymbol{B}^e}\,\boldsymbol{B}^e = \frac{\partial\psi}{\partial\boldsymbol{\varepsilon}^e}\,, \tag{86}$$

and (85) can be re-written as:

$$\dot{\psi} = \frac{1}{2}\,\frac{\partial\psi}{\partial\boldsymbol{\varepsilon}^e} : \dot{\boldsymbol{B}}^e\,\boldsymbol{B}^{e-1} + \frac{1}{\rho_0}\,\boldsymbol{A}\,\dot{\boldsymbol{\alpha}}\,. \tag{87}$$

By definition, $\boldsymbol{B}^e := \boldsymbol{F}^e\boldsymbol{F}^{eT}$, or, in view of the multiplicative elasto-plastic decomposition assumption, $\boldsymbol{B}^e = \boldsymbol{F}(\boldsymbol{F}^p)^{-1}(\boldsymbol{F}^p)^{-T}\boldsymbol{F}^T$. Time differentiation of this last expression and substitution in (87) result, after some straightforward manipulations, in:

$$\begin{aligned}\dot{\psi} &= \frac{\partial\psi}{\partial\boldsymbol{\varepsilon}^e} : \left\{\boldsymbol{D} + \tfrac{1}{2}\left[\boldsymbol{F}^e\boldsymbol{F}^p(\boldsymbol{F}^{p-1})^{\cdot}\boldsymbol{F}^{eT} + \boldsymbol{F}^e(\boldsymbol{F}^{p-T})^{\cdot}\boldsymbol{F}^{pT}\boldsymbol{F}^{e-1}\right]\right\} + \frac{1}{\rho_0}\,\boldsymbol{A}\,\dot{\boldsymbol{\alpha}} \\ &= \frac{\partial\psi}{\partial\boldsymbol{\varepsilon}^e} : \left\{\boldsymbol{D} - \tfrac{1}{2}\boldsymbol{V}^e\boldsymbol{R}^e\left[\bar{\boldsymbol{L}}^p + \bar{\boldsymbol{L}}^{pT}\right]\boldsymbol{R}^{eT}\boldsymbol{V}^{e-1}\right\} + \frac{1}{\rho_0}\,\boldsymbol{A}\,\dot{\boldsymbol{\alpha}}\,,\end{aligned} \tag{88}$$

where use has been made of the relations: $\boldsymbol{F}^p(\boldsymbol{F}^{p-1})^{\cdot} = -\dot{\boldsymbol{F}}^p\boldsymbol{F}^{p-1} =: -\bar{\boldsymbol{L}}^p$ and $(\boldsymbol{F}^{p-T})^{\cdot}\boldsymbol{F}^{pT} = -\boldsymbol{F}^{p-T}(\boldsymbol{F}^{pT})^{\cdot} =: -\bar{\boldsymbol{L}}^{pT}$, obtained, respectively, with time differentiation of the identities: $\boldsymbol{F}^p\boldsymbol{F}^{p-1} = \boldsymbol{I}$ and $\boldsymbol{F}^{p-T}\boldsymbol{F}^{pT} = \boldsymbol{I}$.

Finally, with the introduction of definition (72) of the spatial modified plastic stretching tensor, $\tilde{\boldsymbol{D}}^p$, and by taking into account the elastic isotropy the rate of change of free energy can be expressed as:

$$\dot{\psi} = \frac{\partial\psi}{\partial\boldsymbol{\varepsilon}^e} : \left(\boldsymbol{D} - \tilde{\boldsymbol{D}}^p\right) + \frac{1}{\rho_0}\,\boldsymbol{A}\,\dot{\boldsymbol{\alpha}}\,. \tag{89}$$

Restricted to isothermal processes, the *Clausius-Duhem* inequality (6) can be expressed as:

$$\boldsymbol{\tau} : \boldsymbol{D} - \rho_0\,\dot{\psi} \geq 0\,, \tag{90}$$

so that by introducing (89) one obtains:

$$\left(\boldsymbol{\tau} - \rho_0\,\frac{\partial\psi}{\partial\boldsymbol{\varepsilon}^e}\right) : \boldsymbol{D} + \rho_0\,\frac{\partial\psi}{\partial\boldsymbol{\varepsilon}^e} : \tilde{\boldsymbol{D}}^p - \boldsymbol{A}\,\dot{\boldsymbol{\alpha}} \geq 0\,. \tag{91}$$

From a standard argument, the inequality above implies the following constitutive equation for the Kirchhoff stress:

$$\boldsymbol{\tau} = \rho_0 \, \frac{\partial \psi}{\partial \boldsymbol{\varepsilon}^e} \,, \tag{92}$$

and the non-negative dissipation requirement is reduced to:

$$\boldsymbol{\tau} : \tilde{\boldsymbol{D}}^p - \boldsymbol{A}\,\dot{\boldsymbol{\alpha}} \geq 0 \,. \tag{93}$$

The overall finite strain elasto-plastic constitutive model is summarized in Box 7.1.

(i) Multiplicative decomposition of the deformation gradient

$$\boldsymbol{F} = \boldsymbol{F}^e \boldsymbol{F}^p$$

(ii) Hyperelastic law

$$\boldsymbol{\tau} = \rho_0 \, \frac{\partial \psi(\boldsymbol{\varepsilon}^e, \boldsymbol{\alpha})}{\partial \boldsymbol{\varepsilon}^e}$$

(iii) Evolution equations for $\boldsymbol{F}^p$ and other internal variables $\boldsymbol{\alpha} \equiv \{\alpha_1, ..., \alpha_k\}$

$$\tilde{\boldsymbol{D}}^p := \boldsymbol{R}^e \mathrm{sym}\left[\dot{\boldsymbol{F}}^p \boldsymbol{F}^{p-1}\right] \boldsymbol{R}^{eT} = \dot{\gamma}\, \frac{\partial \Psi}{\partial \boldsymbol{\tau}}$$

$$\dot{\alpha}_i = -\dot{\gamma}\, \frac{\partial \Psi}{\partial A_i} \qquad (i = 1, ..., k)$$

(iv) Loading/unloading criterion

$$\Phi \leq 0 \qquad \dot{\gamma} \geq 0 \qquad \dot{\gamma}\Phi = 0$$

Box 7.1 General finite strain elasto-plastic model

REMARK 7.1 Expressions (92) and (93) as well as the adopted plastic flow rule (81) are completely analogous to their small strain counterparts. In the small strain limit, $\boldsymbol{\varepsilon}^e$ and $\tilde{\boldsymbol{D}}^p$ correspond, respectively, to the standard infinitesimal elastic strain tensor and plastic strain rate. Thus, the present approach allows a natural extension, to the finite strain range, of general isotropic infinitesimal elasto-plastic constitutive models. A generic small strain model defined by an elastic potential ψ_s, a yield function Φ_s and a dissipation potential Ψ_s can be extended to finite strains by adopting, in the constitutive equations above, ψ, Φ and Ψ with the same functional format as the respective small strain counterparts. This procedure will be used later in this section to formulate models for large strain ductile damage. □

REMARK 7.2 With $J^p := \det[\boldsymbol{F}^p]$ we define the *plastic volumetric strain* as:

$$\varepsilon_v^p := \ln J^p = \ln[\lambda^p_{(1)}\, \lambda^p_{(2)}\, \lambda^p_{(3)}] = \ln \lambda^p_1 + \ln \lambda^p_{(2)} + \ln \lambda^p_{(3)} = \mathrm{tr}[\boldsymbol{V}^p] \tag{94}$$

where $\lambda^p_{(i)}$ are the principal *plastic* stretches, i.e., the eigenvalues of the plastic left Cauchy-Green strain tensor, $\boldsymbol{V}^p := \boldsymbol{F}^p \boldsymbol{F}^{p\,T}$. For volume preserving $\boldsymbol{F}^p$,

$$\det[\boldsymbol{F}^p] = 1 \iff \boldsymbol{\varepsilon}^p = 0. \tag{95}$$

It can be easily shown that the plastic flow rule (81) implies that

$$\dot{\varepsilon}^p_v = \dot{\gamma}\ \mathrm{tr}\left[\frac{\partial \Psi}{\partial \boldsymbol{\tau}}\right], \tag{96}$$

so that, as in the infinitesimal theory, dissipation potentials whose derivatives with respect to $\boldsymbol{\tau}$ are traceless (such as the classical Von Mises and Tresca functions) produce *isochoric* plastic flow. □

REMARK 7.3 Analogously to the small strain theory, if Φ is taken as the dissipation potential, then the well known *principle of maximum plastic dissipation* [39] is extended to the finite strain range. In that case, the loading/unloading criterion (83) corresponds to the Kuhn-Tucker optimality condition for the l.h.s. of (93) to reach a maximum subject to the plastic admissibility constraint $\Phi \leq 0$. □

7.1.4 General stress integration procedure. The exponential map algorithm

In the present context, knowing $\boldsymbol{F}^p_n$ and the set $\boldsymbol{\alpha}_n$ of internal variables at time t_n and given the deformation gradient $\boldsymbol{F}_{n+1}$ at time t_{n+1}, the numerical integration of the constitutive equations of Box 7.1 must determine $\boldsymbol{\tau}_{n+1}$, $\boldsymbol{F}^p_{n+1}$ and the updated set $\boldsymbol{\alpha}_{n+1}$ at the subsequent time t_{n+1}.

Due to the underlying additive structure of infinitesimal plasticity, *operator split* algorithms are especially suitable for the numerical integration of small strain elasto-plastic constitutive equations and have been widely used in the computational literature [81, 85, 95, 96]. These methods consist of splitting the problem into two parts: an *elastic predictor*, where the problem is assumed to be purely elastic (no plastic flow or internal variable evolution), and a *plastic corrector*, in which a discrete system of equations comprising the elasticity law, plastic consistency, plastic flow and internal variables evolution is solved, taking the results of the elastic predictor stage as initial conditions. In the present framework for multiplicative finite strain plasticity an operator split algorithm will be adopted to integrate the constitutive equations of Box 7.1. The general algorithm comprises the following steps:

1. Firstly, it is assumed that the pseudo-time increment $[t_n, t_{n+1}]$ is purely elastic (no plastic yielding). The *elastic trial state* at t_{n+1} is, then, defined by the elastic trial deformation gradient:

   $$\boldsymbol{F}^{e\ \mathrm{trial}}_{n+1} := \boldsymbol{F}_{n+1} \boldsymbol{F}^{p\,-1}_n, \tag{97}$$

   with $\boldsymbol{F}^p$ and $\boldsymbol{\alpha}$ *frozen* at t_n:

   $$\boldsymbol{F}^{p\ \mathrm{trial}}_{n+1} = \boldsymbol{F}^p_n \tag{98}$$

   and

   $$\boldsymbol{\alpha}^{\mathrm{trial}}_{n+1} = \boldsymbol{\alpha}_n. \tag{99}$$

   The elastic trial Kirchhoff stress, corresponding to such assumption, is given by:

   $$\boldsymbol{\tau}^{\mathrm{trial}}_{n+1} = \left.\frac{\partial \psi}{\partial \boldsymbol{\varepsilon}^e}\right|_{\substack{\varepsilon^{e\ \mathrm{trial}}_{n+1} \\ \boldsymbol{\alpha}^{\mathrm{trial}}_{n+1}}}. \tag{100}$$

2. If $\Phi(\boldsymbol{\tau}^{\mathrm{trial}}_{n+1}, \boldsymbol{\alpha}^{\mathrm{trial}}_{n+1}) \leq 0$, then the increment is indeed purely elastic and we update:

$$(\cdot)_{n+1} := (\cdot)^{\mathrm{trial}}_{n+1} . \tag{101}$$

3. Otherwise, plastic yielding occurs and the plastic flow rule (81) is discretized by means of a backward *exponential approximation* (see Weber and Anand [118], Eterovic and Bathe [25] and Cuitiño and Ortiz [21]), leading to the following discrete evolution law for $\boldsymbol{F}^p$:

$$\begin{aligned} \boldsymbol{F}^p_{n+1} &= \exp\left[\Delta\gamma\ \boldsymbol{R}^{e\,T}_{n+1} \left.\frac{\partial\Psi}{\partial\boldsymbol{\tau}}\right|_{n+1} \boldsymbol{R}^e_{n+1}\right] \boldsymbol{F}^p_n \\ &= \boldsymbol{R}^{e\,T}_{n+1} \exp\left[\Delta\gamma\ \left.\frac{\partial\Psi}{\partial\boldsymbol{\tau}}\right|_{n+1}\right] \boldsymbol{R}^e_{n+1}\, \boldsymbol{F}^p_n . \end{aligned} \tag{102}$$

In addition, a standard backward Euler scheme is used to integrate the rate evolution equation (82) for the internal variables:

$$\boldsymbol{\alpha}_{n+1} = \boldsymbol{\alpha}_n - \Delta\gamma\ \left.\frac{\partial\Psi}{\partial\boldsymbol{A}}\right|_{n+1} . \tag{103}$$

The incremental plastic multiplier, $\Delta\gamma$, satisfies the discrete counterpart of (83):

$$\Phi_{n+1} \leq 0 \qquad \Delta\gamma \geq 0 \qquad \Delta\gamma\ \Phi_{n+1} = 0 . \tag{104}$$

Consequences of the exponential approximation. The small strain return map
Some crucially important properties result from the use of the exponential map in the discretization the plastic flow rule. Firstly, the incompressibility of the plastic flow for pressure insensitive yield criteria is carried over *exactly* to the incremental rule (102). Indeed, for a traceless flow direction tensor, $\partial\Psi/\partial\boldsymbol{\tau}$, $\det[\exp[\Delta\gamma\ \partial\Psi/\partial\boldsymbol{\tau}]] = 1$ which ensures that the updating formula (102) is volume preserving. In addition, under isotropic conditions, the essential stress updating procedure can be written in the same format as the classical return mapping schemes of infinitesimal elasto-plasticity, with all large strain related operations restricted to the kinematical level. This property is demonstrated in what follows.

Inversion of both sides of (102) followed by their pre-multiplication by $\boldsymbol{F}_{n+1}$ and use of relation (65), gives:

$$\boldsymbol{F}^e_{n+1} = \boldsymbol{F}^{e\ \mathrm{trial}}_{n+1} \boldsymbol{R}^{e\,T}_{n+1} \exp\left[-\Delta\gamma\ \left.\frac{\partial\Psi}{\partial\boldsymbol{\tau}}\right|_{n+1}\right] \boldsymbol{R}^e_{n+1} . \tag{105}$$

Post-multiplication of both sides of (105) by $\boldsymbol{R}^{eT}_{n+1}$ results in:

$$\boldsymbol{V}^e_{n+1} = \boldsymbol{F}^{e\ \mathrm{trial}}_{n+1} \boldsymbol{R}^{e\,T}_{n+1} \exp\left[-\Delta\gamma\ \left.\frac{\partial\Psi}{\partial\boldsymbol{\tau}}\right|_{n+1}\right] , \tag{106}$$

or, equivalently,

$$\boldsymbol{V}^e_{n+1} \exp\left[\Delta\gamma\ \left.\frac{\partial\Psi}{\partial\boldsymbol{\tau}}\right|_{n+1}\right] = \boldsymbol{F}^{e\ \mathrm{trial}}_{n+1} \boldsymbol{R}^{e\,T}_{n+1} . \tag{107}$$

Then, a further post-multiplication of each side by its transpose gives:

$$\boldsymbol{V}^e_{n+1} \exp\left[2\,\Delta\gamma\ \left.\frac{\partial\Psi}{\partial\boldsymbol{\tau}}\right|_{n+1}\right] \boldsymbol{V}^e_{n+1} = (\boldsymbol{V}^{e\ \mathrm{trial}}_{n+1})^2 . \tag{108}$$

(i) Given incr.displ. $\Delta\boldsymbol{u}$, update the deformation gradient

$$\boldsymbol{F}_u := \boldsymbol{I} + \mathrm{Grad}_{\boldsymbol{\varphi}_n}[\Delta\boldsymbol{u}], \qquad \boldsymbol{F}_{n+1} := \boldsymbol{F}_u \boldsymbol{F}_n$$

(ii) Compute elastic trial state

$$\begin{aligned}
\boldsymbol{F}^{e\ \mathrm{trial}}_{n+1} &:= \boldsymbol{F}_{n+1}(\boldsymbol{F}^p_n)^{-1} \\
\boldsymbol{B}^{e\ \mathrm{trial}}_{n+1} &:= \boldsymbol{F}^{e\ \mathrm{trial}}_{n+1}(\boldsymbol{F}^{e\ \mathrm{trial}}_{n+1})^T \\
\boldsymbol{R}^{e\ \mathrm{trial}}_{n+1} &:= (\boldsymbol{V}^{e\ \mathrm{trial}}_{n+1})^{-1}\boldsymbol{F}^{e\ \mathrm{trial}}_{n+1} \\
\boldsymbol{\varepsilon}^{e\ \mathrm{trial}}_{n+1} &:= \ln[\boldsymbol{V}^{e\ \mathrm{trial}}_{n+1}] = \tfrac{1}{2}\ln[\boldsymbol{B}^{e\ \mathrm{trial}}_{n+1}] \\
\boldsymbol{\alpha}^{\mathrm{trial}}_{n+1} &:= \boldsymbol{\alpha}_n
\end{aligned}$$

(iii) **GOTO BOX 7.3** – small strain algorithm (update $\boldsymbol{\tau}$, $\boldsymbol{\varepsilon}^e$ and $\boldsymbol{\alpha}$)

(iv) Update $\boldsymbol{F}^p$ and Cauchy stress.

$$\begin{aligned}
\boldsymbol{V}^e_{n+1} &:= \exp[\boldsymbol{\varepsilon}^e_{n+1}] \\
\boldsymbol{R}^e_{n+1} &:= \boldsymbol{R}^{e\ \mathrm{trial}}_{n+1} \\
\boldsymbol{F}^p_{n+1} &:= (\boldsymbol{R}^e_{n+1})^T(\boldsymbol{V}^e_{n+1})^{-1}\boldsymbol{F}_{n+1} \\
\boldsymbol{\sigma}_{n+1} &:= \det[\boldsymbol{F}_{n+1}]^{-1}\ \boldsymbol{\tau}_{n+1}
\end{aligned}$$

Box 7.2 General integration algorithm for finite multiplicative elastoplasticity

Due to the assumed elastic isotropy, $\boldsymbol{V}^e$ and $\boldsymbol{\tau}$ commute. If the potential Ψ is assumed to be an *isotropic* function of $\boldsymbol{\tau}$, then $\boldsymbol{\tau}$ and $\partial\Psi/\partial\boldsymbol{\tau}$ have the same principal directions so that all terms on the l.h.s. of the above expression commute. Under such assumptions, expression (108) leads to the simpler update formula in terms of the logarithmic eulerian strain tensor:

$$\boldsymbol{\varepsilon}^e_{n+1} = \boldsymbol{\varepsilon}^{e\ \mathrm{trial}}_{n+1} - \Delta\gamma \left.\frac{\partial\Psi}{\partial\boldsymbol{\tau}}\right|_{n+1}, \tag{109}$$

which has the same format of the update formula for the elastic strains of the standard return mapping algorithms of the infinitesimal theory. For the elastic rotation, the following expression is obtained:

$$\boldsymbol{R}^e_{n+1} = \boldsymbol{R}^{e\ \mathrm{trial}}_{n+1}. \tag{110}$$

The resulting algorithm for integration of the large strain elasto-plastic constitutive equations is summarized in Boxes 7.2 and 7.3.

REMARK 7.4 The operations carried out in Box 7.2 are related exclusively to the kinematics of finite strains. Due to the use of logarithmic strains to describe elasticity along with the exponential approximation (102) to the plastic flow rule, the essential material related stress updating procedure, shown in Box 7.3, preserves the small strain format. It corresponds to the well established return mapping procedures of infinitesimal elasto-plasticity. □

(i) Elastic predictor

- Evaluate trial elastic stress

$$\boldsymbol{\tau}_{n+1}^{\text{trial}} = \left.\frac{\partial \psi}{\partial \boldsymbol{\varepsilon}^e}\right|_{\substack{\varepsilon_{n+1}^{e\ \text{trial}} \\ \boldsymbol{\alpha}_{n+1}^{\text{trial}}}}$$

- Check plastic consistency condition

  IF $\Phi(\boldsymbol{\tau}_{n+1}^{\text{trial}}, \boldsymbol{\alpha}_{n+1}^{\text{trial}}) \leq 0$

  THEN

  Set $(\cdot)_{n+1} = (\cdot)_{n+1}^{\text{trial}}$ and RETURN

  ELSE go to (ii)

(ii) Plastic corrector (solve the algebraic system for $\Delta\gamma$, $\boldsymbol{\varepsilon}_{n+1}^e$ and $\boldsymbol{\alpha}_{n+1}$)

$$\left\{ \begin{array}{l} \Phi(\boldsymbol{\tau}_{n+1}, \boldsymbol{\alpha}_{n+1}) \\ \boldsymbol{\varepsilon}_{n+1}^e - \boldsymbol{\varepsilon}_{n+1}^{e\ \text{trial}} + \Delta\gamma\ \left.\frac{\partial \Psi}{\partial \boldsymbol{\tau}}\right|_{n+1} \\ \boldsymbol{\alpha}_{n+1} - \boldsymbol{\alpha}_n + \Delta\gamma\ \left.\frac{\partial \Psi}{\partial \boldsymbol{A}}\right|_{n+1} \end{array} \right\} = \left\{ \begin{array}{c} 0 \\ 0 \\ 0 \end{array} \right\}$$

where

$$\boldsymbol{\tau}_{n+1} = \left.\frac{\partial \psi(\boldsymbol{\varepsilon}^e, \boldsymbol{\alpha})}{\partial \boldsymbol{\varepsilon}^e}\right|_{n+1}$$

(iii) RETURN

Box 7.3 General stress updating procedure – *SMALL STRAINS*

7.1.5 The spatial tangent modulus

The next step towards the complete incorporation of the present model into the numerical framework of Section 5 is the derivation of a closed formula for the spatial tangent modulus $\boldsymbol{a}$, whose general expression is given by (35), consistent with the integration algorithm described above.

In the small strain return mapping of Box 7.3, the updated stress $\boldsymbol{\tau}_{n+1}$ is obtained as a function of $\boldsymbol{\alpha}_n$ and the elastic trial logarithmic strain, so that this procedure can be regarded as an incremental constitutive functional of the form:

$$\boldsymbol{\tau}_{n+1} = \tilde{\boldsymbol{\tau}}(\boldsymbol{\alpha}_n, \boldsymbol{\varepsilon}_{n+1}^{e\ \text{trial}}) . \tag{111}$$

In the general procedure of Box 7.2, $\boldsymbol{\varepsilon}_{n+1}^{e\ \text{trial}}$ is computed as a function of $\boldsymbol{B}_{n+1}^{e\ \text{trial}}$ which, in turn, is a function of $\boldsymbol{F}_n^p$ and $\boldsymbol{F}_{n+1}$. With $\boldsymbol{\varepsilon}_{n+1}^{e\ \text{trial}}$ at hand, the Kirchhoff stress is then updated by means of the incremental functional $\tilde{\boldsymbol{\tau}}$ (small strain algorithm). Thus, the overall procedure defines a function $\hat{\boldsymbol{\tau}}$, for the Kirchhoff stress, that can be generally expressed as:

$$\hat{\boldsymbol{\tau}}(\boldsymbol{\alpha}_n, \boldsymbol{F}_{n+1}) := \tilde{\boldsymbol{\tau}}(\boldsymbol{\alpha}_n, \boldsymbol{\varepsilon}_{n+1}^{e\ \text{trial}}(\boldsymbol{B}_{n+1}^{e\ \text{trial}}(\boldsymbol{F}_n^p, \boldsymbol{F}_{n+1}))) . \tag{112}$$

Clearly, $\hat{\boldsymbol{\tau}}$ is a particular case of the general algorithmic constitutive functional (26).

Application of the chain rule to (112) gives:

$$\frac{\partial \hat{\boldsymbol{\tau}}}{\partial \boldsymbol{F}_{n+1}} = \frac{\partial \tilde{\boldsymbol{\tau}}}{\partial \boldsymbol{\varepsilon}^{e\ \mathrm{trial}}_{n+1}} : \frac{\partial \boldsymbol{\varepsilon}^{e\ \mathrm{trial}}_{n+1}}{\partial \boldsymbol{B}^{e\ \mathrm{trial}}_{n+1}} : \frac{\partial \boldsymbol{B}^{e\ \mathrm{trial}}_{n+1}}{\partial \boldsymbol{F}_{n+1}} . \tag{113}$$

Substitution of this expression into (35) results, after straightforward manipulations, in the following closed formula for the components of the spatial tangent modulus consistent with the present integration algorithm:

$$\boxed{\mathsf{a}_{ijkl} = \frac{1}{2J} [\tilde{\mathsf{h}} : \mathsf{n} : \mathsf{b}]_{ijkl} - \sigma_{il}\, \delta_{jk} ,} \tag{114}$$

where $\tilde{\mathsf{h}}$ is the *small strain elasto-plastic consistent tangent operator*, associated exclusively with the return map algorithm of Box 7.3:

$$\tilde{\mathsf{h}} := \frac{\partial \tilde{\boldsymbol{\tau}}}{\partial \boldsymbol{\varepsilon}^{e\ \mathrm{trial}}_{n+1}} . \tag{115}$$

The fourth order tensor n is defined as:

$$\mathsf{n} := \frac{\partial \ln[\boldsymbol{B}^{e\ \mathrm{trial}}_{n+1}]}{\partial \boldsymbol{B}^{e\ \mathrm{trial}}_{n+1}} , \tag{116}$$

i.e., it is the derivative of the tensor logarithm function at $\boldsymbol{B}^{e\ \mathrm{trial}}_{n+1}$. The tensor logarithm is a member of the class of isotropic tensor functions described in Section A. It is obtained by setting, in expression (176), $y(\cdot) \equiv \ln(\cdot)$ and $\boldsymbol{X} \equiv \boldsymbol{B}^{e\ \mathrm{trial}}_{n+1}$. Thus, the actual computation of n follows the procedure described in Box A.4 in the appendix. Finally, the cartesian components of b are defined by:

$$\mathsf{b}_{ijkl} := \delta_{ik}\, (\boldsymbol{B}^{e\ \mathrm{trial}}_{n+1})_{jl} + \delta_{jk}\, (\boldsymbol{B}^{e\ \mathrm{trial}}_{n+1})_{il} . \tag{117}$$

REMARK 7.5 Note that $\tilde{\mathsf{h}}$ is the *only* material related contribution to the spatial modulus a. All other terms taking part in its assemblage in (114) are related to the geometry of finite deformations and do not depend on the particular material model adopted. Therefore, as far as consistent linearization is concerned, only the derivation of the small strain elasto-plastic consistent tangent operator will be addressed in the following sections. The tensor $\tilde{\mathsf{h}}$ is obtained from the linearization of the algorithm of Box 7.3 by following the classical procedure introduced by Simo and Taylor [99]. □

7.2 Finite Strain Extension of Lemaitre's Ductile Damage Model

The constitutive equations for elastoplasticity coupled with damage adopted here have been originally proposed by Lemaitre [56, 57] in the context of the infinitesimal strain theory. Based on the concept of *effective stress* and the *hypothesis of strain equivalence* Lemaitre's model includes evolution of internal damage as well as non-linear isotropic and kinematic hardening in the description of the behaviour of ductile metals. Within the framework for large strain multiplicative elastoplasticity described above, the extension of Lemaitre's formulation to the finite strain range is presented in the following.

7.2.1 State variables

The starting point of the theory is the assumption that the free energy at a material point can be completely determined by the set $\{\boldsymbol{\varepsilon}^e, R, \boldsymbol{X}, D\}$ of state variables, i.e.,

$$\psi = \psi(\boldsymbol{\varepsilon}^e, R, \boldsymbol{X}, D) \tag{118}$$

where $\boldsymbol{\varepsilon}^e$ is the *logarithmic* elastic strain tensor defined in the previous section and R and D are the *scalar* internal variables associated respectively with *isotropic hardening* and *isotropic damage*. The second order tensor $\boldsymbol{X}$ is the internal variable related to *kinematic hardening*.

From a micromechanical viewpoint, R is intrinsically connected with the density of dislocations in the atomic structure which cause an isotropic increase in resistance to plastic flow. The internal variable $\boldsymbol{X}$ is related to self-equilibrated residual stresses which remain after elastic unloading. These stresses may increase or decrease resistance to slip deformation according to the direction considered. The continuum damage variable D, as discussed in Section 4, can be interpreted as an indirect measure of density of micro voids and microcracks [52]. Such microscopic defects are assumed isotropically distributed and in the present context they will be phenomenologically reflected by the degradation of the elastic modulus. A critical value for D (as an experimentally determined parameter) will define the onset of material instabilities which induce initiation of a macrocrack, i.e., the rupture of a representative volume element [60].

Under the hypothesis of decoupling between elasticity-damage and plastic hardening, the specific free energy is assumed to be given by the sum

$$\psi = \psi^{ed}(\boldsymbol{\varepsilon}^e, D) + \psi^p(R, \boldsymbol{X}) \tag{119}$$

where ψ^{ed} and $\psi^p(R, \boldsymbol{X})$ are, respectively, the elastic-damage and plastic contribution to the free energy.

7.2.2 The elastic-damage potential. Elasticity-damage coupling

Exploiting the kinematical properties of the logarithmic strain in the formulation of finite multiplicative elastoplasticity, Perić *et al.* [85] have employed the *Hencky strain energy function* [37] to describe the elastic response,

$$\rho_0\, \hat{\psi}^e(\lambda_1^e, \lambda_2^e, \lambda_3^e) = \mu \left[(\ln \lambda_1^e)^2 + (\ln \lambda_2^e)^2 + (\ln \lambda_3^e)^2\right] + \tfrac{1}{2}\lambda(\ln J^e)^2 \tag{120}$$

where μ and λ are positive material constants, λ_i^e are the principal elastic stretches and $J^e = \lambda_1^e \lambda_2^e \lambda_3^e$. In the present finite strain extension of Lemaitre's damage model, the *hypothesis of strain equivalence* [60] is introduced in the stored energy function above and the potential ψ^{ed}, written as a function of elastic stretches and damage, is assumed to have the particular form:

$$\rho_0\, \hat{\psi}^{ed}(\lambda_1^e, \lambda_2^e, \lambda_3^e, D) = (1-D)\left\{\mu\left[(\ln \lambda_1^e)^2 + (\ln \lambda_2^e)^2 + (\ln \lambda_3^e)^2\right] + \tfrac{1}{2}\lambda(\ln J^e)^2\right\}, \tag{121}$$

or, equivalently, in terms of the logarithmic elastic strain $\boldsymbol{\varepsilon}^e$,

$$\rho_0\, \psi^{ed}(\boldsymbol{\varepsilon}^e, D) = \tfrac{1}{2}\, \boldsymbol{\varepsilon}^e : (1-D)\boldsymbol{\mathsf{h}} : \boldsymbol{\varepsilon}^e, \tag{122}$$

where $\boldsymbol{\mathsf{h}}$ is the fourth order isotropic tensor represented as:

$$\boldsymbol{\mathsf{h}} = 2\mu \boldsymbol{\mathsf{I}} + \lambda(\boldsymbol{I} \otimes \boldsymbol{I}), \tag{123}$$

with $\boldsymbol{I}$ denoting the identity tensor and $\mathbf{I}$ defined by the cartesian components $\mathsf{I}_{ijkl} := \frac{1}{2}(\delta_{ik}\delta_{jl} + \delta_{il}\delta_{jk})$. For this particular potential, the elasticity law is given by:

$$\boldsymbol{\tau} = \rho_0 \, \frac{\partial \psi}{\partial \boldsymbol{\varepsilon}^e} = (1 - D) \mathbf{I\!h} : \boldsymbol{\varepsilon}^e \, . \tag{124}$$

In this case, the thermodynamical force conjugate to the damage internal variable is given by:

$$Y := \rho_0 \, \frac{\partial \psi}{\partial D} = -\tfrac{1}{2} \, \boldsymbol{\varepsilon}^e : \mathbf{I\!h} : \boldsymbol{\varepsilon}^e \, , \tag{125}$$

or, using the inverse of the elastic stress/strain law,

$$\begin{aligned} Y &= \frac{-1}{2(1-D)^2} \, \boldsymbol{\tau} : \mathbf{I\!h}^{-1} : \boldsymbol{\tau} \\ &= \frac{-q^{\,2}}{2E(1-D)^2} \left[\frac{2}{3}(1+\nu) + 3(1-2\nu) \left(\frac{p}{q} \right)^2 \right] , \end{aligned} \tag{126}$$

where E and ν are, respectively, the Young's modulus and Poisson ratio associated with μ and λ. The hydrostatic *Kirchhoff pressure*, p, is given by:

$$p := \tfrac{1}{3} \, \mathrm{tr}[\boldsymbol{\tau}] \, , \tag{127}$$

and q is the Von Mises equivalent stress defined as:

$$q := \sqrt{3 \, J_2(\boldsymbol{\tau})} = \sqrt{\tfrac{3}{2} \, \mathrm{dev}[\boldsymbol{\tau}] : \mathrm{dev}[\boldsymbol{\tau}]} \, ,$$

with dev[·] standing for the *deviatoric part of* [·].

Commonly known as the *damage energy release rate*, $-Y$ corresponds to the variation of internal energy density due to damage growth at constant stress. It is the continuum damage analogue of the J integral used in fracture mechanics [87]. The product $-Y\,\dot{D}$ represents the power dissipated by the process of internal deterioration (mainly as decohesion of interatomic bonds).

REMARK 7.6 The stress-strain rule (124) has very important experimental consequences. Indeed, with the elasticity-damage coupling introduced via the hypothesis of strain equivalence (stated in Section 4.2), the *effective* elastic modulus of the material, which can be measured from experiments, is given by

$$\mathbf{I\!h}_{\mathrm{eff}} = (1 - D) \mathbf{I\!h} \tag{128}$$

where the damage variable assumes values within the interval [0,1]. In the absence of damage ($D = 0$), the effective modulus corresponds to the modulus $\mathbf{I\!h}$ of the virgin material. For a completely damaged state ($D = 1$), $\mathbf{I\!h}_{\mathrm{eff}} = \mathbf{0}$ corresponding to a total loss of load bearing capacity of the volume element. The identification of a generic damaged state, with $D \in [0,1]$, is then restricted to measurement of the degradation of the current effective elastic modulus with respect to the virgin state ($D = 0$) as described by Lemaitre [56] and Lemaitre and Chaboche [60]. □

7.2.3 The plastic potential

The plastic contribution $\psi^p(R, \boldsymbol{X})$ to the free energy is chosen as:

$$\rho_0\, \psi^p(R, \boldsymbol{X}) = \psi^R(R) + \frac{a}{2}\, \boldsymbol{X} : \boldsymbol{X} \tag{129}$$

where a is a material constant and the isotropic hardening contribution, $\psi^R(R)$, is an arbitrary function of the single argument R. The thermodynamical force associated to isotropic hardening is, then, defined as:

$$K := \rho_0\, \frac{\partial \psi^p(R, \boldsymbol{X})}{\partial R} = \rho_0\, \frac{\partial \psi^R(R)}{\partial R} = K(R)\ . \tag{130}$$

From the plastic potential (129), it follows that the thermodynamic force associated with kinematic hardening, denoted $\boldsymbol{\beta}$, is given by:

$$\boldsymbol{\beta} := \rho_0\, \frac{\partial \psi}{\partial \boldsymbol{X}} = a\, \boldsymbol{X} \tag{131}$$

7.2.4 Yield function and dissipation potential. Internal variables evolution

For the *yield function* Φ the following form is adopted:

$$\Phi(\boldsymbol{\tau}, K, \bar{\boldsymbol{\beta}}, D) = \frac{\sqrt{3\, J_2(\boldsymbol{\tau} - \bar{\boldsymbol{\beta}})}}{1-D} - K - \tau_{y_0} \tag{132}$$

where the material parameter τ_{y_0} is the uniaxial yield stress of the undamaged material and the *spatial* quantity $\bar{\boldsymbol{\beta}}$ is the rotation of the backstress tensor $\boldsymbol{\beta}$ to the spatial configuration:

$$\bar{\boldsymbol{\beta}} := \boldsymbol{R}^e\, \boldsymbol{\beta}\, \boldsymbol{R}^{eT}\ . \tag{133}$$

In addition, *the dissipation potential* is assumed to be given by:

$$\Psi = \Phi + \frac{b}{2\,a} \bar{\boldsymbol{\beta}} : \bar{\boldsymbol{\beta}} + \frac{r}{(1-D)(s+1)} \left(\frac{-Y}{r} \right)^{s+1}, \tag{134}$$

where a, b, r and s are material constants. The damage evolution constants r and s can be identified by integrating the damage evolution law for particular cases of (constant) stress triaxiality rate as described in Section 7.4 of Lemaitre and Chaboche [60]. The constants a and b, associated with kinematic hardening, are obtained from cyclic loading experiments [60].

The convexity of the dissipation potential Ψ with respect to the thermodynamical forces for positive constants a, b, r and s ensures that the dissipation inequality is satisfied *a priori* by the present constitutive model.

The finite strain extension of Lemaitre's ductile damage model is summarized in Box 7.4.

7.2.5 Integration algorithm

Within the present framework, the general algorithm of Box 7.2 is independent of the particular material model adopted. Therefore, only the small strain return mapping algorithm associated with Lemaitre's ductile damage model is addressed below. The algorithm is summarized in Box 7.5. It corresponds to the algorithm originally proposed by Benallal *et al.* [6] in the context of the infinitesimal theory.

(i) Multiplicative decomposition of the deformation gradient

$$\boldsymbol{F} = \boldsymbol{F}^e \boldsymbol{F}^p$$

(ii) Elasticity law

$$\boldsymbol{\tau} = (1 - D)\,\mathbf{I\!h} : \boldsymbol{\varepsilon}^e$$

(iii) Yield function

$$\Phi(\boldsymbol{\tau}, K, \bar{\boldsymbol{\beta}}, D) = \frac{\sqrt{3\, J_2(\boldsymbol{\tau} - \bar{\boldsymbol{\beta}})}}{1 - D} - K - \tau_{y_0}$$

where $\bar{\boldsymbol{\beta}} := \boldsymbol{R}^e \boldsymbol{\beta} \boldsymbol{R}^{eT}$.

(iv) Plastic flow and evolution equations for R, $\boldsymbol{\beta}$ and D

$$\tilde{\boldsymbol{D}}^p = \dot{\gamma}\, \frac{3}{2}\, \frac{\mathrm{dev}[\boldsymbol{\tau} - \bar{\boldsymbol{\beta}}]}{(1 - D)\, \sqrt{3\, J_2(\boldsymbol{\tau} - \bar{\boldsymbol{\beta}})}}$$

$$\dot{R} = \dot{\gamma}$$

$$\dot{\boldsymbol{\beta}} = \dot{\gamma}\, \boldsymbol{R}^{eT} \left[a\, \frac{3}{2}\, \frac{\mathrm{dev}[\boldsymbol{\tau} - \bar{\boldsymbol{\beta}}]}{(1 - D)\, \sqrt{3\, J_2(\boldsymbol{\tau} - \bar{\boldsymbol{\beta}})}} - b\, \bar{\boldsymbol{\beta}} \right] \boldsymbol{R}^e$$

$$\dot{D} = \dot{\gamma}\, \frac{1}{1 - D} \left(\frac{-Y}{r} \right)^s$$

with Y given by (126).

Box 7.4 Finite strain extension of Lemaitre's ductile damage model

It should be noted that, due to the presence of the tensorial kinematic hardening variable, the potential Ψ above is *not* an isotropic function of $\boldsymbol{\tau}$. This is in contradiction with the isotropy hypothesis, made in the previous section, that rendered expression (109) and, consequently, allowed the use of material related integration algorithms with the same format as the infinitesimal return mappings. Nevertheless, it can be shown that, in the present case, (109) approximates (108) to second order in *elastic* strains. Therefore, the neat structure of the stress integration algorithm described in Boxes 7.2 and 7.3 can be recovered so long as the elastic strains remain small. It is emphasized that this condition is, indeed, satisfied in metal plasticity. In the absence of kinematic hardening, Lemaitre's ductile damage model fits *exactly* within this framework independently of the magnitude of the elastic strain.

REMARK 7.7 A study of accuracy and stability properties of the return mapping procedure of Box 7.5 has been carried out in reference [104]. Convergence of the Newton-Raphson scheme used to solve the system of non-linear equations of the plastic corrector stage (item (ii)) has been found to depend crucially on the initial guess supplied, particularly at highly damaged states. Within the finite element context, failure of the return mapping to converge for a single integration point requires that the global incrementation procedure be re-started from the beginning of the current increment with a reduced load step. This may incur a dramatic increase in computational costs, specially for large problems. To tackle

(i) Elastic predictor

- Evaluate trial elastic stress

$$\boldsymbol{\tau}_{n+1}^{\text{trial}} := (1-D_n)\boldsymbol{h} : \boldsymbol{\varepsilon}_{n+1}^{e\ \text{trial}}$$

- Check plastic consistency

IF $\Phi^{\text{trial}} := \frac{\sqrt{3\,J_2(\boldsymbol{\tau}_{n+1}^{\text{trial}}-\boldsymbol{\beta}_n)}}{1-D_n} - K(R_n) - \tau_{y_0} \leq 0$ THEN

Set $(\cdot)_{n+1} = (\cdot)_{n+1}^{\text{trial}}$ and RETURN

ELSE go to (ii)

(ii) Plastic corrector (solve the system for $\boldsymbol{\tau}_{n+1}$, $\bar{\boldsymbol{\beta}}_{n+1}$, D_{n+1} and $\Delta\gamma$)

$$\left\{ \begin{array}{l} \frac{\sqrt{3\,J_2(\boldsymbol{\tau}_{n+1}-\bar{\boldsymbol{\beta}}_{n+1})}}{1-D_{n+1}} - K(R_n+\Delta\gamma) - T_{y_0} \\ \boldsymbol{\tau}_{n+1} - (1-D_{n+1})\ \boldsymbol{h} : (\boldsymbol{\varepsilon}_{n+1}^{e\ \text{trial}} - \Delta\gamma\ \boldsymbol{N}_{n+1}) \\ \bar{\boldsymbol{\beta}}_{n+1} - \bar{\boldsymbol{\beta}}_n - \Delta\gamma\ (a\,\boldsymbol{N}_{n+1} - b\,\bar{\boldsymbol{\beta}}_{n+1}) \\ D_{n+1} - D_n - \frac{1}{1-D_{n+1}}\left(\frac{-Y_{n+1}}{r}\right)^s \Delta\gamma \end{array} \right\} = \left\{ \begin{array}{c} 0 \\ \mathbf{0} \\ \mathbf{0} \\ 0 \end{array} \right\}$$

where $\bar{\boldsymbol{\beta}}_n = \boldsymbol{R}_{n+1}^e \boldsymbol{\beta}_n \boldsymbol{R}_{n+1}^{e\,T}$ and $\boldsymbol{N}_{n+1} = \frac{3}{2}\ \frac{\text{dev}[\boldsymbol{\tau}_{n+1}-\bar{\boldsymbol{\beta}}_{n+1}]}{(1-D_{n+1})\ \sqrt{3\,J_2(\boldsymbol{\tau}_{n+1}-\bar{\boldsymbol{\beta}}_{n+1})}}$.

(iii) Update $\boldsymbol{\varepsilon}^e$, R and $\boldsymbol{\beta}$

$$R_{n+1} := R_n + \Delta\gamma\,, \qquad \boldsymbol{\varepsilon}_{n+1}^e := \boldsymbol{\varepsilon}_{n+1}^{e\ \text{trial}} - \Delta\gamma\ \boldsymbol{N}_{n+1}$$

$$\boldsymbol{\beta}_{n+1} = \boldsymbol{R}_{n+1}^{e\,T} \bar{\boldsymbol{\beta}}_{n+1} \boldsymbol{R}_{n+1}^e$$

(iv) RETURN

Box 7.5 Small strain return mapping algorithm for Lemaitre's model

this problem, the following strategy was proposed in reference [104]:

- Firstly, the Newton-Raphson scheme is applied taking $\boldsymbol{\tau}_n$, $\boldsymbol{\beta}_n$, D_n and $\Delta\gamma = 0$ as initial guesses for the system variables.

- If convergence is not achieved, the N-R scheme is restarted. The initial guess now is $\boldsymbol{\tau}^{\text{proj}}$, $\boldsymbol{\beta}_n$, D_n and $\Delta\gamma = 0$. The *projected stress* $\boldsymbol{\tau}^{\text{proj}}$ is obtained by solving, for $\Delta\lambda$, the *scalar* equation:

$$\Phi(\text{dev}[\boldsymbol{\tau}^{\text{proj}}], R_n, \text{dev}[\bar{\boldsymbol{\beta}}_n], D_n) = 0\,,$$

with

$$\text{dev}[\boldsymbol{\tau}^{\text{proj}}] = \frac{\text{dev}[\boldsymbol{\tau}_{n+1}^{\text{trial}} - \bar{\boldsymbol{\beta}}_n]}{1+\sqrt{\frac{3}{2}}\,\Delta\lambda} + \text{dev}[\bar{\boldsymbol{\beta}}_n]\,,$$

and corresponds to the projection of $\boldsymbol{\tau}_{n+1}^{\text{trial}}$ onto the *frozen* yield surface of time t_n.

This procedure was found to effectively stabilize the local Newton-Raphson algorithm assuring convergence at any stage of damage evolution. □

7.2.6 The small strain elasto-plastic consistent tangent operator

If the outcame $\{\boldsymbol{\tau}_{n+1}, R_{n+1}, \boldsymbol{\beta}_{n+1}, D_{n+1}\}$ of the integration algorithm of Box 7.5 lies inside the elastic domain ($\Phi_{n+1} < 0$) then the corresponding algorithmic constitutive functional for stress,

$$\tilde{\boldsymbol{\tau}}\,(R_n, \bar{\boldsymbol{\beta}}_n, D_n, \boldsymbol{\varepsilon}^{e\ \mathrm{trial}}_{n+1})\,, \tag{135}$$

is differentiable and the consistent tangent operator is simply given by:

$$\tilde{\mathbb{D}} = (1 - D_{n+1})\mathbb{D}. \tag{136}$$

However, if the converged state is on the yield surface ($\Phi_{n+1} = 0$), then plastic loading as well as elastic unloading are possible. Hence, the algorithmic function is *not* differentiable and $\tilde{\mathbb{D}}$ is a one sided derivative of $\tilde{\boldsymbol{\tau}}$. If unloading is assumed to occur, then (136) remains valid. Otherwise, $\boldsymbol{\tau}_{n+1}$ is delivered as the solution of the non-linear system of the plastic corrector stage (item (ii)). In this case, the non-linear system is differentiated leading to the linear form:

$$\begin{bmatrix} A_{1,\tau} & A_{1,D} & A_{1,\Delta\gamma} & A_{1,\bar{\beta}} \\ \boldsymbol{A}_{2,\tau} & \boldsymbol{A}_{2,D} & \boldsymbol{A}_{2,\Delta\gamma} & \boldsymbol{A}_{2,\bar{\beta}} \\ \boldsymbol{A}_{3,\tau} & \boldsymbol{A}_{3,D} & \boldsymbol{A}_{3,\Delta\gamma} & \boldsymbol{A}_{3,\bar{\beta}} \\ A_{4,\tau} & A_{4,D} & A_{4,\Delta\gamma} & \mathbf{0} \end{bmatrix} \begin{bmatrix} \mathrm{d}\boldsymbol{\tau}_{n+1} \\ \mathrm{d}D_{n+1} \\ \mathrm{d}\Delta\gamma \\ \mathrm{d}\bar{\boldsymbol{\beta}}_{n+1} \end{bmatrix} = \begin{bmatrix} 0 \\ (1-D_{n+1})\mathbb{D} : \mathrm{d}\boldsymbol{\varepsilon}^{e\ \mathrm{trial}}_{n+1} \\ \mathbf{0} \\ 0 \end{bmatrix} \tag{137}$$

where the coefficients $\boldsymbol{A}_{1,\tau}$, $A_{1,D}$,... are the partial derivatives of the left hand sides of item (ii) with respect to the system variables computed at the converged solution of the non-linear system of equations of the plastic corrector procedure. Note that the same coefficients matrix is computed for each trial solution obtained during the Newton-Raphson iterations of the plastic corrector stage. Inversion of (137) gives the tangent relations between the system variables ($\boldsymbol{\tau}_{n+1}$, D_{n+1}, $\Delta\gamma$ and $\bar{\boldsymbol{\beta}}_{n+1}$) and $\boldsymbol{\varepsilon}^{e\ \mathrm{trial}}_{n+1}$:

$$\begin{bmatrix} \mathrm{d}\boldsymbol{\tau}_{n+1} \\ \mathrm{d}D_{n+1} \\ \mathrm{d}\Delta\gamma \\ \mathrm{d}\bar{\boldsymbol{\beta}}_{n+1} \end{bmatrix} = \begin{bmatrix} \boldsymbol{C}_{11} & \mathbb{C}_{12} & \mathbb{C}_{13} & \boldsymbol{C}_{14} \\ C_{21} & \boldsymbol{C}_{22} & \boldsymbol{C}_{23} & C_{24} \\ C_{31} & \boldsymbol{C}_{32} & \boldsymbol{C}_{33} & C_{34} \\ \boldsymbol{C}_{41} & \mathbb{C}_{42} & \mathbb{C}_{43} & \boldsymbol{C}_{44} \end{bmatrix} \begin{bmatrix} 0 \\ (1-D_{n+1})\mathbb{D} : \mathrm{d}\boldsymbol{\varepsilon}^{e\ \mathrm{trial}}_{n+1} \\ \mathbf{0} \\ 0 \end{bmatrix}. \tag{138}$$

In particular, for the elasto-plastic consistent tangent operator, one has:

$$\tilde{\mathbb{D}} := \frac{\mathrm{d}\boldsymbol{\tau}_{n+1}}{\mathrm{d}\boldsymbol{\varepsilon}^{e\ \mathrm{trial}}_{n+1}} = (1-D_{n+1})\,\mathbb{C}_{12} : \mathbb{D}\,. \tag{139}$$

A closed formula for the small strain consistent tangent operator, which does not require inversion of the linear system, has been recently derived by Doghri [22] for a variant of the present version of Lemaitre's ductile damage model.

REMARK 7.8 The tangent operator $\tilde{\boldsymbol{h}}$ above is generally *unsymmetric* so that, within the context of finite element computations, an unsymmetric solver is required for solution of the linear system (31) at each iteration of the global Newton-Raphson procedure. Such unsymmetry, however, is immaterial in many situations of industrial interest. In the simulation of metal forming problems, for instance, frictional contact, which inevitably results in unsymmetric tangent stiffnesses, usually plays an essential role and an unsymmetric solver is required regardless of the material model adopted. □

7.3 Finite Strain Extension of Gurson's Voids Growth Model

The constitutive equations presented here have been originally proposed by Gurson [32] to describe the mechanism of internal damaging in the form of voids growth in porous metals. The starting point of Gurson's theory is the microscopic idealization of porous metals as aggregates containing voids of simple geometric shapes embedded in a metallic matrix whose behaviour is governed by a rigid-plastic Von Mises constitutive law. Approximate functional forms for the corresponding macroscopic yield functions are derived based on the analysis of single void cells and use of the upper bound plasticity theorem. In contrast to Lemaitre's damage model, the evolution the damage variable of Gurson's model is *not* associated with a dissipative mechanism. The damage variable D in this case is the *void volume fraction*, i.e., the local fraction of volume occupied by voids and its evolution law follows as a direct consequence of the requirement for mass conservation.

7.3.1 The free energy potential

In the original version of Gurson's ductile damage model [32], the matrix material was assumed incompressible rigid-perfectly plastic and the resulting macroscopic model was compressible rigid-plastic with hardening and softening associated, respectively, with healing and growth of voids. Here, (hyper-) elasticity as well as the possibility of additional isotropic hardening/softening due to straining of the matrix material are introduced and the free energy potential is assumed to be given by:

$$\psi = \psi(\boldsymbol{\varepsilon}^e, R) = \psi^e(\boldsymbol{\varepsilon}^e) + \psi^p(R) \; . \tag{140}$$

The elastic contribution ψ^e is taken as the *Hencky* strain-energy function (120), which, in terms of the logarithmic strain $\boldsymbol{\varepsilon}^e$, reads:

$$\rho_0\, \psi^e(\boldsymbol{\varepsilon}^e) = \tfrac{1}{2}\, \boldsymbol{\varepsilon}^e : \boldsymbol{h} : \boldsymbol{\varepsilon}^e \, , \tag{141}$$

The constitutive equation for the Kirchhoff stress follows as:

$$\boldsymbol{\tau} = \rho_0\, \frac{\partial \psi}{\partial \boldsymbol{\varepsilon}^e} = \boldsymbol{h} : \boldsymbol{\varepsilon}^e \, . \tag{142}$$

As in Lemaitre's model, the isotropic hardening contribution is left as an arbitrary function of a single argument, so that the thermodynamic force K associated with R is given by:

$$K := \rho_0\, \frac{\partial \psi}{\partial R} = \rho_0\, \frac{\partial \psi^p}{\partial R} = K(R) \; . \tag{143}$$

Note that, under the present hypothesis, damage does *not* affect the elastic behaviour.

7.3.2 The yield function and dissipation potential

The yield function of Gurson's theory is expressed by:

$$\Phi(\boldsymbol{\tau}, K, D) := J_2(\boldsymbol{\tau}) - \tfrac{1}{3}\left\{1 + D^2 - 2\,D\cosh\!\left[\tfrac{3\,p}{2\,(K+\tau_{y_0})}\right]\right\}(K+\tau_{y_0})^2\,, \tag{144}$$

where D is the damage variable, τ_{y_0} and $K+\tau_{y_0}$ are, respectively, the initial and current Kirchhoff uniaxial yield stress of the *matrix* material and p is the Kirchhoff pressure. Recall that the damage variable D above is the *void volume fraction*, i.e., the void volume per unit volume. As in Lemaitre's model the damage variable is allowed to range between 0 and 1, with $D=0$ corresponding to the sound (undamaged) material and $D=1$ to the fully damaged state with complete loss of load carrying capacity. Also damage growth induces softening. The function Φ recovers the standard Von Mises yield function for $D=0$ and becomes *pressure sensitive* in the presence of internal voids ($D\neq 0$).

Following the principle of maximum dissipation, the yield function is taken as the dissipation potential in Gurson's model, $\Psi\equiv\Phi$, resulting in the following plastic rule and evolution law for the hardening variable R

$$\tilde{\boldsymbol{D}}^p = \dot{\gamma}\,\frac{\partial\Phi}{\partial\boldsymbol{\tau}} = \dot{\gamma}\,\left\{\mathrm{dev}[\boldsymbol{\tau}] + \tfrac{1}{3}\,D\,(K+\tau_{y_0})\,\sinh\!\left[\tfrac{3\,p}{2\,(K+\tau_{y_0})}\right]\boldsymbol{I}\right\} \tag{145}$$

and

$$\begin{aligned}\dot{R} &= -\dot{\gamma}\,\frac{\partial\Phi}{\partial K}\\ &= \dot{\gamma}\;\frac{\tfrac{2}{3}\left\{1 + D^2 - 2\,D\cosh\!\left[\tfrac{3\,p}{2\,(K+\tau_{y_0})}\right](K+\tau_{y_0})\right\} + p\,D\sinh\!\left[\tfrac{3\,p}{2\,(K+\tau_{y_0})}\right]}{1-D}\end{aligned} \tag{146}$$

REMARK 7.9 Use of property (96) leads to the following expression for the volumetric plastic strain rate in Gurson's damage model:

$$\dot{\varepsilon}^p_v = \dot{\gamma}\,D\,(K+\tau_{y_0})\,\sinh\!\left[\tfrac{3\,p}{2\,(K+\tau_{y_0})}\right]. \tag{147}$$

This implies that Gurson's material is *plastically compressible* in the presence of voids and predicts plastic dilatancy/compression under tensile/compressive pressures. This phenomenon can not be captured by Lemaitre's theory in which damage evolution can cause softening but does not change the original (pressure insensitive) Von Mises shape of the yield surface. □

7.3.3 Damage evolution

Since the present material is assumed to be an aggregate of voids embedded in a solid matrix, the determinant J of the deformation gradient can be split additively as:

$$J = v_m + v_v\,, \tag{148}$$

where v_m and v_v are, respectively, the current matrix and voids volume per unit reference volume. By definition, Gurson's damage variable is the current volume of voids per unit current volume, i.e,

$$D := \frac{v_v}{J}\,, \tag{149}$$

so that the damage rate can be obtained by a direct application of the product rule:

$$\dot{D} = \frac{\dot{v}_v}{J} - D\,\frac{\dot{J}}{J}\,. \tag{150}$$

By assumption, the matrix material is plastically incompressible (Von Mises type). Hence, if elastic volumetric strains are neglected, the following approximation can be made:

$$\dot{v}_m = 0\,. \tag{151}$$

It should be noted that in the original derivation of Gurson's model, the matrix material is assumed rigid-plastic and the above identity holds exactly. From (148) and (151), it then follows that

$$\dot{J} = \dot{v}_m + \dot{v}_v = \dot{v}_v\,, \tag{152}$$

i.e., the macroscopic rate of volume change equals the rate of change of voids volume. At the macroscopic level, the hypothesis of negligible volumetric elastic strains allows the approximation:

$$J = J^p\,; \qquad\qquad \dot{J} = \dot{J}^p\,, \tag{153}$$

where $J^p := \det[\boldsymbol{F}^p]$. Substitution of (152) and (153) into (150) results in

$$\dot{D} = (1-D)\,\frac{\dot{J}^p}{J^p} = (1-D)\,\dot{\varepsilon}^p\,, \tag{154}$$

where use has been made of the identity:

$$\frac{\dot{J}^p}{J^p} \equiv \dot{\varepsilon}^p\,, \tag{155}$$

which follows straightforwardly from the time differentiation of the volumetric plastic strain defined by expression (94). Finally, in view of the constitutive equation (147) for the volumetric plastic flow, the evolution law for the damage variable is obtained as:

$$\dot{D} = \dot{\gamma}\,(D-D^2)\,(K+\tau_{y_0})\sinh\!\left[\tfrac{3\,p}{2\,(K+\tau_{y_0})}\right]. \tag{156}$$

The finite strain extension of Gurson's ductile damage model is summarized in Box 7.6.

7.3.4 Integration algorithm

With the particular definition (145) for the plastic flow rule, if plastic yielding occurs within the time interval of interest, the general expression (109) results, after deviatoric/volumetric decomposition of the elastic strain, in the following update formula:

$$\begin{aligned} \boldsymbol{\varepsilon}^e_{d\,n+1} &= \boldsymbol{\varepsilon}^{e\,\mathrm{trial}}_{d_{n+1}} - \Delta\gamma\;\boldsymbol{\tau}_{d\,n+1}\,,\\ \varepsilon^e_{v\,n+1} &= \varepsilon^{e\,\mathrm{trial}}_{v_{n+1}} - \Delta\gamma\,\left\{D_{n+1}\,[K(R_{n+1})+\tau_{y_0}]\sinh\!\left[\tfrac{3\,p_{n+1}}{2\,(K(R_{n+1})+\tau_{y_0})}\right]\right\}, \end{aligned} \tag{157}$$

where subscripts d and v denote, respectively, deviatoric and volumetric components. Use of the elastic law in the above expression gives:

$$\begin{aligned} \boldsymbol{\tau}_{d\,n+1} &= \tfrac{2\,G}{1+\Delta\gamma\;2\,G}\,\boldsymbol{\varepsilon}^{e\,\mathrm{trial}}_{d_{n+1}}\,,\\ p_{n+1} &= \kappa\,\varepsilon^{e\,\mathrm{trial}}_{v_{n+1}} - \Delta\gamma\,\kappa\,\left\{D_{n+1}\,[K(R_{n+1})+\tau_{y_0}]\sinh\!\left[\tfrac{3\,p_{n+1}}{2\,(K(R_{n+1})+\tau_{y_0})}\right]\right\}. \end{aligned} \tag{158}$$

(i) Multiplicative decomposition of the deformation gradient

$$\boldsymbol{F} = \boldsymbol{F}^e \boldsymbol{F}^p$$

(ii) Elasticity law

$$\boldsymbol{\tau} = \mathbb{H} : \boldsymbol{\varepsilon}^e$$

(iii) Yield function

$$\Phi(\boldsymbol{\tau}, K, D) = J_2(\boldsymbol{\tau}) - \tfrac{1}{3}\left\{1 + D^2 - 2\,D \cosh\!\left[\tfrac{3\,p}{2\,(K+\tau_{y0})}\right]\right\}(K+\tau_{y0})^2$$

(iv) Plastic flow and evolution equations for R and D

$$\tilde{\boldsymbol{D}}^p = \dot{\gamma}\left\{\mathrm{dev}[\boldsymbol{\tau}] + \tfrac{1}{3}\,D\,(K+\tau_{y0})\sinh\!\left[\tfrac{3\,p}{2\,(K+\tau_{y0})}\right]\boldsymbol{I}\right\}$$

$$\dot{R} = \dot{\gamma}\,\frac{\frac{2}{3}\left\{1+D^2-2\,D\cosh\!\left[\frac{3\,p}{2(K+\tau_{y0})}\right](K+\tau_{y0})\right\}+p\,D\sinh\!\left[\frac{3\,p}{2(K+\tau_{y0})}\right]}{1-D}$$

$$\dot{D} = \dot{\gamma}\,(D-D^2)\,(K+\tau_{y0})\sinh\!\left[\tfrac{3\,p}{2\,(K+\tau_{y0})}\right]$$

where $K := K(R)$ is a given hardening function.

Box 7.6 Finite strain extension of Gurson's ductile damage model

With introduction of the above update formula for the deviatoric Kirchhoff stress into the definition (144) of Gurson's model yield function, the following algorithmic counterpart of Φ is obtained:

$$\tilde{\Phi}(p_{n+1}, R_{n+1}, D_{n+1}, \Delta\gamma) = \left(\tfrac{2\,G}{1+2\,G\,\Delta\gamma}\right)^2 J_2(\boldsymbol{\varepsilon}^{e\ \mathrm{trial}}_{d_{n+1}}) - \tfrac{1}{3}\,a\,[K(R_{n+1})+\tau_{y0}]^2\,, \tag{159}$$

with a defined as:

$$a \equiv 1+D^2_{n+1}-2D_{n+1}\cosh\!\left[\tfrac{3\,p_{n+1}}{2[K(R_{n+1})+\tau_{y0}]}\right].$$

Thus, for the present material model, the plastic corrector stage comprises the requirement of plastic consistency by means of the algorithmic yield function above, the pressure update $(158)_2$ and the backward Euler discrete counterparts of the evolution equations (146) and (156). The return mapping algorithm is summarized in Box 7.7. Note that, here, a set of only four coupled non-linear equations has to be solved in the plastic corrector phase for any stress state. In contrast, Lemaitre's model requires, in the simplest case (plane stress state), that eight equations be solved simultaneously. In the most general situation (3-D analysis) the number of non-linear equations reaches fourteen. It is emphasized, however, that in the absence of kinematic hardening, the non-linear system can be reduced to only *two* coupled equations for any stress state. In the simplified version of Lemaitre's theory implemented by Steinmann *et al.* [107], which excludes kinematic hardening and does not account for the effect of stress triaxiality on damage evolution, the plastic corrector comprises two scalar equations.

(i) Elastic predictor

- Evaluate trial elastic stress

$$\boldsymbol{\tau}_{n+1}^{\text{trial}} := \mathbb{D} : \boldsymbol{\varepsilon}_{n+1}^{e\ \text{trial}}$$

- Check plastic consistency

$$\Phi^{\text{trial}} := J_2(\boldsymbol{\tau}_{n+1}^{\text{trial}}) - \frac{1}{3}\left\{1+D_n^2-2D_n\cosh\left[\frac{3\,p_n}{2[K(R_n)+\tau_{y_0}]}\right]\right\}[K(R_n)+\tau_{y_0}]^2$$

IF $\Phi^{\text{trial}} \leq 0$ THEN

Set $(\cdot)_{n+1} = (\cdot)_{n+1}^{\text{trial}}$ and RETURN

ELSE go to (ii)

(ii) Plastic corrector (solve the system for the scalars p_{n+1}, R_{n+1}, D_{n+1} and $\Delta\gamma$)

$$\left\{\begin{array}{l} \left(\frac{2\,G}{1+2\,G\,\Delta\gamma}\right)^2 J_2(\boldsymbol{\varepsilon}_{d_{n+1}}^{e\ \text{trial}}) - \frac{1}{3}\,a\,[K(R_{n+1})+\tau_{y_0}]^2 \\ p_{n+1} - \kappa\,\varepsilon_{v_{n+1}}^{e\ \text{trial}} + \Delta\gamma\,\kappa\,b\,[K(R_{n+1})+\tau_{y_0}] \\ D_{n+1} - D_n - \Delta\gamma\,b\,\left(D_{n+1}-D_{n+1}^2\right)[K(R_{n+1})+\tau_{y_0}] \\ R_{n+1} - R_n - \Delta\gamma\,\frac{1}{1-D_{n+1}}\left\{\frac{2}{3}a\,[K(R_{n+1})+\tau_{y_0}] + b\,p_{n+1}\,D_{n+1}\right\} \end{array}\right\} = \left\{\begin{array}{c} 0 \\ 0 \\ 0 \\ 0 \end{array}\right\}$$

where $a \equiv 1+D_{n+1}^2-2D_{n+1}\cosh\left[\frac{3\,p_{n+1}}{2[K(R_{n+1})+\tau_{y_0}]}\right]$ and $b \equiv \sinh\left[\frac{3\,p_{n+1}}{2[K(R_{n+1})+\tau_{y_0}]}\right]$.

(iii) Update $\boldsymbol{\varepsilon}^e$ and $\boldsymbol{\tau}$

$$\boldsymbol{\varepsilon}_{n+1}^{e} := \frac{1}{1+2G\,\Delta\gamma}\,\boldsymbol{\varepsilon}_{d_{n+1}}^{e\ \text{trial}} + \frac{p_{n+1}}{\kappa}\,\boldsymbol{I}$$

$$\boldsymbol{\tau}_{n+1} := \frac{2G}{1+2G\,\Delta\gamma}\,\boldsymbol{\varepsilon}_{d_{n+1}}^{e\ \text{trial}} + p_{n+1}\,\boldsymbol{I}$$

(iv) RETURN

Box 7.7 Small strain return mapping algorithm for Gurson's model

It is remarked that, as in Lemaitre's model, instabilities have been detected in the Newton-Raphson scheme adopted to solve the equations of the plastic corrector phase of Box 7.7. To improve the Newton method convergence behaviour, a line search procedure (as suggested by Steinmann *et al.* [107]) has been added to the standard Newton algorithm.

7.3.5 The small strain consistent tangent operator

If the current state lies in the elastic domain or it is on the yield surface and elastic unloading is assumed to occur, the tangent operator consistent with the algorithmic stress update function:

$$\tilde{\boldsymbol{\tau}}\,(R_n, D_n, \varepsilon_{n+1}^{e\ \text{trial}})\,, \tag{160}$$

defined by Box 7.7, is simply the standard small strain elasticity tensor:

$$\tilde{\mathbb{D}} = \mathbb{D}. \tag{161}$$

If, on the other hand, plastic loading is assumed to occur, the procedure described for Lemaitre's model is followed. The system of equations of the plastic corrector phase is differentiated at the converged state resulting in the identity:

$$\begin{bmatrix} A_{1,\Delta\gamma} & A_{1,p} & A_{1,D} & A_{1,R} \\ A_{2,\Delta\gamma} & A_{2,p} & A_{2,D} & A_{2,R} \\ A_{3,\Delta\gamma} & A_{3,p} & A_{3,D} & A_{3,R} \\ A_{4,\Delta\gamma} & A_{4,p} & A_{4,D} & A_{4,R} \end{bmatrix} \begin{bmatrix} \mathrm{d}\Delta\gamma \\ \mathrm{d}p_{n+1} \\ \mathrm{d}D_{n+1} \\ \mathrm{d}R_{n+1} \end{bmatrix} = \begin{bmatrix} -A_{1,\varepsilon^{e\,\mathrm{trial}}_{d_{n+1}}} : \mathrm{d}\boldsymbol{\varepsilon}^{e\,\mathrm{trial}}_{d_{n+1}} \\ -A_{2,\varepsilon^{e\,\mathrm{trial}}_{v_{n+1}}}\, \mathrm{d}\varepsilon^{e\,\mathrm{trial}}_{v_{n+1}} \\ 0 \\ 0 \end{bmatrix}, \tag{162}$$

where $A_{1,\Delta\gamma}$, $A_{1,p}$,... denote the derivatives of the plastic corrector system components. Inversion of the above expression then leads to:

$$\begin{bmatrix} \mathrm{d}\Delta\gamma \\ \mathrm{d}p_{n+1} \\ \mathrm{d}D_{n+1} \\ \mathrm{d}R_{n+1} \end{bmatrix} = \begin{bmatrix} C_{11} & C_{12} & C_{13} & C_{14} \\ C_{21} & C_{22} & C_{23} & C_{24} \\ C_{31} & C_{32} & C_{33} & C_{34} \\ C_{41} & C_{42} & C_{43} & C_{44} \end{bmatrix} \begin{bmatrix} -A_{1,\varepsilon^{e\,\mathrm{trial}}_{d_{n+1}}} : \mathrm{d}\boldsymbol{\varepsilon}^{e\,\mathrm{trial}}_{d_{n+1}} \\ -A_{2,\varepsilon^{e\,\mathrm{trial}}_{v_{n+1}}}\, \mathrm{d}\varepsilon^{e\,\mathrm{trial}}_{v_{n+1}} \\ 0 \\ 0 \end{bmatrix}, \tag{163}$$

which provides the tangent relations between the system variables ($\Delta\gamma$, p, D and R) and the system input $\boldsymbol{\varepsilon}^{e\,\mathrm{trial}}_{n+1}$. Note that, since the stress tensor is one of the system variables in Lemaitre's model, the tangent operator $\tilde{\boldsymbol{h}}$ in that case is obtained directly from the inversion of the system derivative. Here, the consistent tangent operator can be obtained by differentiating the stress update formula of item (iii) of Box 7.7, which gives:

$$\mathrm{d}\boldsymbol{\tau}_{n+1} = \tfrac{2G}{1+2G\,\Delta\gamma}\, \mathrm{d}\boldsymbol{\varepsilon}^{e\,\mathrm{trial}}_{d_{n+1}} - \left(\tfrac{2G}{1+2G\,\Delta\gamma}\right)^2 \mathrm{d}\Delta\gamma\;\; \boldsymbol{\varepsilon}^{e\,\mathrm{trial}}_{d_{n+1}} + \mathrm{d}p_{n+1}\, \boldsymbol{I}. \tag{164}$$

Then, substitution of $\mathrm{d}\Delta\gamma$ and $\mathrm{d}p_{n+1}$ by the relations given in (163) and use of the identities:

$$A_{1,\varepsilon^{e\,\mathrm{trial}}_{d_{n+1}}} = \left(\tfrac{2G}{1+2G\,\Delta\gamma}\right)^2 \boldsymbol{\varepsilon}^{e\,\mathrm{trial}}_{d_{n+1}}; \qquad\qquad A_{2,\varepsilon^{e\,\mathrm{trial}}_{v_{n+1}}} = -\kappa,$$

results, after some straightforward manipulations, in the following expression for the elastoplastic consistent tangent operator:

$$\begin{aligned} \tilde{\boldsymbol{h}} := \frac{\mathrm{d}\boldsymbol{\tau}_{n+1}}{\mathrm{d}\boldsymbol{\varepsilon}^{e\,\mathrm{trial}}_{n+1}} = g\,[\boldsymbol{I} - \tfrac{1}{3}\,\boldsymbol{I}\otimes\boldsymbol{I}] + g^{2}\,\boldsymbol{\varepsilon}^{e\,\mathrm{trial}}_{d_{n+1}} \otimes [C_{11}\,g^2\,\boldsymbol{\varepsilon}^{e\,\mathrm{trial}}_{d_{n+1}} - C_{12}\,\kappa\,\boldsymbol{I}] \\ - \boldsymbol{I}\otimes[C_{21}\,g^2\,\boldsymbol{\varepsilon}^{e\,\mathrm{trial}}_{d_{n+1}} - C_{22}\,\kappa\,\boldsymbol{I}], \end{aligned} \tag{165}$$

where

$$g \equiv \left(\tfrac{2G}{1+2G\,\Delta\gamma}\right).$$

Note that, as in Lemaitre's model, the resulting tangent operator $\tilde{\boldsymbol{h}}$ is generally *unsymmetric*.

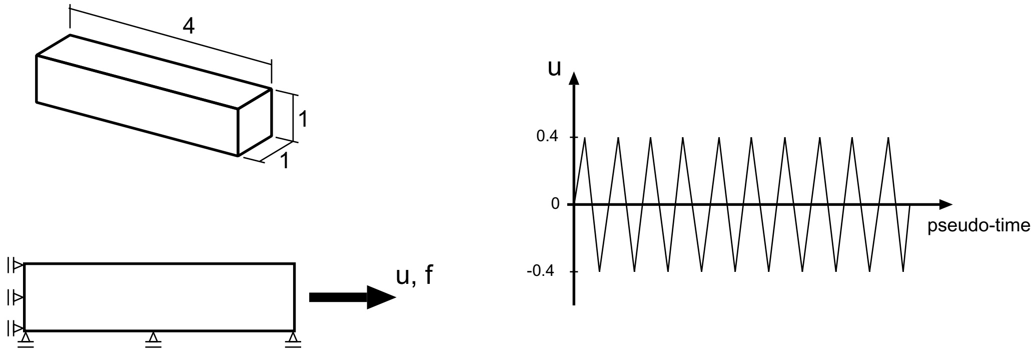

Figure 14. The model problem. Geometry and loading

7.4 Numerical Examples

EXAMPLE 7.1 The model problem. The finite element analysis of a uniaxially stressed bar subjected to cyclic loading is carried out in this example. This problem serves to highlight the fundamental differences that exist between the two ductile damage models described above. The dimensions of the bar and the boundary conditions are shown in Figure 14. The load consists of ten compression/extension cycles obtained by imposing, at one end of the bar, the displacement function u illustrated in the graph of Figure 14. The extreme displacements during each cycle correspond to $+10\%$ and -10% straining of the bar. The boundary conditions ensure that the bar is subjected to a uniform state of uniaxial stress. The simulation is executed with Lemaitre's and Gurson's damage models. The material parameters are:

$$E = 210000\,; \qquad \nu = 0.3\,; \qquad \tau_{y_0} = 520,$$

with the following damage growth constants required by Lemaitre's model:

$$r = 1.0\,; \qquad s = 3.5\,.$$

For the Gurson model simulation, an initial voids fraction:

$$D_0 = 0.05\,,$$

is assumed. No hardening is taken into account in the present simulations so that, for both models,

$$K(R) \equiv 0,$$

and, in addition, the constants a and b of Lemaitre's model are set to zero. Two three-noded triangular elements of unit thickness (under plane stress) are used along the longitudinal axis of the bar in the simulation with Lemaitre's model. For the Gurson model, a single eight node tri-linear brick is employed to discretize the bar. If a full 3-D discretization of the bar with a sufficiently fine mesh were adopted, issues such as strain localization would arise. Nevetheless, the coarse meshes adopted here are adequate for the purpose of the present analysis, whose objective is to study the behaviour of the two models under uniform uniaxial stress states.

The axial reaction force f obtained in the simulations is plotted in Figure 15 against the imposed displacement u. Figures 15.a and b show, respectively, the results for Lemaitre's and Gurson's model. For Lemaitre's model simulation, the reaction force is progressively

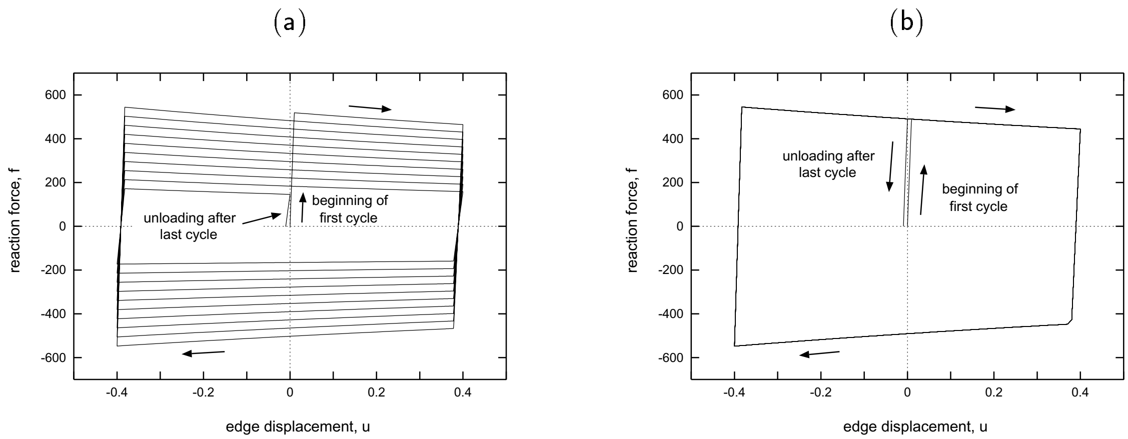

Figure 15. The model problem. Cyclic extension/compression without hardening. Force-displacement curves obtained for: (a) Lemaitre's model and; (b) Gurson's model

	Lemaitre		Gurson	
cycle	$u = 0.4$	$u = -0.4$	$u = 0.4$	$u = -0.4$
1	0.0171	0.0531	0.0535	0.0464
2	0.0890	0.1250	0.0535	0.0464
3	0.1610	0.1970	0.0535	0.0464
4	0.2330	0.2690	0.0536	0.0464
5	0.3050	0.3410	0.0536	0.0465
6	0.3770	0.4130	0.0536	0.0465
7	0.4490	0.4850	0.0536	0.0465
8	0.5210	0.5570	0.0536	0.0465
9	0.5930	0.6290	0.0536	0.0465
10	0.6650	0.7010	0.0536	0.0465

Table 7.1 The model problem. Cyclic extension/compression without hardening. Damage variable evolution

decreasing over the cycles. This is a direct result of damage accumulation and consequent material softening. Also as a result of damage accumulation, the progressive degradation of the elastic modulus makes the slope of the f–u curve smaller when the load is reversed after each cycle. This is particularly evident during the elastic unloading after the end of the last cycle. In contrast, the reaction forces obtained with Gurson's model are practically constant over the cycles. Indeed, for this model, damage growth resulting from the extension of the bar is compensated by damage healing that occurs during compression. Essentially, in this case, no cumulative damage occurs and the damage variable returns to its initial value after each cycle. This does not correspond to the experimental observation of progressive damaging in cyclic tests with ductile metals. The use of Gurson's model under such a condition would lead to erroneous predictions. The values of the damage variable obtained at the extreme displacements for each cycle are shown in Table 7.1 for both material models. Note that only a very small variation of damage occurs between the states of maximum extension and maximum compression for the present simulation with Gurson's model. Thus, the corresponding softening/hardening of the material has little influence on the overall response of the bar and the apparent softening/hardening

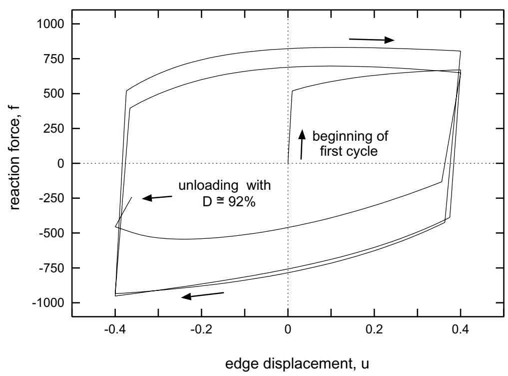

Figure 16. The model problem. Cyclic extension/compression with Lemaitre's model including damage, isotropic and kinematic hardening. Force-displacement curve

observed during extension/compression in Figure 15.b is mostly due the geometrical effect of reduction/increase of the cross section of the bar.

To illustrate the generality of Lemaitre's model, a similar simulation including isotropic and kinematic hardening evolution is also carried out. In this case, the same material parameters employed in the simulation above with Lemaitre's model are used, except that the hypothesis of perfect plasticity is replaced by the saturation hardening law:

$$K(R) = R_\infty[1 - \exp(-\gamma R)],$$

with $R_\infty = 4305$ and $\gamma = 0.2$, and the kinematic hardening evolution constants are taken as:

$$a = 2\,500\,; \qquad\qquad b = 2\,0.$$

These constants (with E, τ_{y_0}, R_∞, a and s measured in MPa) have been used by Benallal *et al.* [6] in small strain simulations. Figure 16 shows the force-displacement curve obtained. The interaction of complex phenomena such as damage growth and non-linear isotropic and kinematic hardening in the finite strain range is clearly illustrated. In this case, due to the rapid evolution of damage, the simulation is terminated before the third load cycle is completed. In the last elastic unloading, the damage variable is approximately 92% and failure is imminent.

EXAMPLE 7.2 Stretching of a thin perforated rectangular plate. This example presents the numerical simulation of a thin perforated plate subjected to stretching along its longitudinal axis. As in the previous example, both Lemaitre's and Gurson's model are used for comparison. The geometry, boundary conditions and material parameters are shown in Figure 17. In the simulation with Lemaitre's model, a mesh containing 576 three-node constant strain triangular plane stress elements was used in the finite element approximation. In Gurson's model simulation, a mesh of 288 eight-node *F-bar* brick elements is employed (refer to [102] for a full description of this element). Figures 18 and 19 show the meshes in their initial configuration as well as in their final deformed configurations with $U_2 = 2.65$. In both figures, the damage variable field obtained at the end of the simulation is plotted on the deformed mesh. In both cases it can be seen that, due to strain localization, the plastic-damage process is confined to a band along the narrowest section of the plate and maximum damage is observed near its internal boundary. The peak values of the damage

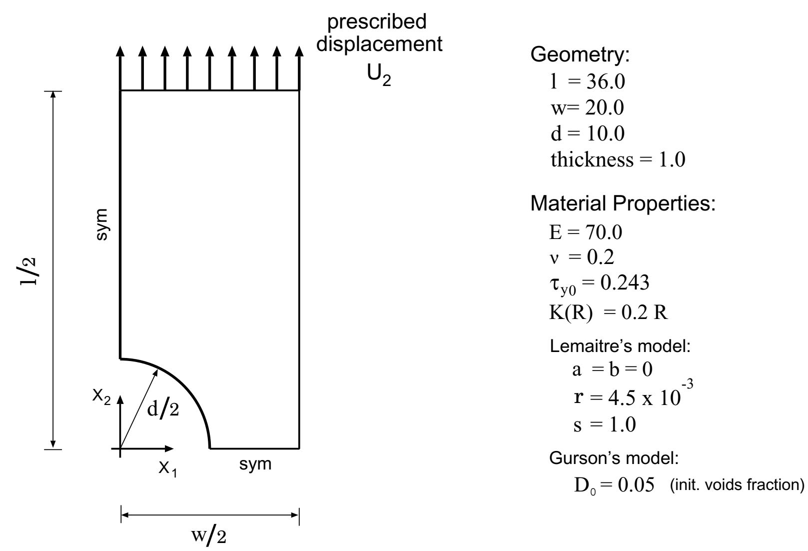

Figure 17. Perforated plate. Geometry and material parameters

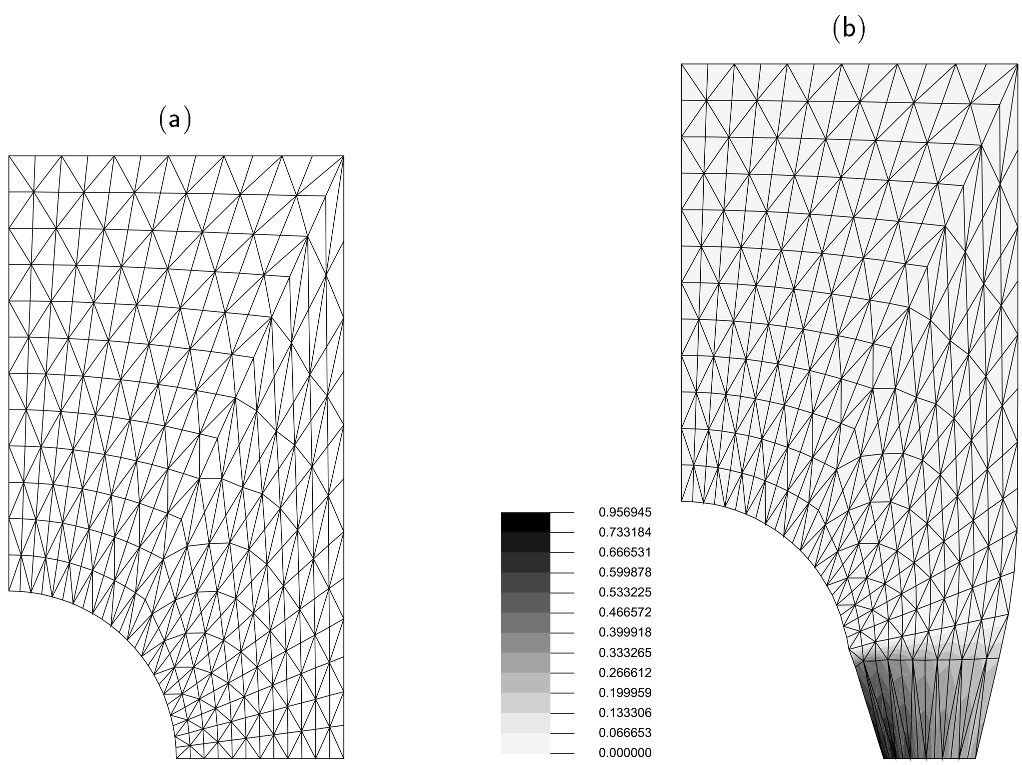

Figure 18. Perforated plate. Finite elemen t meshes for Lemaitre's model simulation. (a) Initial configuration; and (b) Damage con tour plot on deformed configuration at $U_2 = 2.65$

variable are approximately 96% and 34%, respectively, for the sim ulations with Lemaitre's and Gurson's model.

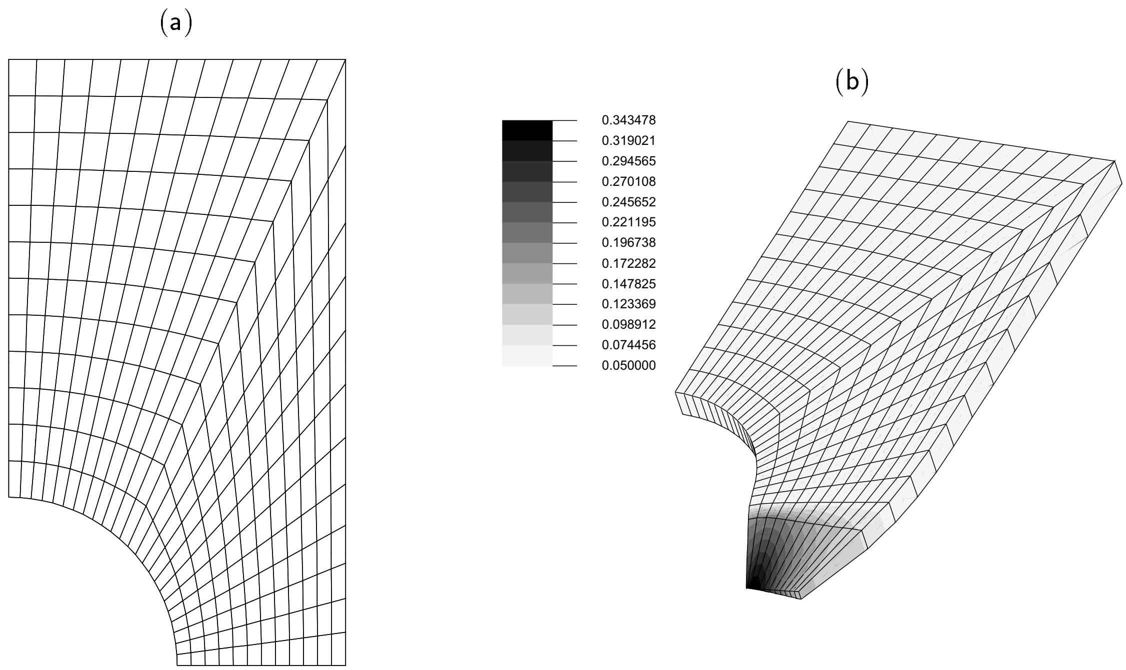

Figure 19. Perforated plate. Finite element meshes for Gurson's model simulation. (a) Initial configuration. Frontal view; and (b) Damage contour plot on deformed configuration at $U_2 = 2.65$

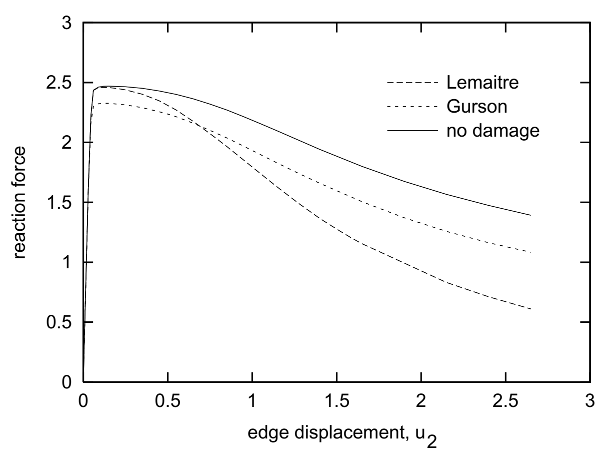

Figure 20. Perforated plate. Reaction-displacement curves

The reaction forces obtained on the restrained edge during the loading process in each simulation are compared with the result presented in [82] where the purely elasto-plastic model was used (this result is reproduced here by setting $r = \infty$ in Lemaitre's model or $D_0 = 0$ in Gurson's model, i.e, no damage evolution). The reaction-displacement curves are plotted in Figure 20. The influence of damage in the global behaviour of the structure is clearly shown. Both damage models predict a drop in reaction forces when compared to the purely plastic theory. This is an obvious consequence of material softening induced by damage growth at the local level. The lower force corresponding to plastic yielding observ in the simulation with Gurson's theory is due to the initial value of the damage variable, set to $D_0 = 5\,\%$. Recall that, since no mechanism of voids nucleation is incorporated in this theory, a non-zero initial voids volume ratio is required to produce damage evolution. Inclusion of a voids nucleation contribution to damage growth (such as the nucleation laws employed by Tvergaard [114] and Tvergaard and Needleman [116]) would allow damage growth with zero initial voids ratio. Also, it should be noted that, as a result of the relatively slow damage growth predicted by Gurson's theory, the final reaction force obtained is higher than that predicted by Lemaitre's model. Acceleration of damage growth could be easily incorporated by modifying Gurson's macroscopic yield criterion as suggested by Tvergaard [113, 114, 115].

To reach the end of the loading process ($U_2 = 2.65$), 24 increments were applied in both simulations. The tolerance for convergence in the overall Newton-Raphson procedure was 10^{-6} in the euclidean norm of residual forces normalized by the external forces. In both cases, an average of about 5 iterations per increment was necessary for convergence. Table 7.2 shows the residuals during global Newton-Raphson iterations for typical increments at different stages of the process. The high rates of convergence achieved by means of the consistent linearization of the incremental boundary value problem are significant.

	Lemaitre		Gurson	
iteration	incr. 6	incr. 18	incr. 6	incr. 18
1	0.131046E-01	0.881843E-01	0.325069E+01	0.405738E+02
2	0.329877E-02	0.746851E+00	0.239389E+00	0.254875E+01
3	0.381935E-03	0.414897E-02	0.118506E-01	0.502956E-01
4	0.397149E-06	0.515920E-04	0.100894E-05	0.682371E-04
5	0.102422E-09	0.964154E-08	0.628288E-10	0.348303E-09

Table 7.2 Perforated plate. Residuals norm ratio

EXAMPLE 7.3 Thin sheet metal forming application. This example considers the simulation of a thin sheet metal forming process, in which Lemaitre's model is employed to account for damage evolution. The problem consists of a thin circular sheet stretched by a rigid spherical punch. The sheet lies on a rigid cylindrical die and its edge is assumed clamped. The geometry and material parameters (with exception of the damage evolution parameter r) are shown in Figure 21. Due to the symmetry of the problem, only one quarter of the domain is considered in the finite element simulation. A mesh with 736 three-noded membrane elements is used in the discretization of the sheet. The algorithm described in [83] is employed in the treatment of the frictional contact between the sheet, punch and die. The surfaces of the punch and the die are discretized respectively by 2145 and 612 flat triangular elements. Figure 22 shows the finite element meshes used.

Four different damage evolution parameters are considered: $r = \infty$, $r = 10, 5$ and $2.5 N/mm^2$. The results for $r = \infty$ correspond to the original elastoplastic model (with no damage evolution) and were taken from reference [84]. Figure 23.a shows the uniaxial stress-strain curves for each r. The corresponding punch reaction forces obtained in the simulations are presented in Figure 23.b. The maximum value of the punch reaction was obtained at $d_p = 3$ 55, 32.5, 29.5 and $26.5 mm$ respectively for $r = \infty$, 10, 5 and $2.5 N/mm^2$. As expected, the use of softer materials (lower values of r) reduces the maximum punch reaction attained during the process.

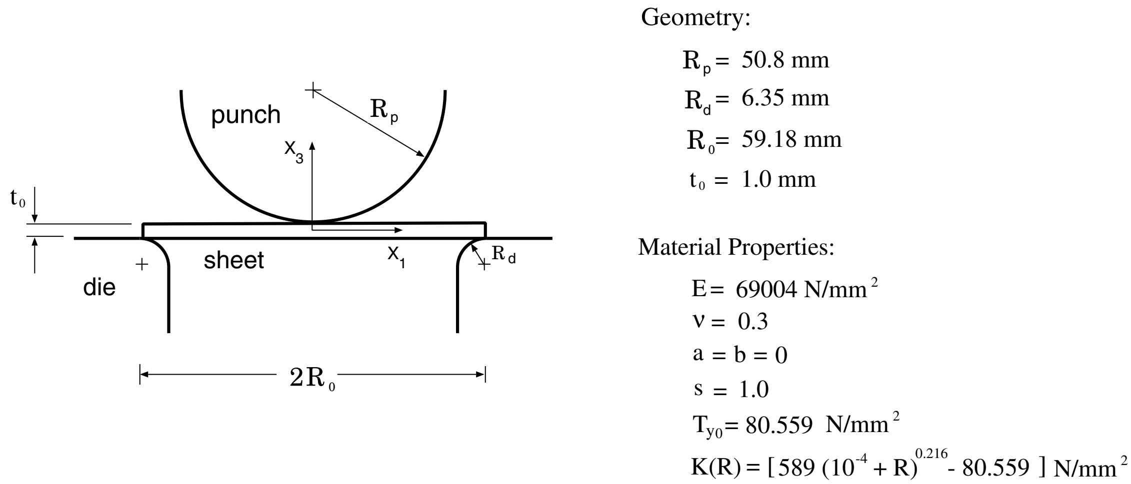

Figure 21. Thin sheet metal forming. Tool/workpiece configuration

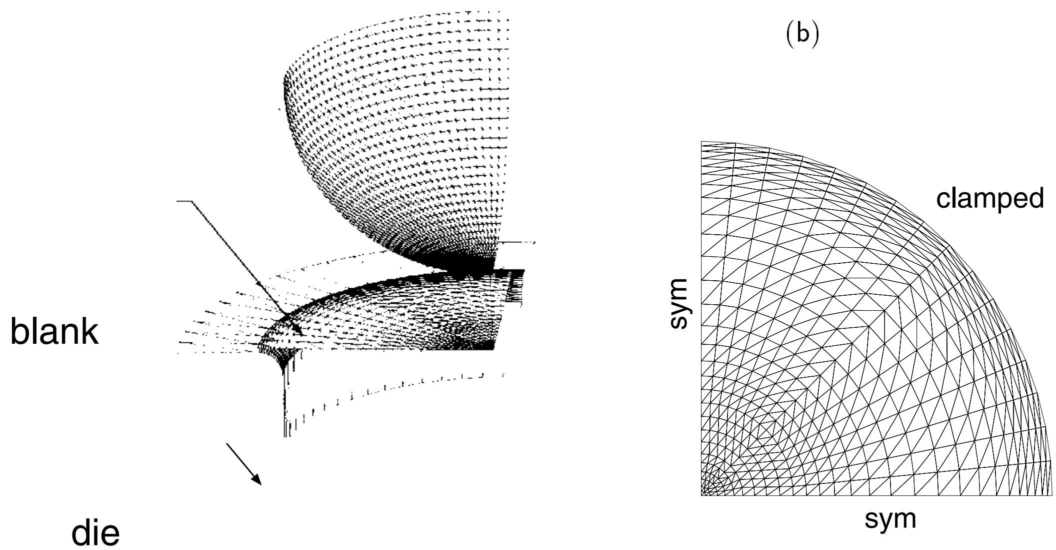

Figure 22. Thin sheet metal forming. (a) Finite element discretization of the sheet, die and punch; and, (b) Finite element mesh and boundary conditions for the sheet

Figure 24 shows the distribution of radial thickness along the sheet radius obtained for each damage parameter r considered. The results are plotted for 10, 20, 30 and $40mm$ of punch displacement (d_p). With $r = 2.5N/mm^2$, the numerical limit of the damage variable (99.99%) was reached for $d_p = 3\,009mm$ when the computations were stopped. Thus, in this case, results are shown only for $d_p = 10$, 20 and $30mm$

In the present computations, the convergence tolerance for the global Newton-Raphson scheme was 10^{-5} in the euclidean norm of residual forces normalized by the external forces. For the local N-R procedure (plastic corrector phase of the stress integration algorithm) the convergence tolerance used was 10^{-10} in the residual vector norm. The total number

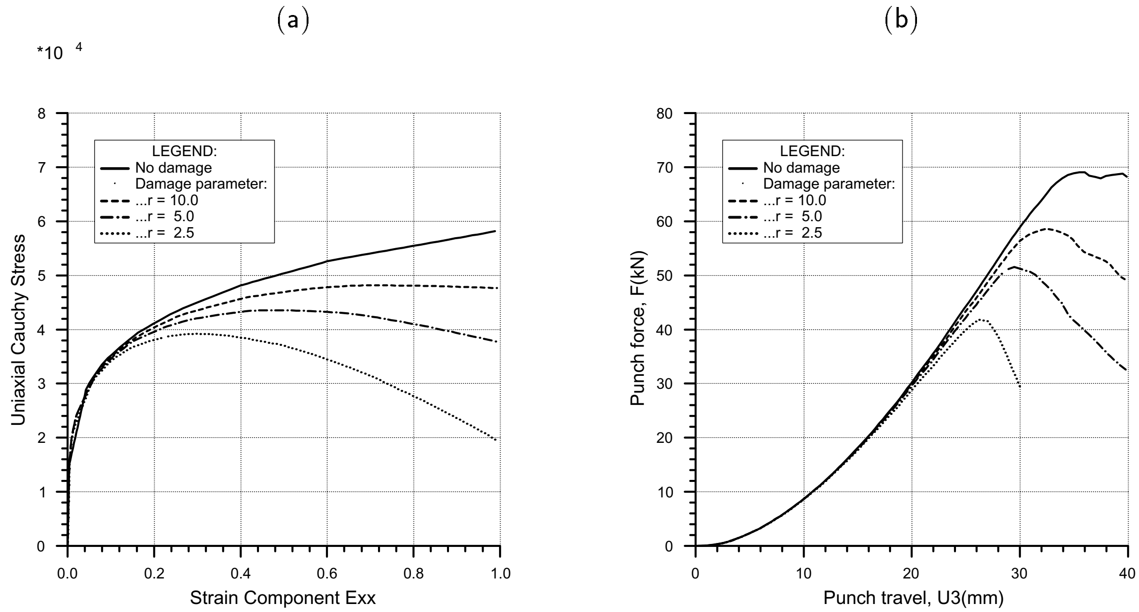

Figure 23. Thin sheet metal forming. (a) Uniaxial stress–strain curves; and (b) Reaction forces on punch

of increments and global Newton-Raphson iterations required to reach the final deformed configuration ($d_p = 40mm$) as well as the number of increments to attain the maximum punch reaction are shown in Table 7.3 for each parameter r.

Damage parameter r	∞^a	10	5	2.5
Total number of load increments	183	161	181	98^b
Total number of global N-R iterations	973	961	999	530^b
Number of increments to attain max.reaction on punch	147	108	96	63

[a]original elasto-plastic model
[b]results up to $d_p = 30.09mm$

Table 7.3 Increments and Newton-Raphson iterations

It is noted that the inclusion of fully coupled elasto-plastic damage constitutive equations did not affect the performance of the original model. For all cases the results were obtained in a reasonable number of increments.

Table 7.4 presents the residuals during the global Newton-Raphson iterations for typical increments at different values of punch displacement. It corresponds to the simulation with $r = 5N/mm^2$. As in the previous example, high rates of convergence are observed as a result of the consistent linearization of the incremental boundary value problem.

It can be seen in Figures 24 that the softening effect of damage growth triggered strain localization at lower values of punch displacement. It also moved the strain localization point towards the centre of the sheet.

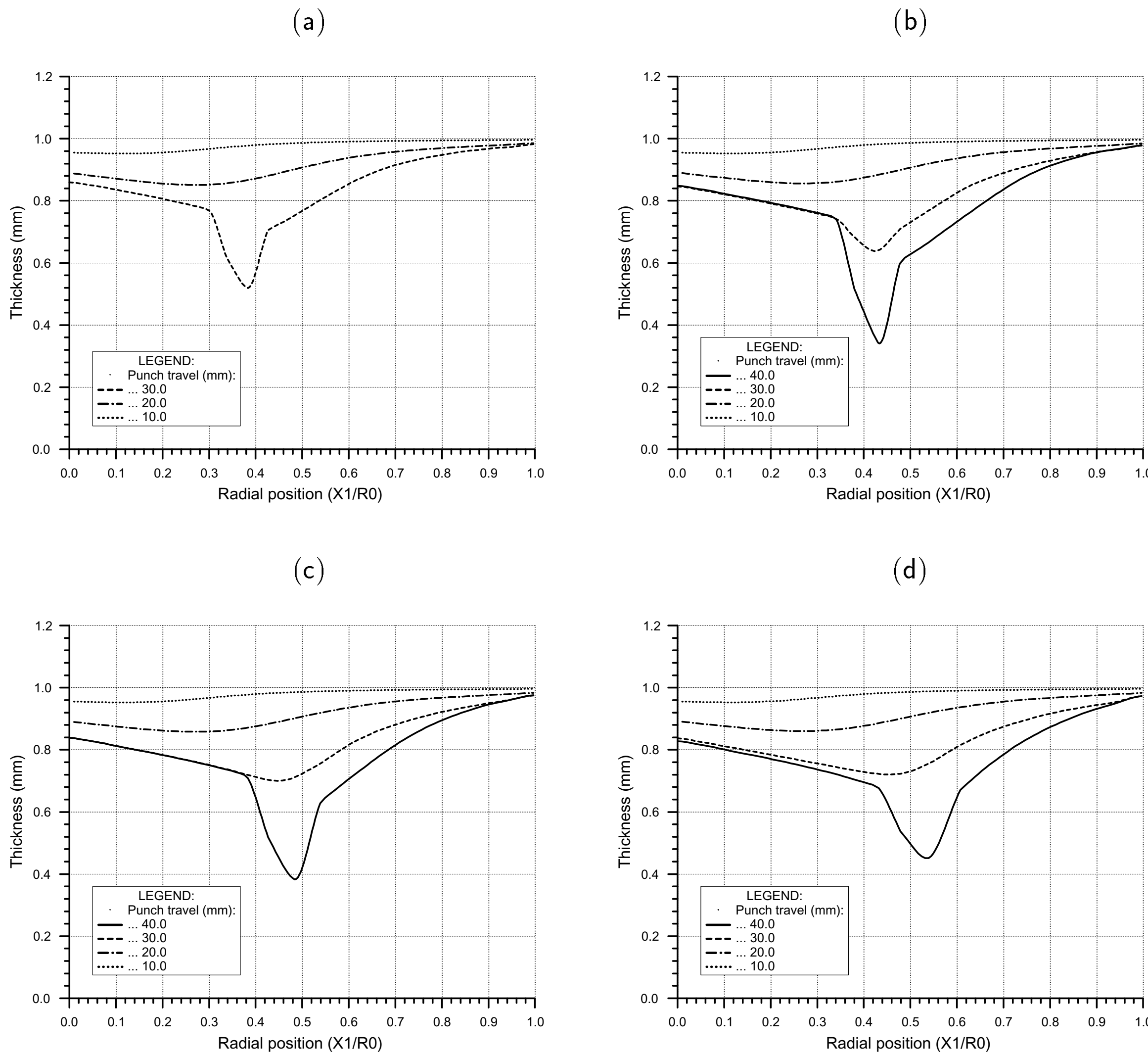

Figure 24. Thin sheet metal forming. Thickness distributions plotted over the initial configuration. *Damage p arameters:* (a) $r = 2.5$; (b) $r = 5$; (c) $r = 10$; and (d) No damage

n_{iter}	$d_p = 10mm$	$d_p = 20mm$	$d_p = 30mm$	$d_p = 40mm$
1	0.475099E-01	0.446032E-01	0.415027E-01	0.347834E+00
2	0.473760E-01	0.574047E-01	0.558268E-01	0.145966E+00
3	0.114935E-01	0.147966E-01	0.147191E-01	0.142490E-01
4	0.210567E-02	0.727378E-02	0.529641E-01	0.453278E-03
5	0.163940E-04	0.673537E-03	0.604233E-03	0.139017E-04
6	0.607955E-08	0.779331E-05	0.114828E-05	0.435165E-08

Table 7.4 Thin sheet metal forming. Residuals norm ratio

8 SUMMARY AND CONCLUSIONS

Based on Continuum Damage Mechanics and on a fully implicit finite element scheme set on the spatial configuration, a general framework for constitutive modelling and numerical simulation of internal damage in finitely deformed solids has been described. Aspects of the micromechanical characterization of damage and its representation within the context of continuum thermodynanics have been discussed and a brief historical review of Continuum Damage Mechanics has been presented. On the numerical side, a general procedure for the simulation of finite strain problems involving dissipative material has been described in detail. In this context, issues related to the derivation of algorithms for integration of path dependent constitutive equations have been discussed and particular attention has been focused on the derivation of the corresponding consistent tangent operators – essential for the overall efficiency of the Newton-Raphson procedure for solution of the implicit finite element equations.

Within the described framework, three particular models have been formulated: A model for elastic damage in highly filled polymers and finite strain extensions to Lemaitre's and Gurson's ductile damage theories. Numerical examples have demonstrated the efficiency of the adopted scheme in the simulation of complex phenomena such as the Mullin's effect in rubbery polymers or combined effects of damage evolution, isotropic and kinematic hardening in ductile metals in the finite strain range.

Good qualitative agreement has been found between the numerical results presented and the actual behaviour of damaging materials under finite strain conditions. This, in conjunction with the overall efficiency of the computational scheme, indicates the present constitutive-numerical framework to be an attractive alternative for incorporation of material deterioration effects into the simulation of large scale finite strain industrial problems.

REFERENCES

1 D.H. Allen, E. Harris and S.E. Groves (1987), "A thermomechanical constitutive theory for elastic composites with distributed damage – I. Theoretical development and II. Application to matrix cracking in laminated composites", *Int. J. Solids Struct.*, **23**(9), 1301–1338.

2 R.G.C. Arridge (1985), *An Introduction to Polymer Mechanics*, Taylor & Francis, London.

3 M. Basista, D. Krajčinović, and D. Šumarac (1992), "Micromechanics, phenomenology and statistics of brittle deformation", In D.R.J. Owen, E. Oñate, and E. Hinton, editors, *Proceedings of the Third International Conference on Computational Plasticity: Fundamentals and Applications – Barcelona, April 1992*, pages 1479–1490, Swansea, Pineridge Press.

4 K.J. Bathe (1982), *Finite Element Procedures in Engineering Analysis*, Prentice-Hall, Englewood Cliffs, New Jersey.

5 M.F. Beatty (1987), "Topics in finite elasticity: Hyperelasticity of rubber, elastomers, and biological tissues – with examples", *Appl. Mech. Rev.*, **40**, 1699–1734.

6 A. Benallal, R. Billardon, and I. Doghri (1988), "An integration algorithm and the corresponding consistent tangent operator for fully coupled elastoplastic and damage equations", *Comm. Appl. Num. Meth*, **4**, 731–740.

7 F. Bueche (1960), "Molecular basis for the Mullins effect", *J. Appl. Poly. Sci*, **4**(10), 107–114.

8 F. Bueche (1961), "Mullins effect and rubber-filler interaction", *J. Appl. Poly. Sci.*, **5**(15), 271–281.

9 J.L. Chaboche (1978), "Description thermodynamique et phénoménologique de la viscoplasticité cyclique avec endommagement", Technical Report 1978–3, Office National d'Etudes et de Recherches Aérospatiales.

10 J.L. Chaboche (1981), "Continuous damage mechanics – a tool to describe phenomena before crack initiation", *Nuclear Engng. Design*, **64**, 233–247.

11 J.L. Chaboche (1984), "Anisotropic creep damage in the framework of continuum damage mechanics", *Nuclear Engng. Design*, **79**, 309–319.

12 J.L. Chaboche (1988), "Continuum damage mechanics: Part I – General concepts and Part II – Damage growth, crack initiation and crack growth", *J. Appl. Mech.*, **55**, 59–72.

13 C.L. Chow and T.J. Lu (1989), "On evolution laws of anisotropic damage", *Engng. Fract. Mech.*, **34**(3), 679–701.

14 B.D. Coleman (1964), "Thermodynamics of materials with memory", *Arch. Rat. Mech. Anal.*, **17**, 1–46.

15 B.D. Coleman and M.E. Gurtin (1967), "Thermodynamics with internal state variables", *J. Chemical Physics*, **47**(2), 597–613.

16 B.D. Coleman and W. Noll (1963), "The thermodynamics of elastic materials with heat conduction and viscosity", *Arch. Rat. Mech. Anal.*, **13**, 167–178.

17 J.P. Cordebois (1983), *Criteres d'Instabilite Plastique et Endommagement Ductile en Grandes Deformations*, Thèse de Doctorat d'Etat, Univ. Pierre et Marie Curie.

18 J.P. Cordebois and F. Sidoroff (1979), "Damage induced elastic anisotropy", In *Euromech 115 – Villard de Lans – Juin 1979*, pages 761–774.

19 J.P. Cordebois and F. Sidoroff (1982), "Endomagement anisotrope en élasticité et plasticité", *Journal de Mećanique Théorique et Appliquée*, pages 45–60. Numéro spécial.

20 M.A. Crisfield (1991), *Non-linear Finite Element Analysis of Solids and Structures, Volume 1: Essentials*, John Wiley & Sons, Chichester.

21 A. Cuitiño and M. Ortiz (1992), "A material-independent method for extending stress update algorithms from small-strain plasticity to finite plasticity with multiplicative kinematics", *Engng. Comp.*, **9**, 437–451.

22 I. Doghri (1995), "Numerical implementation and analysis of a class of metal plasticity models coupled with ductile damage", *Int. J. Num. Meth. Engng.*, **38**, 3403–3431.

23 A. Dragon and A. Chihab (1985), "On finite damage: Ductile fracture-damage evolution", *Mech. of Materials*, **4**, 95–106.

24 L. Engel and H. Klingele (1981), *An Atlas of Metal Damage*, Wolfe Science Books.

25 A.L. Eterovic and K.-J. Bathe (1990), "A hyperelastic based large strain elasto-plastic constitutive formulation with combined isotropic-kinematic hardening using the logarithmic stress and strain measures", *Int. J. Num. Meth. Engng.*, **30**, 1099–1114.

26 G.U. Fonseka and D. Krajčinović (1981), "The continuous damage theory of brittle materials – Part 2: Uniaxial and plane response modes", *J. Appl. Mech.*, **48**, 816–824.

27 J.C. Gelin and A. Danescu (1992), "Constitutive model and computational strategies for finite-strain elasto-plasticity with isotropic or anisotropic ductile damage", In D.R.J. Owen, E. Oñate, and E. Hinton, editors, *Proceedings of the Third International Conference on Computational Plasticity: Fundamentals and Applications – Barcelona, April 1992*, pages 1413–1424, Swansea, Pineridge Press.

28 J.C. Gelin and A. Mrichcha (1992), "Computational procedures for finite strain elasto plasticity with isotropic damage", In D.R.J. Owen, E. Oñate, and E. Hinton, editors, *Proceedings of the Third International Conference on Computational Plasticity: Fundamentals and Applications – Barcelona, April 1992*, pages 1401–1412, Swansea, Pineridge Press.

29 O.A.J. Gonçalves F° and D.R.J. Owen (1983), "Creep and viscoelastic brittle rupture of structures by the finite element method", In B. Wilshire and D.R.J. Owen, editors, *Engineering Approach to High Temperature Design*, Swansea, Pineridge Press.

30 S. Govindjee and J. Simo (1991), "A micro-mechanically based continuum damage model for carbon black-filled rubbers incorporating Mullins' effect", *J. Mech. Phys. Solids*, **39**(1), 87–112.

31 S. Govindjee and J.C. Simo (1992), "Mullins' effect and the strain amplitude dependence of the storage modulus", *Int. J. Solids Structures*, **20**, 1737–1751.

32 A.L. Gurson (1977), "Continuum theory of ductile rupture by void nucleation and growth – Part I: Yield criteria and flow rule for porous media", *J. Engng. Mat. Techn.*, **99**, 2–15.

33 M.E. Gurtin (1981), *An Introduction to Continuum Mechanics*, Academic Press.

34 M.E. Gurtin and E.C. Francis (1981), "Simple rate-independent model for damage", *J. Spacecraft*, **18**(3), 285–286.

35 M.E. Gurtin and K. Spear (1983), "On the relationship between the logarithmic strain rate and the stretching tensor", *Int. J. Solids Struct.*, **19**(5), 437–444.

36 M.E. Gurtin and O.W. Williams (1967), "An axiomatic foundation of continuum thermodynamics", *Arch. Rat. Mech. Anal.*, **27**, 83–117.

37 H. Hencky (1933), "The elastic behavior of vulcanized rubber", *J. Appl. Mech.*, **1**, 45–53.

38 G. Herrmann and J. Kestin (1989), "On thermodynamic foundations of a damage theory in elastic solids", In J. Mazars and Z.P. Bazant, editors, *Cracking and Damage, Strain Localization and Size Effect*, pages 228–232, Amsterdam, Elsevier.

39 R. Hill (1950), *The Mathematical Theory of Plasticity*, Oxford Univ. Press, London.

40 A. Hoger (1986), The material time derivative of the logarithmic strain. *Int. J. Solids Struct.*, **22**(9), 1019–1032.

41 A. Hoger (1987), "The stress conjugate to logarithmic strain", *Int. J. Solids Struct.*, **23**(12), 1645–1656.

42 H. Horii and S. Nemat-Nasser (1983), "Overall moduli of solids with microcracks: Load induced anisotropy", *J. Mech. Phys. Solids*, **31**(2), 155–171.

43 J. Janson (1978), "A continuous damage approach to the fatigue process", *Engng. Fract. Mech.*, **10**, 651–657.

44 L.M. Kachanov (1958), "Time of the rupture process under creep condition", *Izv. Akad. Nauk. SSSR, Otd. Tekhn. Nauk*, **8**, 26–31.

45 L.M. Kachanov (1977), "Creep and rupture under complex loading", *Problemi Prochnosti*, **6**.

46 J. Kestin and J. Bataille (1977), "Irreversible thermodynamics of continua and internal variables", In *Proceedings of the Int. Symp. on Continuum Models of Discrete Systems*, pages 39–67. Univ. of Waterloo Press.

47 D. Krajčinović (1983), "Constitutive equations for damaging materials", *J. Appl. Mech.*, **50**, 355–360.

48 D. Krajčinović (1985), "Continuous damage mechanics revisited: Basic concepts and definitions", *J. Appl. Mech.*, **52**, 829–834.

49 D. Krajčinović (1989), "Damage mechanics", *Mech. of Materials*, **8**, 117–197.

50 D. Krajčinović and G.U. Fonseka (1981), "The continuous damage theory of brittle materials – Part 1: General theory", *J. Appl. Mech.*, **48**, 809–815.

51 F.A. Leckie and D.R. Hayhurst (1974), "Creep rupture of structures", *Proc. Roy. Soc. Lond. A*, **340**, 323–347.

52 F.A. Leckie and E.T. Onat (1981), "Tensorial nature of damage measuring internal variables", In *Proceedings of the IUTAM Symposium on Physical Nonlinearities in Structures*, pages 140–155, Springer.

53 E.H. Lee (1969), "Elastic-plastic deformation at finite strains", *J. Appl. Mech.*, **36**, 1–6.

54 J. Lemaitre (1983), "A three-dimensional ductile damage model applied to deep-drawing forming limits", In *ICM 4 Stockholm*, Volume **2**, pages 1047–1053.

55 J. Lemaitre (1984), "How to use damage mechanics", *Nuclear Engng. Design*, **80**, 233–245.

56 J. Lemaitre (1985), "A continuous damage mechanics model for ductile fracture", *J. Engng. Mat. Tech.*, **107**, 83–89.

57 J. Lemaitre (1985), "Coupled elasto-plasticity and damage constitutive equations", *Comp. Meth. Appl. Mech. Engng.*, **51**, 31–49.

58 J. Lemaitre (1987), "Formulation and identification of damage kinetic constitutive equations", In D. Krajčinović and J. Lemaitre, editors, *Continuum Damage Mechanics: Theory and Applications*, pages 37–89, Springer-Verlag.

59 J. Lemaitre (1990), "Micro-mechanics of crack initiation", *Int. J. Fracture*, **42**, 87–99.

60 J. Lemaitre and J.L. Chaboche (1990), *Mechanics of Solid Materials*, Cambridge Univ. Press.

61 J. Lemaitre and J. Dufailly (1987), "Damage measurements", *Engng. Fract. Mech.*, **28**(8), 643–661.

62 J.E. Mark (1984), "The rubber elastic state", In *Physical Properties of Polymers*, pages 1–54, Washington, American Chemical Society.

63 D. Marquis and J. Lemaitre (1988), "Constitutive equations for the coupling between elasto-plasticity damage and aging", *Revue Phys. Appl.*, **23**, 615–624.

64 F. A. McClintock (1968), "A criterion for ductile fracture by the growth of holes", *J. Appl. Mech.*, **35**, 363–371.

65 G.P. Mitchell (1990), *Topics in the Numerical Analysis of Inelastic Solids*, PhD thesis, Dept. of Civil Engineering, Univ. Coll. of Swansea.

66 B. Moran, M. Ortiz, and F. Shih (1990), "Formulation of implicit finite element methods for multiplicative finite deformation plasticity", *Int. J. Num. Meth. Engng.*, **29**, 483–514.

67 L. Mullins (1969), "Softening of rubber by deformation", *Rubber Chemistry and Technology*, **42**, 339–351.

68 S. Murakami (1987), "Anisotropic aspects of material damage and application of continuum damage mechanics", In D. Krajčinovió and J. Lemaitre, editors, *Continuum Damage Mechanics: Theory and Applications*, pages 91–133, Springer-Verlag.

69 S. Murakami (1988), "Mechanical modeling of material damage", *J. Appl. Mech.*, **55**, 280–286.

70 S. Murakami and T. Imaizumi (1982), "Mechanical description of creep damage state and its experimental verification", *Journal de Mécanique Théorique et Appliquée*, **1**(5), 743–761.

71 S. Murakami and N. Ohno (1981), "A continuum theory of creep and creep damage", In A.R.S. Ponter (ed.), *Proceedings of the IUTAM Symposium on Creep in Structures, Leicester, 1980*, pages 422–443, Berlin, Springer.

72 J.C. Nagtegaal (1982), "On the implementation of inelastic constitutive equations with special reference to large deformation problems", *Comp. Meth. Appl. Mech. Engng.*, **33**, 469–484.

73 S. Nemat-Nasser (1982), "On finite deformation elasto-plasticity", *Int. J. Solids Structures*, **18**(10), 857–872.

74 E. Oñate, M. Kleiber, and C. Agelet de Saracibar (1988), "Plastic and viscoplastic flow of void-containing metals. Applications to axisymmetric sheet forming problems", *Int. J. Num. Meth. Engng.*, **25**, 227–251.

75 J.T. Oden (1972), *Finite Elements of Nolinear Continua*, McGraw-Hill, London.

76 R.W. Ogden (1972), "Large deformation isotropic elasticity – on the correlation of theory and experiment for incompressible rubberlike solids", *Proc. R. Soc. Lond. A*, **326**, 565–584.

77 R.W. Ogden (1984), *Non-Linear Elastic Deformations*, Ellis Horwood, Chichester.

78 E.T. Onat (1986), "Representation of mechanical behaviour in the presence of internal damage", *Engng. Fract. Mech.*, **25**, 605–614.

79 E.T. Onat and F.A. Leckie (1988), "Representation of mechanical behavior in the presence of changing internal structure", *J. Appl. Mech.*, **55**, 1–10.

80 M. Ortiz and E.P. Popov (1985), "Accuracy and stability of integration algorithms for elasto-plastic constitutive relations", *Int. J. Num. Meth. Engng.*, **21**, 1561–1576.

81 D.R.J. Owen and E. Hinton (1980), *Finite Elements in Plasticity: Theory and Practice*, Pineridge Press, Swansea.

82 D. Perić (1993), "On a class of constitutive equations in viscoplasticity: Formulation and computational issues", *Int. J. Num. Meth. Engng.*, **36**, 1365–1393.

83 D. Perić and D.R.J. Owen (1992), "Computational model for 3-D contact problems with friction based on the penalty method", *Int. J. Num. Meth. Engng.*, **35**, 1289–1309.

84 D. Perić and D.R.J. Owen (1992), "A model for large deformation of elasto-viscoplastic solids at finite strains: Computational issues", In D. Besdo and E. Stein, editors, *Proceedings of the IUTAM Symposium on Finite Inelastic Deformations – Theory and Applications*, pages 299–312, Berlin, Springer.

85 D. Perić, D.R.J. Owen, and M.E. Honnor (1992), "A model for finite strain elasto-plasticity based on logarithmic strains: Computational issues", *Comp. Meth. Appl. Mech Engng.*, **94**, 35–61.

86 Y.N. Rabotnov (1963), "On the equations of state for creep", In *Progress in Applied Mechanics, Prager Anniversary Volume*, page 307, New York, MacMillan.

87 J.R. Rice (1968), "A path independent integral and the approximate analysis of strain concentration by notches and cracks", *J. Appl. Mech.*, **35**, 379–386.

88 J.R. Rice (1969), "On the ductile enlargement of voids in triaxial stress fields", *J. Mech. Phys. Solids*, **17**, 201–217.

89 R.T. Rockafellar (1970), *Convex Analysis*, Princeton University Press.

90 R. Rubinstein and S.N. Atluri (1983), "Objectivity of incremental constitutive relations over finite time steps in computational finite deformation analysis", *Comp. Meth. Appl. Mech. Engng.*, **36**, 277–290.

91 K. Saanouni, J.L. Chaboche, and P.M. Lesne (1989), "Creep crack-growth prediction by a non-local damage formulation", In J. Mazars and Z.P. Bazant, editors, *Cracking and Damage, Strain Localization and Size Effect*, pages 404–414, Amsterdam, Elsevier.

92 F. Sidoroff (1981), "Description of anisotropic damage application to elasticity", In J. Hult and J. Lemaitre, editors, *Proceedings of the IUTAM Symposium on Physical Non-Linearities in Structural Analysis – Senlis (France) – 1980*, Springer-Verlag.

93 J.C. Simo (1985), "On the computational significance of the intermediate configuration and hyperelastic stress relations in finite deformation elastoplasticity", *Mech. of Materials*, **4**, 439–451.

94 J.C. Simo (1987), "On a fully three-dimensional finite-strain viscoelastic damage model: Formulation and computational aspects", *Comp. Meth. Appl. Mech. Engng.*, **60**, 153–173.

95 J.C. Simo (1992), "Algorithms for static and dynamic multiplicative plasticity that preserve the classical return mapping schemes of the infinitesimal theory", *Comp. Meth. Appl. Mech. Engng.*, **99**, 61–112.

96 J.C. Simo and T.R.J. Hughes (1987), "General return mapping algorithms for rate-independent plasticity", In C.S. Desai *et al.*, editor, *Constitutive Laws for Engineering Materials: Theory and Applications*, pages 221–231, Elsevier.

97 J.C. Simo and J.W. Ju (1987), "Strain- and stress-based continuum damage models – I. Formulation and II. Computational aspects", *Int. J. Solids Struct.*, **23**, 821–869.

98 J.C. Simo and C. Miehe (1992), "Associative coupled thermoplasticity at finite strains: Formulation, numerical analysis and implementation", *Comp. Meth. Appl. Mech. Engng.*, **98**, 41–104.

99 J.C. Simo and R.L. Taylor (1985), "Consistent tangent operators for rate-independent elastoplasticity", *Comp. Meth. Appl. Mech. Engng.*, **48**, 101–118.

100 E.A. de Souza Neto and D. Perić (1996), "A computational framework for a class of models for fully coupled elastoplastic damage at finite strains with reference to the linearization aspects", *Comp. Meth. Appl. Mech. Engng.*, **130**, 179–193.

101 E.A. de Souza Neto and D. Perić (1996), "On the computation of general isotropic tensor functions of one tensor and their derivatives", (submitted for publication).

102 E.A. de Souza Neto, D. Perić, M. Dutko, and D.R.J. Owen (1996), "Design of simple low order finite elements for large strain analysis of nearly incompressible solids", *Int. J. Solids Struct.*, **33**, 3277–3296.

103 E.A. de Souza Neto, D. Perić, and D.R.J. Owen (1992), "A computational model for ductile damage at finite strains", In D.R.J. Owen, E. Oñate, and E. Hinton, editors, *Proceedings of the Third International Conference on Computational Plasticity: Fundamentals and Applications – Barcelona, April 1992*, pages 1425–1441, Swansea, Pineridge Press.

104 E.A. de Souza Neto, D. Perić, and D.R.J. Owen (1994), "A model for elasto-plastic damage at finite strains: Computational issues and applications", *Engng. Comp.*, **11**(3), 257–281.

105 E.A. de Souza Neto, D. Perić, and D.R.J. Owen (1994), "A phenomenological three-dimensional rate-independent continuum damage model for highly filled polymers: Formulation and computational aspects", *J. Mech. Phys. Solids*, **42**(10), 1533–1550.

106 E.A. de Souza Neto, D. Perić, and D.R.J. Owen (1995), "Finite elasticity in spatial description: Linearization aspects with 3-D membrane applications", *Int. J. Num. Meth. Engng.*, **38**, 3365–3381.

107 P. Steinmann, C. Miehe, and E. Stein (1994), "Comparison of different finite deformation inelastic damage models within multiplicative elastoplasticity for ductile metals", *Computational Mechanics*, **13**, 458–474.

108 H.J. Stern (1967), *Rubber: Natural and Synthetic*, McLaren and Sons.

109 W.H. Tai (1990), "Plastic damage and ductile fracture in mild metals", *Engng. Fract. Mech.*, **37**(4), 853–880.

110 L.R.G. Treloar (1967), *The Physics of Rubber Elasticity*, Oxford Univ. Press, 2^{d} edition.

111 C. Truesdell (1969), *Rational Thermodynamics*, McGraw-Hill, New York.

112 C. Truesdell and W. Noll (1965), "The non-linear field theories of mechanics", In S. Flügge, editor, *Handbuch der Physik*, Volume III/3. Springer-Verlag.

113 V. Tvergaard (1981), "Influence of voids on shear band instabilities under plane strain conditions", *Int. J. Fracture*, **17**, 389–407.

114 V. Tvergaard (1982), "Material failure by void coalescence in localized shear bands", *Int. J. Solids Struct.*, **18**, 659–672.

115 V. Tvergaard (1982), "On localization in ductile materials containing spherical voids", *Int. J. Fracture*, **18**, 237–252.

116 V. Tvergaard and A. Needleman (1984), "Analysis of the cup-cone fracture in a round tensile bar", *Acta Metall.*, **32**, 157–169.

117 S. Valliappan, V. Murti, and Z. Wohua (1990), "Finite element analysis of anisotropic damage mechanics problems", *Engng. Fracture Mech.*, **35**(6), 1061–1071.

118 G. Weber and L. Anand (1990), "Finite deformation constitutive equations and a time integration procedure for isotropic, hyperelastic-viscoplastic solids", *Comp. Meth. Appl. Mech. Engng.*, **79**, 173–202.

119 Y.Y. Zhu, S. Cescotto, and A-M. Habraken (1992), "A fully coupled elastoplastic damage theory based on energy equivalence", In D.R.J. Owen, E. Oñate, and E. Hinton, editors, *Proceedings of the Third International Conference on Computational Plasticity: Fundamentals and Applications – Barcelona, April 1992*, pages 1455–1466, Swansea, Pineridge Press.

120 O.C. Zienkiewicz and R.L. Taylor (1989), *The Finite Element Method – Vol.1: Basic Formulation and Linear Problems*, McGraw-Hill.

121 O.C. Zienkiewicz and R.L. Taylor (1991), *The Finite Element Method – Vol.2: Solid and Fluid Mechanics, Dynamics and Non-Linearity*, McGraw-Hill.

Please address your comments or questions on this paper to:
International Center for Numerical Methods in Engineering
Edificio C-1, Campus Norte UPC
Grand Capitán s/n
08034 Barcelona, Spain
Phone: 34-93-4106035; Fax: 34-93-4016517

A COMPUTATION OF ISOTROPIC TENSOR FUNCTIONS OF A TENSOR AND THEIR DERIVATIVES

A.1 General Isotropic Tensor-valued Functions of a Tensor

Consider a generic real symmetric second order tensor $\boldsymbol{X}$ in three-dimensional space. Its spectral decomposition gives:

$$\boldsymbol{X} = \sum_{i=1}^{3} x_i \, \boldsymbol{e}_i \otimes \boldsymbol{e}_i \tag{166}$$

where x_i are the *eigenvalues* of $\boldsymbol{X}$ and $\boldsymbol{e}_i$ are corresponding unit *eigenvectors*. Alternatively, with $p \leq 3$ defined as the number of *distinct* eigenvalues of $\boldsymbol{X}$, one may write:

$$\boldsymbol{X} = \sum_{i=1}^{p} x_i \, \boldsymbol{E}_i \, . \tag{167}$$

where the *eigenprojection* tensor $\boldsymbol{E}_i$ is the orthogonal projection operator on the characteristic space of $\boldsymbol{X}$ associated with x_i, i.e, the space containing all vectors $\boldsymbol{v}$ that satisfy:

$$\boldsymbol{X}\,\boldsymbol{v} = x_i\,\boldsymbol{v} \, . \tag{168}$$

The eigenprojections have the property:

$$\boldsymbol{I} = \sum_{i=1}^{p} \boldsymbol{E}_i \, , \tag{169}$$

and, if an eigenvalue x_i is not repeated, then

$$\boldsymbol{E}_i = \boldsymbol{e}_i \otimes \boldsymbol{e}_i \qquad \text{(no sum)} \, . \tag{170}$$

We are concerned in this section with general isotropic tensor-valued functions of one tensor constructed as follows. Given the generic tensor $\boldsymbol{X}$ and a scalar function $y : \mathbb{R}^3 \to \mathbb{R}$, the tensor function $\boldsymbol{Y}$ is defined by:

$$\boldsymbol{Y}(\boldsymbol{X}) := \sum_{i=1}^{p} y_i \, \boldsymbol{E}_i \tag{171}$$

where the eigenvalues y_i of $\boldsymbol{Y}$ are obtained from the eigenvalues x_i of $\boldsymbol{X}$ as:

$$\begin{aligned} y_1 &:= y(x_1, x_2, x_3) \\ y_2 &:= y(x_2, x_3, x_1) \\ y_3 &:= y(x_3, x_1, x_2) \, , \end{aligned} \tag{172}$$

and the isotropy of $\boldsymbol{Y}$ requires that

$$y(a, b, c) = y(a, c, b) \tag{173}$$

for arbitrary a, b and c.

REMARK A.1 It should be noted that *any* isotropic tensor-valued function of one tensor can be expressed in the above form. A simple example is given by the *deviatoric projection* of a symmetric tensor, defined as:

$$\boldsymbol{Y}(\boldsymbol{X}) := \boldsymbol{X}_d = \boldsymbol{X} - \tfrac{1}{3}\,\mathrm{tr}[\boldsymbol{X}]\,\boldsymbol{I}\,.$$

Is this case, the function y, in 3-D, reads:

$$y(x_i, x_j, x_k) = x_i - \tfrac{1}{3}\,(x_i + x_j + x_k)\,.$$

For functions such as the one above, in which $\boldsymbol{Y}$ is expressed as a function of $\boldsymbol{X}$ in a tensorial compact form, $\boldsymbol{Y}$ can be computed directly from its definition. Compact representation, however, is usually not possible and the computation of $\boldsymbol{Y}(\boldsymbol{X})$ requires, in general, the use of the procedure described in the sequel. □

A.1.1 Function computation

The computational procedure for evaluation of the general tensor functions of the above class is carried out based on *closed form* expressions for eigenvalues and eigenprojections of a tensor. It is summarized in Box A.1.

(i) Given $\boldsymbol{X}$, compute its eigenvalues, x_i, and eigenprojections, $\boldsymbol{E}_i$ (GOTO Box A.2).

(ii) Compute the eigenvalues of $\boldsymbol{Y}$ as:

$$\begin{aligned} y_1 &:= y(x_1, x_2, x_3) \\ y_2 &:= y(x_2, x_3, x_1) \\ y_3 &:= y(x_3, x_1, x_2) \end{aligned}$$

(iii) Assemble $\boldsymbol{Y}$:

$$\boldsymbol{Y}(\boldsymbol{X}) := \sum_{i=1}^{p} y_i\,\boldsymbol{E}_i\,,$$

where p is the number of distinct eigenvalues.

Box A.1 Computation of general isotropic tensor functions of a tensor

REMARK A.2 In practical computations, the signs $=$ and $\neq$, that decide which formula is to be used in Boxes A.2 and A.3, as well as in what follows, are replaced by a check that takes into account the numerical precision of the machine used. For generic eigenvalues x_i and x_j we proceed as follows:

$$\text{If}\quad \left|\frac{x_i - x_j}{x_i}\right| < \mathrm{tol}\,,\qquad \text{then assume}\quad x_i = x_j\,.$$

Otherwise, assume $x_i \neq x_j$. Where tol is a machine dependent numerical tolerance. □

(i) Given $\boldsymbol{X}$ compute its principal invariants:

$$I_X = \mathrm{tr}[\boldsymbol{X}] = x_1 + x_2 + x_3$$
$$II_X = \frac{1}{2}\{(\mathrm{tr}\,\boldsymbol{X})^2 - \mathrm{tr}[\boldsymbol{X}^2]\} = x_1\,x_2 + x_2\,x_3 + x_1\,x_3$$
$$III_X = \det[\boldsymbol{X}] = x_1\,x_2\,x_3$$

(ii) Compute the eigenvalues of $\boldsymbol{X}$:

$$R = \frac{-2\,I_X^3 + 9\,I_X\,II_X - 27\,III_X}{54}$$
$$\theta = \cos^{-1}\left[\frac{R}{\sqrt{Q^3}}\right]$$
$$Q = \frac{I_X^2 - 3\,II_X}{9}$$
$$x_1 = -2\,\sqrt{Q}\,\cos\left[\frac{\theta}{3}\right] + \frac{I_X}{3}$$
$$x_2 = -2\,\sqrt{Q}\,\cos\left[\frac{\theta+2\pi}{3}\right] + \frac{I_X}{3}$$
$$x_3 = -2\,\sqrt{Q}\,\cos\left[\frac{\theta-2\pi}{3}\right] + \frac{I_X}{3}$$

(iii) Compute eigenprojections of $\boldsymbol{X}$:

- If $x_i \neq x_2 \neq x_3$, then for $i = 1, 2, 3$,

$$\boldsymbol{E}_i = \frac{x_i}{2\,x_i^3 - I_X\,x_i^2 + III_X}\left[\boldsymbol{X}^2 - (I_X - x_i)\,\boldsymbol{X} + \frac{III_X}{x_i}\,\boldsymbol{I}\right]$$

- Else, if $x_i \neq x_j = x_k$, then compute $\boldsymbol{E}_i$ using the expression above and

$$\boldsymbol{E}_j = \boldsymbol{I} - \boldsymbol{E}_i$$

- Else $(x_1 = x_2 = x_3)$,

$$\boldsymbol{E}_1 = \boldsymbol{I}$$

Box A.2 Computation of eigen values and eigenprojections

A.1.2 Computation of the function derivative

As in the function evaluation described in Box A.1, closed form expressions are also used to compute the function derivative. The derivation of the adopted closed formulae for the general isotropic function derivative is described in detail in reference [101].

The computational procedure for computation of $\mathrm{d}\boldsymbol{Y}/\mathrm{d}\boldsymbol{X}$ is described in Box A.3 where $\boldsymbol{I}$ denotes the fourth order tensor defined by the cartesian components $I_{ijkl} = \frac{1}{2}(\delta_{ik}\delta_{jl} + \delta_{il}\delta_{jk})$, $\mathrm{d}\boldsymbol{X}^2/\mathrm{d}\boldsymbol{X}$ is the derivative of the square of a tensor with cartesian components given by:

$$\left[\frac{\mathrm{d}\boldsymbol{X}^2}{\mathrm{d}\boldsymbol{X}}\right]_{ijkl} = \frac{1}{2}\,(\delta_{ik}X_{lj} + \delta_{il}X_{kj} + \delta_{jl}X_{ik} + \delta_{kj}X_{il}) \tag{174}$$

and the scalars s_1, s_2,..., s_6 have been defined as:

$$
\begin{aligned}
s_1 &= \frac{y_a - y_c}{(x_a - x_c)^2} + \frac{1}{x_a - x_c}\left(\frac{\partial y_c}{\partial x_b} - \frac{\partial y_c}{\partial x_c}\right) \\
s_2 &= 2x_c\,\frac{y_a - y_c}{(x_a - x_c)^2} + \frac{x_a + x_c}{x_a - x_c}\left(\frac{\partial y_c}{\partial x_b} - \frac{\partial y_c}{\partial x_c}\right) \\
s_3 &= 2\,\frac{y_a - y_c}{(x_a - x_c)^3} + \frac{1}{(x_a - x_c)^2}\left(\frac{\partial y_a}{\partial x_c} + \frac{\partial y_c}{\partial x_a} - \frac{\partial y_a}{\partial x_a} - \frac{\partial y_c}{\partial x_c}\right) \\
s_4 &= 2x_c\,\frac{y_a - y_c}{(x_a - x_c)^3} + \frac{1}{x_a - x_c}\left(\frac{\partial y_a}{\partial x_c} - \frac{\partial y_c}{\partial x_b}\right) + \frac{x_c}{(x_a - x_c)^2}\left(\frac{\partial y_a}{\partial x_c} + \frac{\partial y_c}{\partial x_a} - \frac{\partial y_a}{\partial x_a} - \frac{\partial y_c}{\partial x_c}\right) \\
s_5 &= 2x_c\,\frac{y_a - y_c}{(x_a - x_c)^3} + \frac{1}{x_a - x_c}\left(\frac{\partial y_c}{\partial x_a} - \frac{\partial y_c}{\partial x_b}\right) + \frac{x_c}{(x_a - x_c)^2}\left(\frac{\partial y_a}{\partial x_c} + \frac{\partial y_c}{\partial x_a} - \frac{\partial y_a}{\partial x_a} - \frac{\partial y_c}{\partial x_c}\right) \\
s_6 &= 2x_c^2\,\frac{y_a - y_c}{(x_a - x_c)^3} + \frac{x_a x_c}{(x_a - x_c)^2}\left(\frac{\partial y_a}{\partial x_c} + \frac{\partial y_c}{\partial x_a}\right) - \frac{x_c^2}{(x_a - x_c)^2}\left(\frac{\partial y_a}{\partial x_a} + \frac{\partial y_c}{\partial x_c}\right) - \frac{x_a + x_c}{x_a - x_c}\,\frac{\partial y_c}{\partial x_b}
\end{aligned}
\tag{175}
$$

The subscripts (a, b, c) above and in Box A.4 are cyclic permutations of (1,2,3).

A.2 A Particular Class of Isotropic Tensor Functions

Assume now that y is a function of a single argument. Given $y : \mathbb{R} \to \mathbb{R}$, an isotropic tensor function of $\boldsymbol{X}$ can be constructed as:

$$
\boldsymbol{Y}(\boldsymbol{X}) := \sum_{i=1}^{p} y(x_i)\, \boldsymbol{E}_i\,, \tag{176}
$$

REMARK A.3 Functions expressed as such define an important class of isotropic tensor valued functions of a tensor and are, obviously, particular cases of the general form (171). Note that the function given as example in Remark A.1 does *not* admit representation by means of (176). The *tensor logarithm*:

$$
\boldsymbol{Y}(\boldsymbol{X}) := \ln[\boldsymbol{X}]\,,
$$

is a particularly important member of this class of functions. Is this case, the function y, in 3-D, reads:

$$
y(x_i) = \ln x_i\,.
$$

Functions such as the tensor square root and the tensor exponential can also be expressed in the format (176) by setting $y(x_i) = \sqrt{x_i}$ and $y(x_i) = \exp(x_i)$, respectively. □

Since (176) is a particular case of (171), the computational procedures for evaluation of $\boldsymbol{Y}(\boldsymbol{X})$ and its derivative are entirely analogous to the procedures described in the previous section. The computation of the function value, $\boldsymbol{Y}(\boldsymbol{X})$, follows exactly the steps of Box A.1 except that, in item (ii), the function eigenvalues are computed as:

$$
y_i := y(x_i)\,, \tag{177}
$$

for $i = 1, 2, 3$. The computation of the derivative $\mathrm{d}\boldsymbol{Y}/\mathrm{d}\boldsymbol{X}$ is summarized in Box A.4 where the scalars s_1,...,s_6 are now defined by:

(i) Given $\boldsymbol{X}$, compute its eigenvalues, x_i, and eigenprojections, $\boldsymbol{E}_i$ (GOTO Box A.2).

(ii) Compute the eigenvalues y_i of $\boldsymbol{Y}$ and their derivatives $\partial y_i/\partial x_j$ for $i,j=1,2,3$

(iii) Assemble the derivative $\dfrac{\mathrm{d}\boldsymbol{Y}}{\mathrm{d}\boldsymbol{X}}$

$$\frac{\mathrm{d}\boldsymbol{Y}}{\mathrm{d}\boldsymbol{X}} = \begin{cases} \displaystyle\sum_{a=1}^{3} \frac{y_a}{(x_a-x_b)(x_a-x_c)} \Big\{ \frac{\mathrm{d}\boldsymbol{X}^2}{\mathrm{d}\boldsymbol{X}} - (x_b+x_c)\,\boldsymbol{I} \\ \qquad - [(x_a-x_b)+(x_a-x_c)]\,\boldsymbol{E}_a\otimes\boldsymbol{E}_a \\ \qquad\qquad - (x_b-x_c)\,(\boldsymbol{E}_b\otimes\boldsymbol{E}_b - \boldsymbol{E}_c\otimes\boldsymbol{E}_c)\Big\} \\ \qquad\qquad\qquad + \displaystyle\sum_{i=1}^{3}\sum_{j=1}^{3} \frac{\partial y_i}{\partial x_j}\,\boldsymbol{E}_i\otimes\boldsymbol{E}_j & \text{if } x_1\neq x_2\neq x_3 \\ s_1\,\dfrac{\mathrm{d}\boldsymbol{X}^2}{\mathrm{d}\boldsymbol{X}} - s_2\,\boldsymbol{I} - s_3\,\boldsymbol{X}\otimes\boldsymbol{X} + s_4\,\boldsymbol{X}\otimes\boldsymbol{I} + s_5\,\boldsymbol{I}\otimes\boldsymbol{X} - s_6\,\boldsymbol{I}\otimes\boldsymbol{I} & \text{if } x_a\neq x_b = x_c \\ \left(\dfrac{\partial y_1}{\partial x_1} - \dfrac{\partial y_1}{\partial x_2}\right)\boldsymbol{I} + \dfrac{\partial y_1}{\partial x_2}\,\boldsymbol{I}\otimes\boldsymbol{I} & \text{if } x_1=x_2=x_3 \end{cases}$$

Box A.3 Computation of the derivative of a general isotropic tensor function

$$\begin{aligned} s_1 &= \frac{y(x_a)-y(x_c)}{(x_a-x_c)^2} - \frac{y'(x_c)}{x_a-x_c} \\ s_2 &= 2x_c\,\frac{y(x_a)-y(x_c)}{(x_a-x_c)^2} - \frac{x_a+x_c}{x_a-x_c}\,y'(x_c) \\ s_3 &= 2\,\frac{y(x_a)-y(x_c)}{(x_a-x_c)^3} - \frac{y'(x_a)+y'(x_c)}{(x_a-x_c)^2} \\ s_4 &= s_5 = x_c\,s_3 \\ s_6 &= x_c^2\,s_3\,. \end{aligned} \tag{178}$$

Again, the subscripts (a,b,c) are cyclic permutations of $(1,2,3)$.

(i) Given $\boldsymbol{X}$ compute its eigenvalues, x_i, and eigenprojections, $\boldsymbol{E}_i$ (GOTO Box A.2).

(ii) Compute the eigenvalues of $\boldsymbol{Y}$, $y_i := y(x_i)$, and their derivatives, $y'(x_i)$ for $i = 1, 2, 3$.

(iii) Assem ble the derivative $\dfrac{\mathrm{d}\boldsymbol{Y}}{\mathrm{d}\boldsymbol{X}}$

$$\frac{\mathrm{d}\boldsymbol{Y}}{\mathrm{d}\boldsymbol{X}} = \begin{cases} \displaystyle\sum_{a=1}^{3} \left\{ \frac{y(x_a)}{(x_a - x_b)(x_a - x_c)} \left[\frac{\mathrm{d}\boldsymbol{X}^2}{\mathrm{d}\boldsymbol{X}} - (x_b + x_c)\, \mathsf{I} \right.\right. \\ \qquad - [(x_a - x_b) + (x_a - x_c)]\, \boldsymbol{E}_a \otimes \boldsymbol{E}_a \\ \qquad\qquad \left.\left. - \ (x_b - x_c)\, (\boldsymbol{E}_b \otimes \boldsymbol{E}_b - \boldsymbol{E}_c \otimes \boldsymbol{E}_c) \right] + \ y'(x_a)\ \boldsymbol{E}_a \otimes \boldsymbol{E}_a \right\} \\ \hfill \text{if } x_1 \neq x_2 \neq x_3 \\ \\ s_1 \dfrac{\mathrm{d}\boldsymbol{X}^2}{\mathrm{d}\boldsymbol{X}} - s_2\, \mathsf{I} - s_3\, \boldsymbol{X} \otimes \boldsymbol{X} + s_4\, \boldsymbol{X} \otimes \boldsymbol{I} + s_5\, \boldsymbol{I} \otimes \boldsymbol{X} - s_6\, \boldsymbol{I} \otimes \boldsymbol{I} \\ \hfill \text{if } x_a \neq x_b = x_c \\ \\ y'(x_1)\, \mathsf{I} \hfill \text{if } x_1 = x_2 = x_3 \end{cases}$$

Bo x A.4 Computation of the deriv ative for a particular class of isotropic tensor functions